Hawke's Bay 3D Aquifer Mapping Project:

Hydrogeological interpretation of SkyTEM-derived resistivity models within the Poukawa and Otane basins

February 2024
Hawkes Bay Regional Council Publication No. 5628

HAWKES BAY
REGIONAL COUNCIL
TE KAUNIHERA Ā-ROHE O TE MATAU-A-MĀUI

ISSN 2703-2051 (Online)
ISSN 2703-2043 (Print)

HAWKES BAY REGIONAL COUNCIL
TE KAUNIHERA Ā-ROHE O TE MATAU-A-MĀUI

(06) 835 9200
0800 108 838
Private Bag 6006 Napier 4142
159 Dalton Street . Napier 4110

Environmental Science

Hawke's Bay 3D Aquifer Mapping Project:

Hydrogeological interpretation of SkyTEM-derived resistivity models within the Poukawa and Otane basins

February 2024
Hawkes Bay Regional Council Publication No. 5628

Prepared By:
GNS Science

ZJ Rawlinson TR Sahoo
RL Kellett SG Cameron

For: Hawke's Bay Regional Council

Reviewed by:
S Harper, Hawke's Bay Regional Council
R Westerhoff, GNS Science
C Tschritter, GNS Science

ISSN 2703-2051 (Online)
ISSN 2703-2043 (Print)

.

Hawke's Bay 3D Aquifer Mapping Project: Hydrogeological interpretation of SkyTEM-derived resistivity models within the Poukawa and Otane basins

ZJ Rawlinson
RL Kellett
TR Sahoo
SG Cameron

GNS Science Consultancy Report 2021/12
February 2024

GNS SCIENCE
TE PŪ AO

DISCLAIMER

This report has been prepared by the Institute of Geological and Nuclear Sciences Limited (GNS Science) exclusively for and under contract to Hawke's Bay Regional Council. Unless otherwise agreed in writing by GNS Science, GNS Science accepts no responsibility for any use of or reliance on any contents of this report by any person other than Hawke's Bay Regional Council and shall not be liable to any person other than Hawke's Bay Regional Council, on any ground, for any loss, damage or expense arising from such use or reliance.

Use of Data:

Date that GNS Science can use associated data: February 2024

BIBLIOGRAPHIC REFERENCE

Rawlinson ZJ, Sahoo TR, Kellett RL, Cameron SG. 2024. Hawke's Bay 3D Aquifer Mapping Project: hydrogeological interpretation of the SkyTEM-derived resistivity models within the Poukawa and Otane basins. Wairakei (NZ): GNS Science. 96 p. Consultancy Report 2021/12.

CONTENTS

FIGURES

TABLES

APPENDICES

APPENDIX FIGURES

APPENDIX TABLES

EXECUTIVE SUMMARY

This report focuses on the mapping of groundwater systems in the Poukawa and Otane basins as part of the Hawke's Bay 3D Aquifer Mapping Project (3DAMP).

3DAMP is a four-year initiative (2019–2023) jointly funded by the Provincial Growth Fund, Hawke's Bay Regional Council (HBRC) and GNS Science's (GNS) Groundwater Strategic Science Investment Fund research programme. The project applies SkyTEM technology to improve mapping and modelling of groundwater resources within the Heretaunga Plains, Ruataniwha Plains and Poukawa and Otane basins. 3DAMP involves collaboration between HBRC, GNS and the Aarhus University HydroGeophysics Group.

SkyTEM is a geophysical technique that uses electromagnetic waves to investigate the shallow (up to 500 m) resistivity structure of the earth. Resistivity models were developed for the Poukawa and Otane basins by Rawlinson et al. (2021). This report describes a hydrogeological interpretation of these resistivity models.

As the Poukawa and Otane basin survey area is not a priority research area within the 3DAMP project, the hydrogeological interpretation undertaken was required to be limited in scope. Key objectives for the Poukawa and Otane basins interpretation were discussed and prioritised with HBRC as follows:

1. The 3D lithological structure of relevance to groundwater, particularly:
    a. Waipawa River and Papanui Stream bed delineation.
    b. Depth to limestone (Mangaheia Group).
    c. Base of limestone (Mangaheia Group).
    d. Thickness of any unconfined layer in the Poukawa area.
    e. Any differences within the limestone, e.g. permeability/fracture zones.
    f. Peat thickness.
2. Connection to the Heretaunga Plains.
3. Delineation of main faults.

Where feasible, the hydrogeological interpretations were to be provided by the delivery of 2D and 3D map products that address the above objectives, including the development of 3D datasets suitable for display within an online 3D visualisation tool.

There are no unique mathematical equations established that directly link geological material with resistivity values. Supporting local information is therefore required to interpret the resistivity models. Within the study area, such information is relatively limited in both quantity and quality.

A combined approach of manual delineation and automated thresholding was considered an effective way to deal with a resistivity dataset that displayed many overlapping values from different lithological units, limited supporting datasets and non-linear relationships between resistivity and permeability in some areas. Both the smooth and sharp resistivity models were utilised for the manual delineation, but only the smooth model was used for the automated thresholding.

A series of 3D models were developed with 50 x 50 m grid cells horizontally and 2-m-thick grid cells vertically. The 3D models developed are as follows:

- An interpolated resistivity (res) model.
- A major Hydrogeological Unit (HU) model.
- A resistivity facies (facies) model.
- An Aquifer Potential (AP) model.

2D maps/models were also developed:

- Near-surface properties (res, facies and AP) for the upper 5 m, 10 m, 15 m, 20 m, 30 m, 50 m, 75 m, 100 m and 150 m, using the geometric and harmonic mean.
- Manually delineated surfaces describing: top of limestone, base of limestone and base of riverbeds.

3D model datasets were created and saved in an accessible *.csv* format, with x,y,z defining the centre of each grid cell. This format enables rapid model visualisation in an interactive online webmap and as 3D block models within a Leapfrog software viewer file. A selection of these models was also converted to multi-band raster format, enabling further accessibility, such as visualisation of elevation slices within GIS software. 2D models were developed in raster format.

The datasets from this study enable a 3D view of the subsurface geology and hydrogeology not previously possible, providing refinement of the existing understanding of groundwater resources in the Poukawa and Otane basins.

Recommendations for future work aim to refine interpretations and reduce uncertainties through drilling, additional electromagnetic measurements (ground-based, bore-based or sample-based) and more detailed local studies.

1.0 INTRODUCTION

This report focuses on the mapping of groundwater aquifers in the Poukawa and Otane basins (Figure 1.1) as part of the Hawke's Bay 3D Aquifer Mapping Project (3DAMP).

3DAMP is a four-year initiative (2019–2023) jointly funded by the Provincial Growth Fund, Hawke's Bay Regional Council (HBRC) and GNS Science's (GNS) Groundwater Strategic Science Investment Fund research programme. The project applies SkyTEM technology to improve mapping and modelling of groundwater resources within the Heretaunga Plains, Ruataniwha Plains and Poukawa and Otane basins. 3DAMP involves collaboration between HBRC, GNS and the Aarhus University HydroGeophysics Group (HGG).

SkyTEM is a geophysical technique that uses electromagnetic waves to investigate the shallow (up to 500 m depth) resistivity structure of the earth. SkyTEM data were collected in the Hawke's Bay region during January/February 2020 (SkyTEM Australia Pty Ltd [2020]). Resistivity models were developed for the Poukawa and Otane basins by Rawlinson et al. (2021). This report describes a hydrogeological interpretation of these resistivity models.

1.1 Objectives

Key interpretation objectives for the Poukawa and Otane basins survey area (Figure 1.1) were discussed and prioritised with HBRC as follows:

1. The 3D lithological structure of relevance to groundwater, particularly:
    a. Waipawa River and Papanui Stream bed delineation.
    b. Depth to limestone (Mangaheia Group).
    c. Base of limestone (Mangaheia Group).
    d. Thickness of any unconfined layer in the Poukawa area.
    e. Any differences within the limestone, e.g. permeability/fracture zones.
    f. Peat thickness.
2. Connection to the Heretaunga Plains.
3. Delineation of main faults.

Where feasible, the hydrogeological interpretations were to be provided by the delivery of 2D and 3D map products that address the above objectives, including developing 3D datasets suitable for display within an online 3D visualisation tool.

The online visualisation tool was developed after the completion of the draft version of this report, with the draft datasets and models utilised for iterative testing. It was determined during this testing that a separation between consolidated and unconsolidated sediments was useful for simplified visualisation and understanding. This timeline impacted some of the methodological approach taken.

As the Poukawa and Otane basin survey area is not a priority research area within the 3DAMP project, the hydrogeological interpretation undertaken was required to be limited in scope (compared to the Heretaunga and Ruataniwha Plains hydrogeological interpretations; see Rawlinson [2023] and Rawlinson [2024]). Items outside the scope of this work or below the resolution of the SkyTEM data were to be identified but not discussed in full.

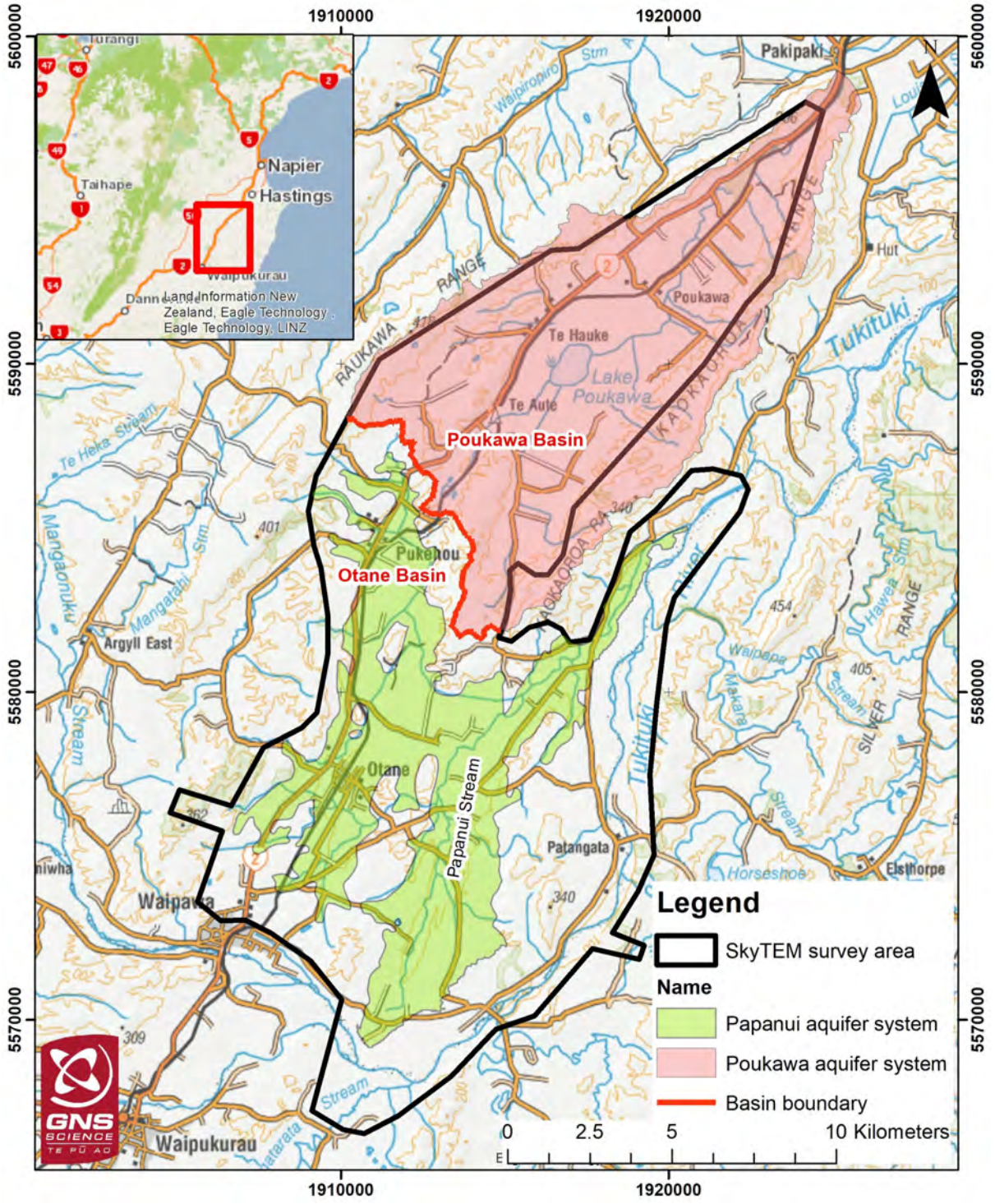

Figure 1.1 Location map of the Poukawa and Otane basins and the SkyTEM survey area. The light shaded areas show the aquifers in these basins as currently defined by HBRC.

1.2 Resistivity Models from SkyTEM Data

The SkyTEM airborne geophysical technique is a transient (time-domain) electromagnetic method (TEM) capable of investigating the shallow (usually up to 500 m deep) electrical resistivity structure of the earth (Sørensen and Auken 2004). The resistivity structure can then be interpreted in terms of geology (e.g. groundwater aquifers) and used to inform and improve geological and hydrological models. In February 2020, 1235.4 km of SkyTEM data were collected over the Poukawa and Otane basins with a line spacing of ~200 m to evaluate the groundwater aquifer systems.

Rawlinson et al. (2021) processed these data to remove electromagnetic noise/artefacts and to develop resistivity models. The resistivity models have 35 layers extending to a depth of 500 m. The shallowest layer has a thickness of 1 m, and the thickness of each layer increases gradually with depth. Each layer is composed of a uniform resistivity value. As undertaking inversion modelling to develop resistivity models is a non-unique mathematical process, both smooth and sharp resistivity models were developed. The smooth model inversion considers absolute changes in resistivity and provides smooth resistivity transitions both vertically and horizontally. In contrast, the sharp model inversion favours resistivity changes above a certain size and provides relatively sharp resistivity transitions.

The quality and reliability of these resistivity models depend on the SkyTEM system set-up, the geological setting, the flight altitude and any electromagnetic noise caused by man-made structures. During data processing, two depth of investigations (DOI) were estimated to highlight the limits of reliable interpretation – standard and conservative (also referred to as ‘DOI Lower’ and ‘DOI Upper’, respectively). The standard DOI varies from 60 to 490 m (Figure 1.2). As a guideline, resistivity structures above the DOI conservative (DOI Upper) value are considered ‘well determined’ (i.e. the inversion modelling is primarily informed by the data), and resistivity structures below the DOI standard (DOI Lower) value are considered ‘weakly determined’ (i.e. the inversion modelling is primarily guided by mathematical regularisation). Between the DOI conservative and the DOI standard, the resistivity model is informed by a combination of data and mathematical regularisation. Details on the SkyTEM data acquisition and processing can be found in SkyTEM Australia Pty Ltd ([2020]), Auken et al. (2009) and Rawlinson et al. (2021).

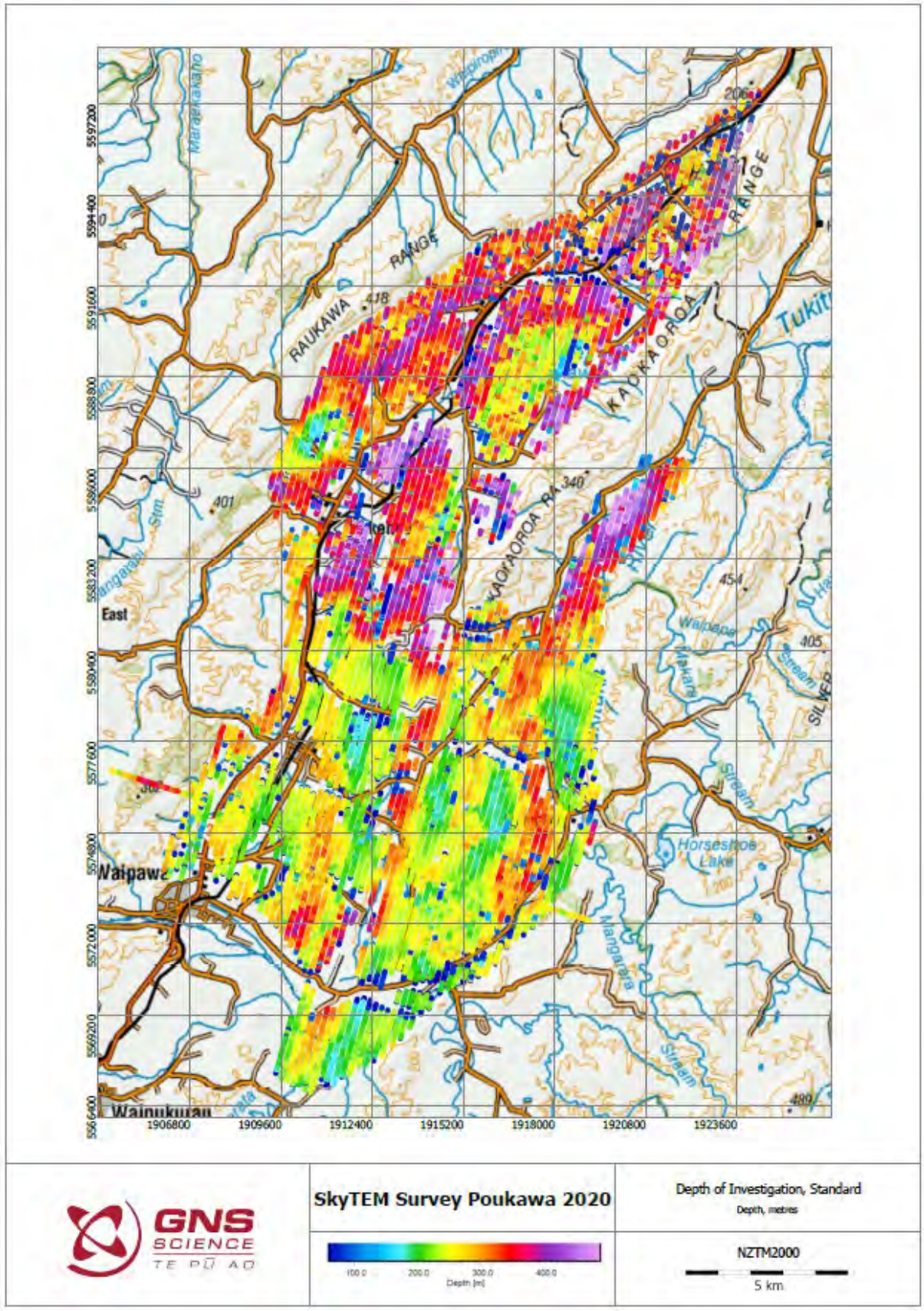

Figure 1.2 Standard depth of investigation for the smooth resistivity model. Figure from Rawlinson et al. (2021).

1.3 What is Hydrogeological Interpretation?

Hydrogeological interpretation of resistivity models is a process of translating resistivity values (typically represented by the unit ohm.m or Ω·m) to categorical or numerical values of more immediate use to a hydrogeologist.

The numerical values present in a resistivity model are a function of complex relationships between porosity, permeability, grain size and sorting, mineralogical content such as clay, and fluid properties. There are no unique mathematical equations established that directly link geological material with resistivity values. Wide ranges of resistivity values have been empirically correlated to various unconsolidated and consolidated lithologies (e.g. Figure 1.3). These values will be locale-specific and may be spatially variable within a locale due to subtle geological variations (e.g. different facies or depositional processes).

Supporting local information is therefore required to interpret the resistivity models. This includes information such as surface geological maps and subsurface geological logs from drilling (Figure 1.4; see Section 3 and Appendix 1). The reliability of interpretations is therefore biased by the quality of local information and to areas with more information to compare to the resistivity models. Within the study area, such information is relatively limited in both quantity and quality (Figure 1.4; see Section 3 and Appendix 1).

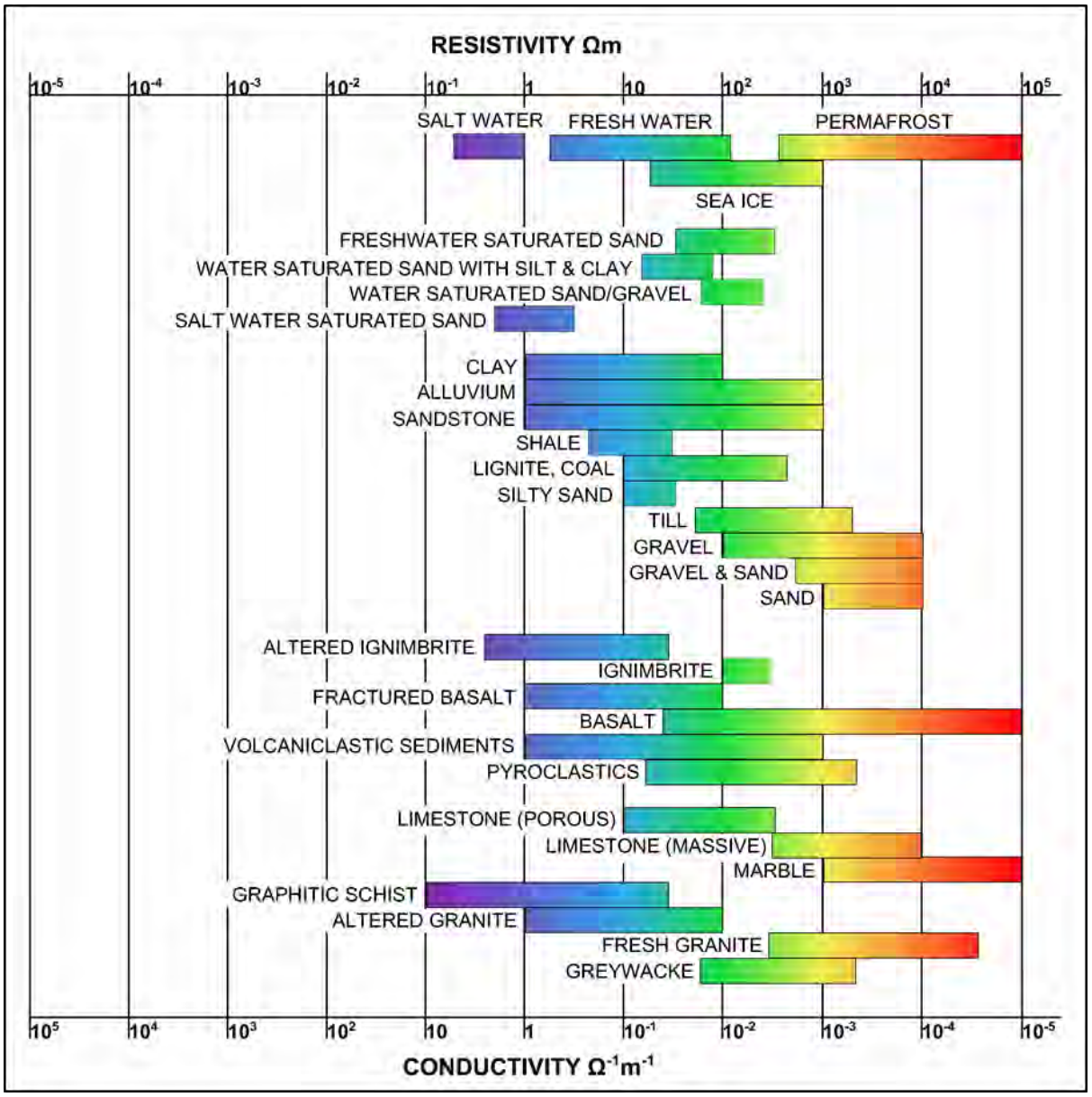

Figure 1.3 Ranges of electrical resistivity for some common lithologies measured in-situ, compiled from a variety of publications. Figure from Rawlinson (2013).

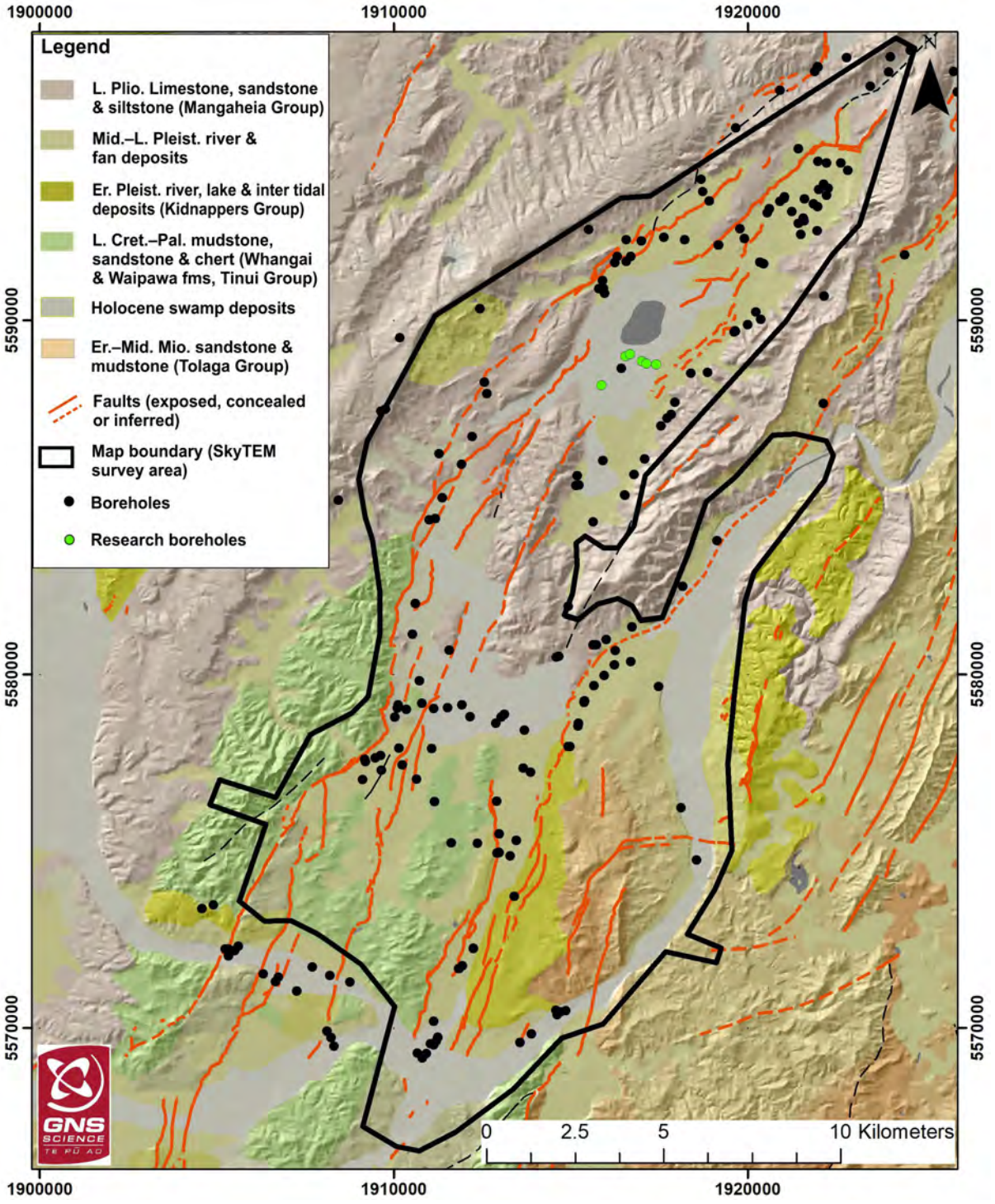

Figure 1.4 Surface geological map (QMAP) draped over a digital elevation model, showing locations of boreholes and research wells. Abbreviations: L. Plio. = Late Pliocene, Mid.-L. Pleist. = Mid to Late Pleistocene, Er. Pleist. = Early Pleistocene, L. Cret.-Pal. = Late Cretaceous to Paleocene, Er.-Mid. Mio. = Early to Mid-Miocene.

2.0 HYDROGEOLOGICAL REVIEW

This section provides a summary of the geological and hydrogeological setting of the Poukawa and Otane area, including major geological formations and their hydrogeological characteristics that are relevant to the SkyTEM survey. The primary sources of geological information for both areas are:

- Kingma (1971): Geology of the Te Aute subdivision.
- Lee et al. (2011): Geology of the Hawke's Bay area (QMAP).

For the Poukawa area:

Geology

- Beu (1995): Pliocene limestones and scallops
- Fellows (1984): Lake Poukawa drilling project
- Hull (1990): Tectonics of the 1931 Hawke's Bay earthquake
- Kelsey et al. (1993, 1998): Geology of southern Hawke's Bay; paleoseismology of an active reverse fault in a forearc setting: the Poukawa Fault Zone
- Robinson et al. (1984): Lithologic log of Lake Poukawa drilling project hole 5 (LPDP 5)
- Beanland et al. (1998): Poukawa Fault Zone seismic interpretation
- Cashman and Kelsey (1990): Tectonics
- Robertson (1978): Quaternary geology
- Howorth et al. (1980): Tephra chronology.

Hydrogeology

- Dravid (1993): Geology and groundwater conditions around Lake Poukawa
- Brown et al. (1998): Availability of sustainable groundwater resource in Poukawa Basin
- Cameron and others (Cameron 2002; Cameron and Gusyev 2011a, b; Cameron and Minni 2009; Cameron and Reeves 2004; Cameron and White 1999, 2001): Pumptest and groundwater modelling consultancy reports on assessment of groundwater abstraction for resource consenting purposes for Brownrigg Agriculture.

For the Otane area:

Geology and hydrogeology

- Harper (2012): Tukituki Catchment groundwater resources
- Barber (2019): Papanui catchment groundwater study – dissolved reactive phosphorus
- Morgenstern and Gordon (2017): Surface water and groundwater quality and isotope survey
- Rissmann and Lovett (2016): Otane sewage discharge investigation.

2.1 Overview

The Poukawa Basin, south-central Hawke's Bay, is located within a NE–SW-trending tectonic depression. The sediments infilling the basin are overlain by soils derived from detritus washed into the basin from the surrounding limestone/siltstone/sandstone hills (Mangaheia Group at the surface) and from organic material associated with Lake Poukawa and fringing swamps

(Figures 1.4 and 2.1). The soil is naturally fertile, and high yields of squash, corn, onions and potatoes can be produced with irrigation. The surface water system of the basin drains to the north to the Heretaunga Plains.

The Otane Basin shares its northern boundary with the Poukawa Basin and lies immediately to the south. It is more commonly referred to as the Papanui catchment in HBRC groundwater publications, reflecting the main drainage system of the basin. The basin drains to the northeast into the Tukituki River. The basin is surrounded by erosion-resistant limestone hills, with a faulted mudstone (shale) basin floor, which are the Whangai and Waipawa formations at the surface (Figure 1.4; Lee et al. 2011). The low-lying basin plains are infilled with recent fan and alluvial deposits, including Waipawa River sediments. The plains once supported extensive wetlands and peat development.

2.2 Poukawa

2.2.1 Geology

The Poukawa Basin is a depression or syncline (Figures 1.4 and 2.1) formed from warping of Pliocene–Pleistocene sediments. These limestone, siltstone and sandstone sediments of the Mangaheia Group form the adjacent hills and underlie the basin to form an asymmetrical syncline flanked by two rising anticlines (Kingma 1971). The main Pliocene–Pleistocene rock types are the soft, barnacle-rich, creamy-yellow Rotookiwa Limestone; yellow-grey, cross-bedded, barnacle-rich Awapapa Limestone (variably cemented and sandy); and coarse-grained shelly textured Te Aute Limestone. The Raukawa Range on the western flank of the basin is composed of Pliocene sediments, including the Te Aute limestone (which was the Te Onepu Limestone of Beu [1995]) dipping to the northwest. On the basin's eastern flank, the Kaokaoroa Range is mainly composed of Rotookiwa Limestone (Beu 1995) dipping 10–25° northwest beneath the Basin. An isopach map of limestone indicates that the limestone aquifer thickness is between approximately 150 and 450 m in the basin (Figure 2.2).

Between the Poukawa Basin and the Heretaunga Plains, Pliocene–Pleistocene sandstone and siltstone outcrops have been preserved in the syncline. These sandstone–siltstone sediments overlie the limestones in the north. Older sandstone sediments underlie the limestone. The basin is infilled with Quaternary sediments that are more than 234 m thick in test bore LPDP 5 in the vicinity of Lake Poukawa. Northeast-trending faults (Poukawa Fault Zone; Kelsey et al. 1993) disrupt the strata and infilling sediments of the basin, including the fault trace along the western margin of the basin on which movement occurred during the 1931 Hawke's Bay earthquake (Hull 1990).

The strata and infilling sediments are penetrated by groundwater wells and test bores described in Beu (1995), Fellows (1994) and Dravid (1993). The deepest test bore drilled (LPDP 5) was 234 m deep and located about 500 m south of Lake Poukawa at a site where the maximum thickness of infilling sediment was thought to occur. The test bore penetrated alternating layers of peats, lake silts and fine silty sands (Fellows 1984). Only a few gravel layers were encountered, and these consisted of sub-rounded to sub-angular pebbles of limestone and mudstone of local origin. The sediments contained a high proportion of re-worked shell fragments derived from the adjacent limestone hills. In March–April 1997, a test bore (Poukawa 97-1) was drilled nearby LPDP 5 for a School of Earth Sciences, Victoria University of Wellington project investigating the paleoclimatic record in the sediments infilling the Poukawa Basin. The test bore was drilled to a depth of 197.7 m.

Based on the lithostratigraphy of the two test bores, Shulmeister et al. (1998) considered that the Quaternary sediments were deposited during the last three full glacial–interglacial cycles (~300,000 years). Shane et al. (2002) extended this dating using tephra chronology, yielding an age of 120 Ka for the base of the section drilled at Poukawa 97-1 (197.7 m).

The absence of greywacke gravel clasts is significant, as it is evidence that the valley has not been occupied by a river (e.g. Waipawa River) with a greywacke rock catchment for at least the last 120,000 years. Greywacke gravel deposits could be present overlying the Pliocene–Pleistocene siltstone/sandstone/limestone in the deepest part of the basin.

2.2.2 Hydrology

Lake Poukawa occupies the centre of the enclosed basin and is the result of rainfall runoff from the surrounding hills. There is potential for lateral leakage into the lake from shallow groundwater within the surrounding unconfined aquifer and/or upward leakage of groundwater from deeper confined aquifers.

The lake and swamp sediments penetrated by the test bores show that a lake has occupied the Poukawa Basin for at least most of the last 120,000 years. The enclosed form of the basin has protected the lake from marine incursion from the sea from the north and from major fluvial sediment deposition by rivers from the south.

Lake Poukawa is almost circular, being about 1.5 km in diameter. The lake is approximately 20 m above mean sea level and is usually less than 1 m deep. Lake levels fluctuate seasonally, and flooding of the surrounding peat swamp often occurs. For example, in August 1977, the lake extended to the west as far as State Highway 2 (SH 2) and covered at least three times its normal area. A study of diatoms in the lake sediments to a depth of 6 m showed that the lake has varied in size but has always been shallow for the last 5000 years (Harper et al. 1986).

The Poukawa Basin has drained to the north throughout the late Quaternary. The sinter deposits in the west (Kingma 1971) and the extensive peat and lake deposits penetrated by test bores and wells suggest that Lake Poukawa was once larger than the present lake. Judging from the terraces in the east of the basin mapped by Kingma (1971), the lake, and possibly the river draining the lake to the north, was capable of eroding the lake and river valley deposits when the gradient was steeper. To the west of the Poukawa Fault Zone, on the fault scarp between the railway line and SH 2 in the vicinity of Mahanga Road, there is an incised abandoned channel of the Poukawa Stream immediately south of Pekapeka Swamp. This change of course by the stream was a result of tectonic uplift about 12,000–15,000 years ago (Kelsey et al. 1993) and demonstrates that tectonic uplift would be a major influence on drainage. Pekapeka Swamp is a product of the low gradient of Poukawa Stream. In 1931, a drain was dug from Lake Poukawa to Poukawa Stream to increase drainage and maintain a lower lake level. Today, Lake Poukawa is drained via this man-made outlet to the northeast to Poukawa Stream and Pekepeka Swamp before joining the Awanui Stream and Karamu Stream on the Heretaunga Plains (Howorth et al. 1980). The level of the lake is controlled by a control gate structure on the outlet channel (Jellyman and Sykes 2009).

2.2.3 Hydrogeology

Dravid (1993) lists and plots 15 wells in the Poukawa Basin that have well logs suggesting that three aquifer systems are present to 108 m, the total depth of the deepest water well (well 1410 – screened in sandstone). Low-yielding and low-transmissivity aquifers are present in the Late Quaternary sediments and Pliocene–Pleistocene sediments that underlie the basin and outcrop on the hills surrounding the basin (Dravid 1993).

Groundwater in a shallow unconfined aquifer within the fluvial and lake sediments is the result of local rain and stream infiltration. The aquifer is in the depth range of 2–10 m and Lake Poukawa is basically a component of this aquifer, with the lake level corresponding to the water table (Figure 2.3). Near Te Mahanga Road, a low-yielding confined aquifer within the infilling Quaternary sediments is hosted in Late Quaternary fluvial and lacustrine sand and silty sand deposits below a depth of about 38.5 m, with groundwater pressure sufficient to produce a flowing artesian well. Artesian heads up to 9 m above ground level have been measured (Dravid 1993).

Dravid (1993) lists several wells in the northern area of the Poukawa Basin between Douglas Road and Pekapeka Swamp, with well logs showing groundwater derived from sandstone aquifers. This is the Pliocene–Pleistocene sandstone mapped by Kingma (1971) as overlying the limestone. Static water levels range from 7.6 m above ground level to 6.4 m below ground level. The synclinal structure of the Poukawa Basin suggests that this sandstone strata could also underlie the Quaternary sediments in the central part of the basin. Limestone aquifers may underlie the sandstone in the northern sector of the basin.

Groundwater wells located to the south of Douglas Road along the eastern margin of the Poukawa Basin encounter confined groundwater in aquifers associated with the limestone strata underlying Quaternary lacustrine and fluvial sediments. Static water levels are variable, with both flowing artesian wells and sub-artesian wells depending on site elevation. The synclinal structure of the Poukawa Basin suggests that the limestone strata and associated aquifers will underlie the Quaternary sediments over the whole basin. Hydrostatic pressure of the groundwater will be high because of the head imposed by groundwater recharge into the limestone strata on the adjacent hills. Fault dislocation of limestone strata might also affect groundwater pressure and aquifer distribution.

Six bores were drilled for research purposes during the Lake Poukawa Drilling Project (LPDP) from 1976 to 1984 and the Victoria University of Wellington paleoclimate study in 1996. Cameron and White (1999, 2001) assessed data from these test bores, combined with geological mapping, and suggested that the hydrogeology may be more complex than the three-aquifer system identified by Dravid (1993). Groundwater pressure and pockets of gas caused the dilution of drilling mud viscosity and infilling of the casing with heaving sand during the drilling of test bores LPDP 5 and 97-1. Fellows (1984) records problems with drilling LPDP 5 due to groundwater and gas pressure at 107 m, 144 m, 159 m and 214 m. Shulmeister et al. (1998) records problems at 38.5 m, 54.9 m, 75.1 m, 91.4 m, 106.0 m and 138.4 m. These variations in depth and location support the Dravid (1993) observation that aquifers within the fluvial and lake sediments “appear to be patchy with wide variation in static water levels”. Quaternary greywacke-derived gravel clasts of a paleo-Waipawa River channel may be present in the deepest part of the basin.

Cameron et al. (2011) presented a conceptual model of the Poukawa Basin to underpin groundwater flow model development to support consenting of groundwater abstraction from Brownrigg Agriculture (Figure 2.3). The conceptual model contains a low permeability zone at the margins of the shallow unconfined aquifer between Lake Poukawa and surrounding limestone hills. The presence of this zone was inferred in the groundwater flow model calibration to maintain observed heads in the limestone aquifer and baseflows in spring-fed streams that drain the limestone hills in the vicinity of Brownrigg Agriculture. The extent of this low-permeability zone may extend much closer to the lake than defined by Cameron et al. (2011) (Figure 2.3).

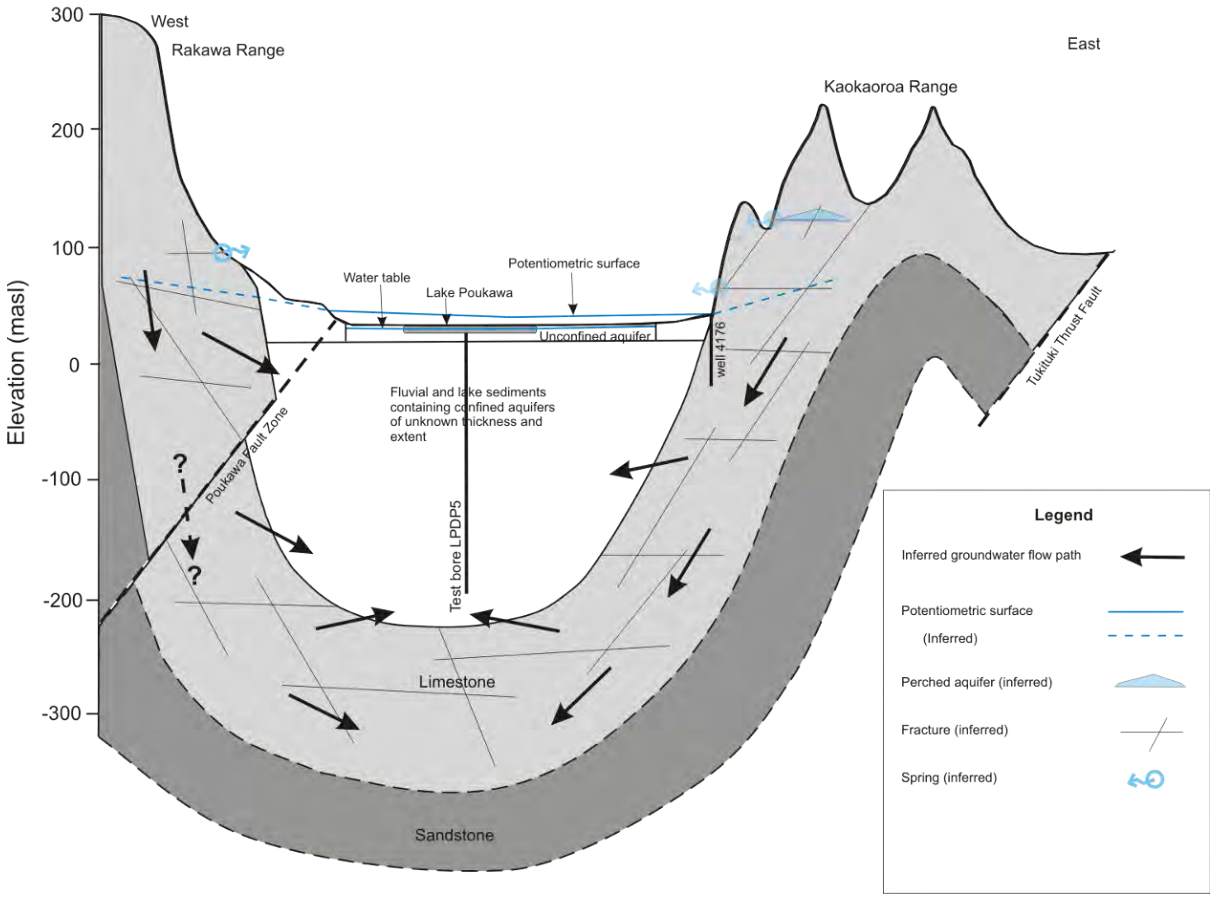

Figure 2.1 Schematic west-east hydrogeological cross-section through the central area of Poukawa Basin with vertical exaggeration. Figure from Cameron et al. (2011).

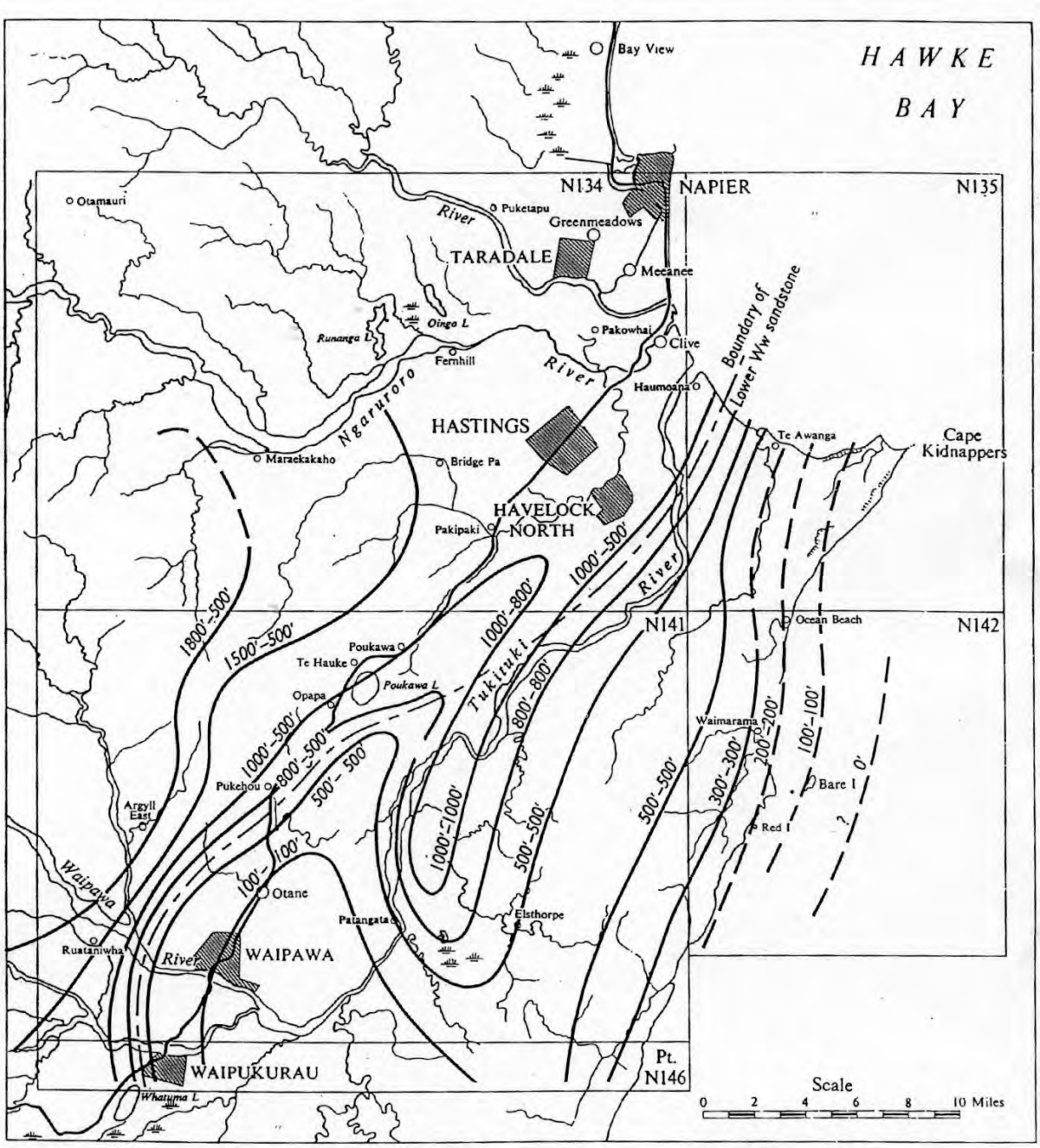

Figure 2.2 Isopach map of Waitotarian Stage and limestone in top part of sequence. The figures preceding the hyphen denote total thickness in feet; the second group of figures denotes thickness of the limestone in the top part of the sequence along that particular isopach. Figure from Kingma (1971).

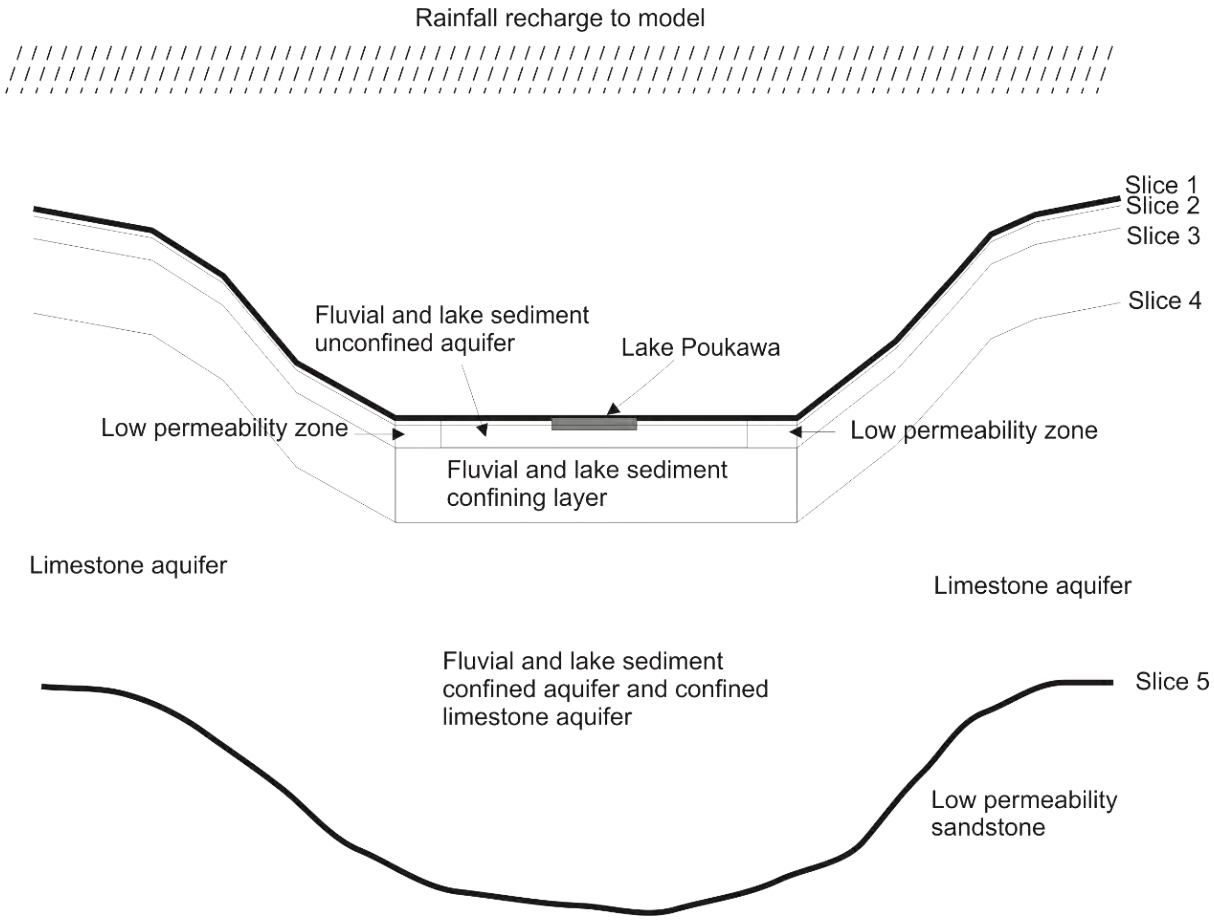

Figure 2.3 Conceptual hydrogeological model. Figure from Cameron et al. (2011).

2.3 Otane Basin

The geology and hydrogeology of the Otane Basin is less understood and documented than the Poukawa Basin.

2.3.1 Geology

'Basement' rock in the Otane Basin is the Whangai Formation and Waipawa Formation of the Tinui Group (Kingma 1971). These are Late Cretaceous to Paleocene alternating mudstone and sandstone, with the main rock type being mudstone. Late Pliocene Mangaheia Group marine sediments are exposed at ground surface along the Raukawa Ranges, Pukeora Hills and Mount Vernon and form the western and southern margins of the Otane Basin. These sediments are mostly sandstone, mudstone and minor shell lenses, with sandstone being the main rock type (Figure 1.4). Between Waipukurau and Otane, sediments from landslides, swamp deposits and old riverbeds form alluvial plains between the faulted hill country (Lee et al. 2011).

2.3.2 Hydrology, Soil and Land Use

The surface water systems of the Otane Basin comprise the Kaikora Stream, the Papanui Stream and their tributaries (Figure 2.4). The main soil type in the basin is silt loam, but it also has a large area of peat and peat loam soils located within the Otane Plains (Barber 2019). Pasture and forestry dominate the lowlands and hill country.

2.3.3 Hydrogeology

The groundwater system within Otane Basin is shallow (<100 m deep), typically unconfined and hydraulically connected to surface waters. Groundwater discharges as seeps and springs maintaining surface water baseflows (Barber 2019). Groundwater flow is believed to follow the topographic gradients of the catchment, travelling southwest to northeast along the old Waipawa River channel and converging at the confluence of the Papanui Stream and Tukituki River (Figure 2.4).

Young groundwater sourced from the Waipawa River enters the Papanui Stream midway along its course (Morgenstern and Gordon 2017). This contrasts with the presence of much older groundwater in the upper Papanui and the lower Kaikora catchments, in both the shallow and deeper aquifer layers. Upwelling of very old groundwater occurs within the low-lying area of the plains to the northeast, where water exits the basin to the Tukituki River. Rainfall that does not run off to streams percolates into the basin and contributes to groundwater recharge (Harper 2012; Morgenstern and Gordon 2017; Barber 2019).

Harper (2012) made the following observations from the distribution of groundwater wells and their bore logs:

- Groundwater is abstracted from most geological formations in the basin, as indicated by the presence of wells relative to geology (Figure 2.5).
- The most productive aquifer is the Quaternary gravel deposits of the Waipawa River and the Papanui Stream.
- Gravel alluvium is deepest at the southern end of the catchment, near the middle of the old Waipawa riverbed, where it is at least up to 50 m deep.
- Further north, along the Papanui Stream, alluvium is up to 30 m thick. Wells here are screened in both younger gravels and older mudstone or weathered limestone.
- In the middle of the catchment, along Drumpeel Road, the aquifer system pinches out or grades into Quaternary swamp deposits.
- Less productive aquifers are found within limestones from the Mangaheia Group located in the north of the catchment.

Aquifer test data in the area indicate that the Quaternary aquifer system beneath the old Waipawa riverbed and Papanui Stream (gravel-dominated in well lithology) includes semi-confined conditions and transmissivity values between 502 and 11,129 m^2/day (Harper 2012). Toward the west, along Drumpeel Road and near Otane, aquifer test data indicate that groundwater resources are generally less transmissive and more confined. This is consistent with well lithology, which shows thick layers of silt, clay and mud (Harper 2012).

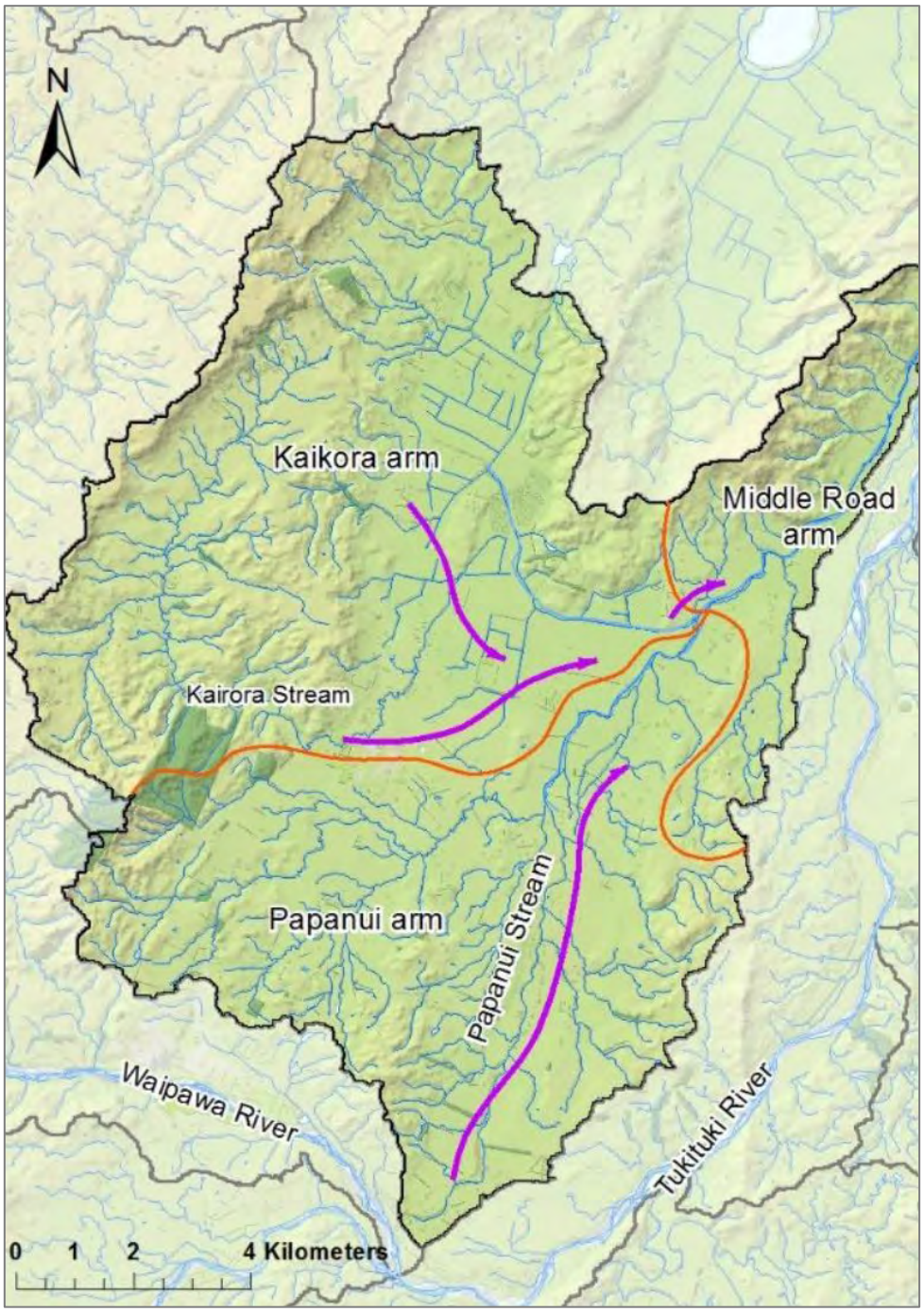

Figure 2.4 The Papanui catchment water bodies, comprising the Kaikora Stream, Papanui Stream and their tributaries. The catchment has been divided into three arms (orange lines): Kaikora, Papanui and Middle Road. The overall groundwater flow direction (pink lines) is north-east towards the confluence with the Tukituki River. Figure from Barber (2019).

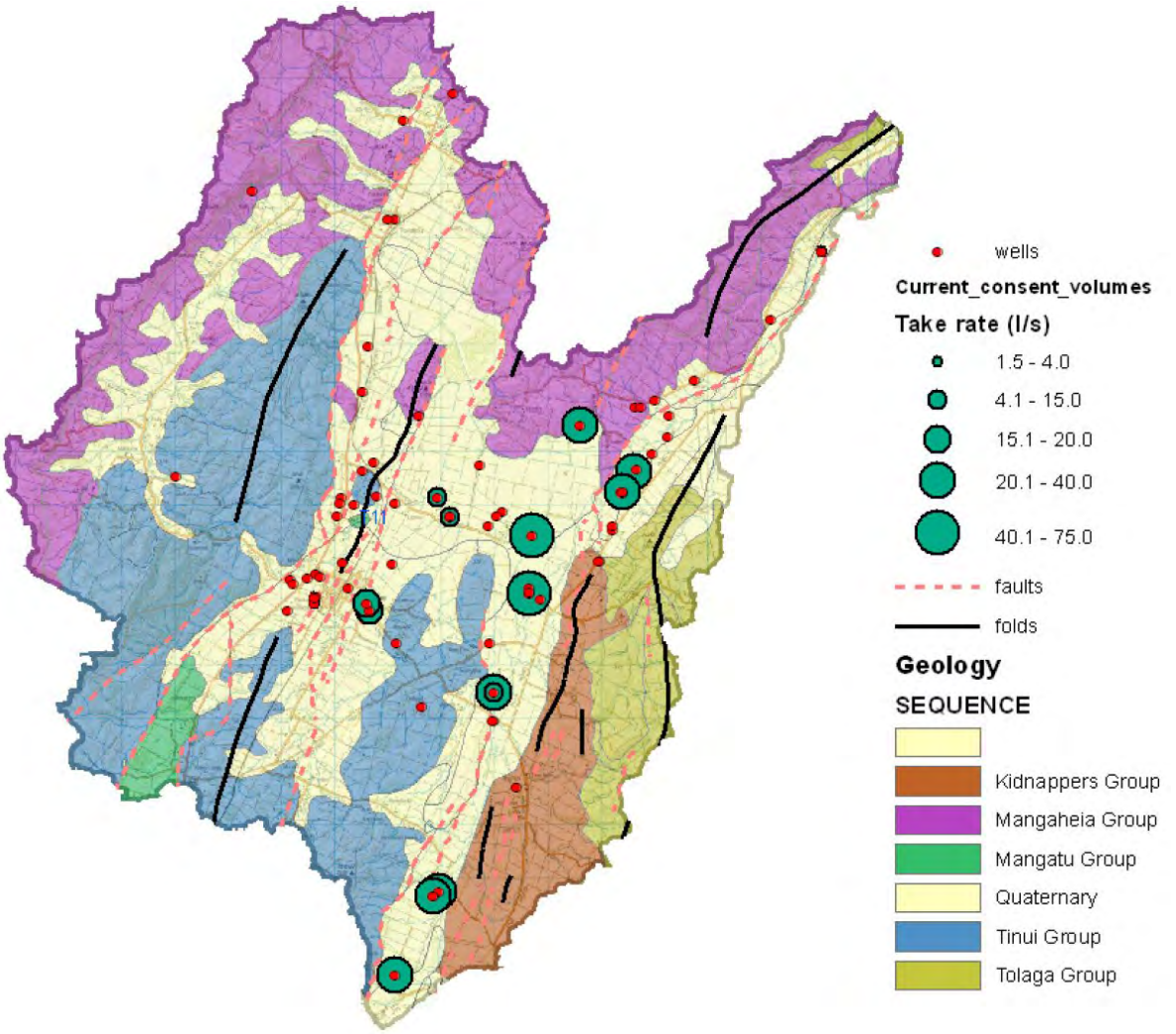

Figure 2.5 Location of wells and relative magnitude of groundwater consented-take rates. Figure from Harper (2012).

3.0 METHOD

The resistivity models consist of a large amount of data: 925,715 data points in each resistivity model. It is beyond the scope of this work to inspect small volumes of data at the local scale. Here, we assess the entire volume of data at the catchment scale, which necessitates a methodology that can handle the inspection of a large amount of data.

To manage the inspection of this large amount of data, as well as the relatively sparse supporting datasets, a combined approach of manual and automated methods for interpretation was utilised, including:

- Automated and manual assessments of resistivity data values against datasets relevant to hydrogeology (see Appendix 1).
- Manual delineation of major hydrogeological boundaries using GeoScene3D software (see Section 3.1).
- Development of 3D models for online visualisation, including automated and manual refinement to assess fine-scale variations (see Section 3.2).
- Development of 2D maps of near-surface properties (see Section 3.3).

3.1 Manual Delineation of Major Hydrogeological Boundaries

SkyTEM (resistivity models), topography (Digital Elevation Model [DEM]), and borehole and surface geological (QMAP) data (Figure 3.1) were utilised to identify and map different hydrogeological units within the near subsurface (up to ~500 m) of relevance to groundwater.

The SkyTEM survey reveals a detailed 3D resistivity model of the subsurface (Rawlinson et al. 2021). The DEM has a resolution of 10 m. This was developed by down-sampling a 5 m DEM provided by HBRC, who combined LiDAR and SRTM V2 (Shuttle Radar Topography Mission) data (Farrier 2020). There were >200 boreholes with lithological log data distributed over the study area. Borehole data (Harper 2019) and QMAP (Heron 2020) provided lithological and geological information that was used to assess the surrounding resistivity models from the SkyTEM data.

GeoScene3D software was used to integrate all of the input data and interpret the resistivity data manually. Manual interpretation was selected for the following reasons:

1. There are sparse supporting datasets with limited spatial coverage.
2. As discussed in Section 4.1 and Appendix 1, the resistivity values overlap for different lithological units.
3. There is lateral variation of resistivity within different lithologies and geological units.
4. There are finer scale variations of resistivity within the broader hydrogeological units.

Cross-sections were viewed along flight lines, upon which resistivity models were displayed alongside the DEM and lithological log information from boreholes. A maximum distance of 200 m was applied for the projection of boreholes onto the cross-sections. Resistivity models were displayed with a range of 0–200 ohm.m to highlight the resistivity contrasts identified on preliminary inspections of the data.

Based on the objectives of this study (Section 1.1) and initial assessments of the resistivity values and contrasts (Appendix 1) visualised within Geoscene3D cross-sections, a simplified hydrogeological framework was developed that consists of the following hydrogeological units (Figure 3.2):

1. Swamp and fan deposits (Swamp and Fan HU).
2. Riverbed deposits (Riverbed HU).
3. Limestone (Limestone HU).
4. Hydrogeological basement (Basement HU; Whangai and Waipawa formations).

To delineate these hydrogeological units, three boundaries were manually delineated (Figure 3.2):

1. Riverbed HU base.
2. Limestone HU top.
3. Limestone HU base.

Boundary delineation within Geoscene3D software was undertaken as follows:

- Seed points (manually placed interpretation points) were interpreted in the cross-sections where sharp resistivity contrasts were observed (Figures 3.2 and 3.3).
- Seed points were gridded with a node spacing of 200 m to create 3D boundaries (hydrogeological boundaries) using a 2D inverse distance weighting interpolation function with a 500 m search radius in the x and y directions and a 50 m search radius in the z direction.
- The 3D boundaries were reviewed, and additional seed points added where needed, to ensure boundary consistency with information such as structural geology, surface geology (Heron 2020) and borehole lithology (particularly in areas with gaps in the resistivity data, or shallow DOIs).
- The three gridded surfaces defining the hydrogeological boundaries (Riverbed HU base, Limestone HU top, Limestone HU base) were exported from Geoscene3D (Section 4.2), re-sampled to 10 m grids using bi-linear interpolation within ArcGIS and then exported as ascii files.

The smooth resistivity model was primarily used for boundary mapping. The sharp resistivity model was used as a supporting reference and to assist with mapping of the hydrogeological boundaries with greater certainty, particularly in areas of increased ambiguity (e.g. Figure 3.4). Resistivity contrasts were analysed along with the borehole lithology, QMAP surface geology and mapped faults to understand their relationship with any hydrogeological boundaries. In structurally complex areas (e.g. close to faults) and in areas where resistivity data is poor (has a shallow DOI) or missing, QMAP geology, borehole lithology and DEM data provided regional geological and structural information to enable boundary delineation. In general, the uncertainty in boundary interpretation is higher in structurally complex areas (close to the faults) and close to the hills. Uncertainty also increases with distance from seed points due to boundary interpolation uncertainties.

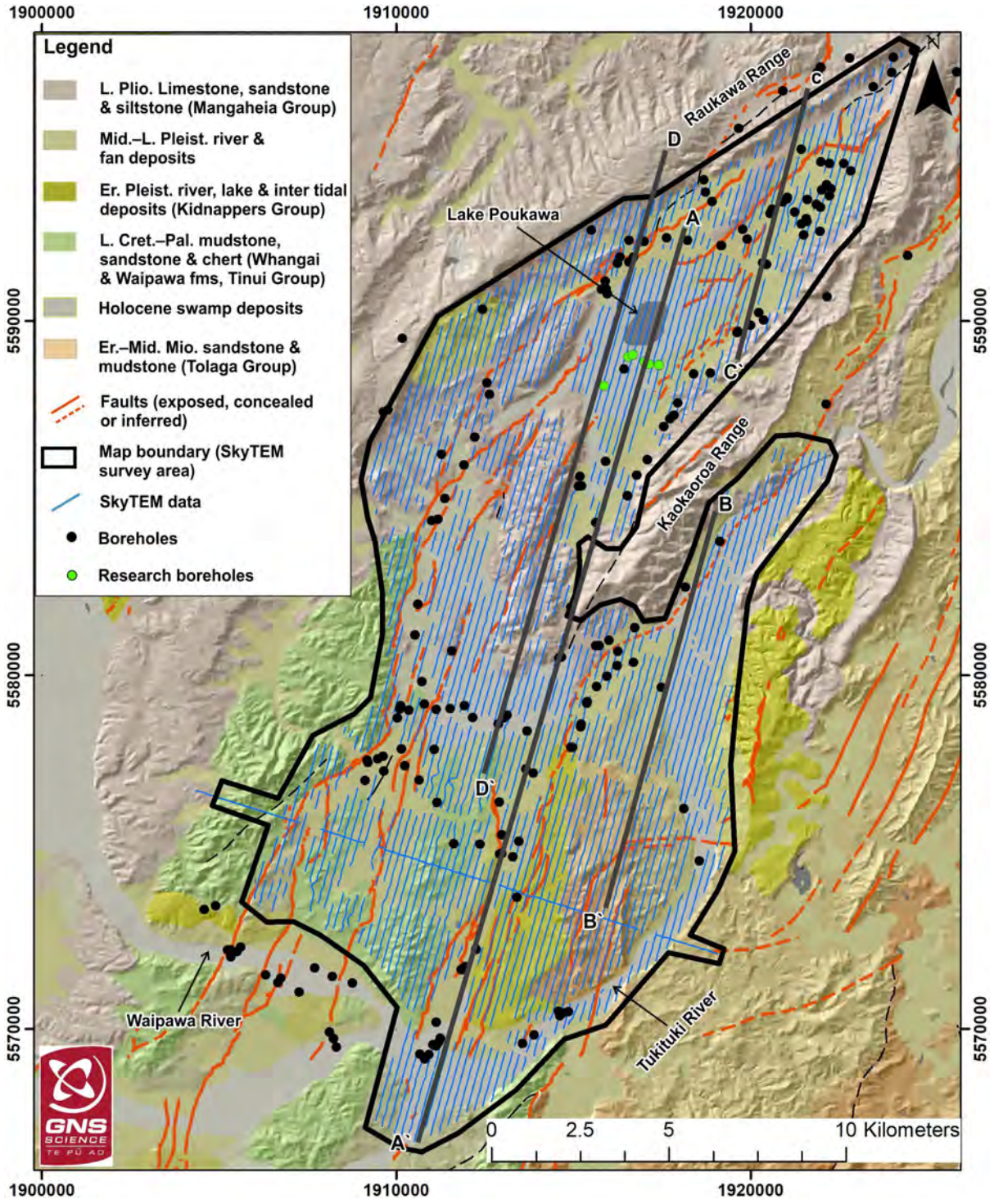

Figure 3.1 Surface geological map (QMAP) draped over a digital elevation model, showing coverage of SkyTEM data, locations of boreholes and research wells. Resistivity profiles along A–A`, B–B`, C–C` and D–D` are shown in Figures 3.2, 3.4, 5.1 and 5.2, respectively. Abbreviations: L. Plio. = Late Pliocene, Mid.-L. Pleist. = Mid to Late Pleistocene, Er. Pleist. = Early Pleistocene, L. Cret.-Pal. = Late Cretaceous to Paleocene, Er.-Mid. Mio. = Early to Mid-Miocene.

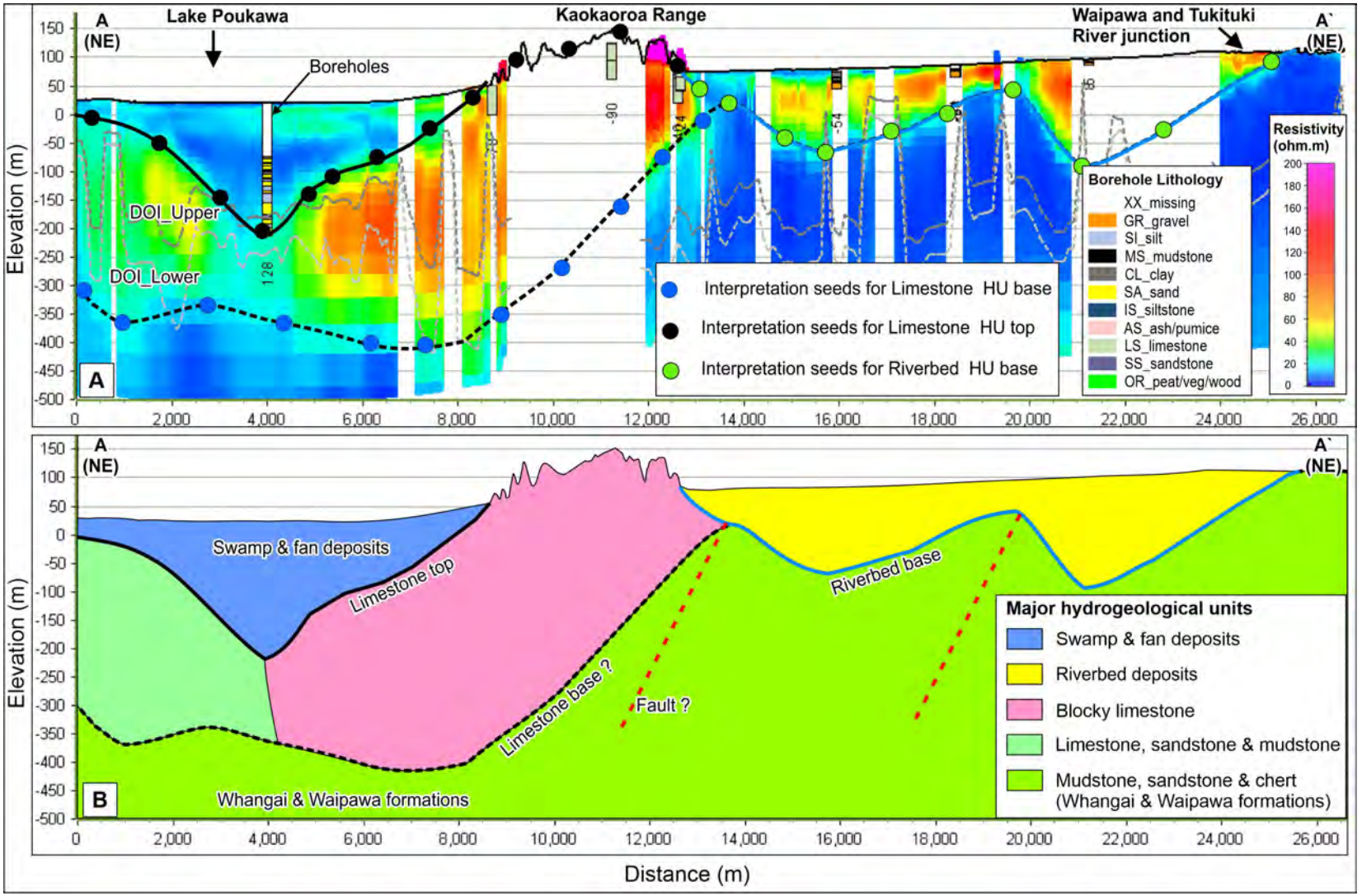

Figure 3.2 (A) An example showing an uninterpreted N–S resistivity profile (A–A`; see location in Figure 3.1) across the study area. DOI Lower and DOI Upper are shown as grey dashed lines on the resistivity data. Projection distance of wells are shown below the wells. (B) Interpreted profile with major hydrogeological boundaries. Borehole data and QMAP surface geology provide calibration for the major hydrogeological units.

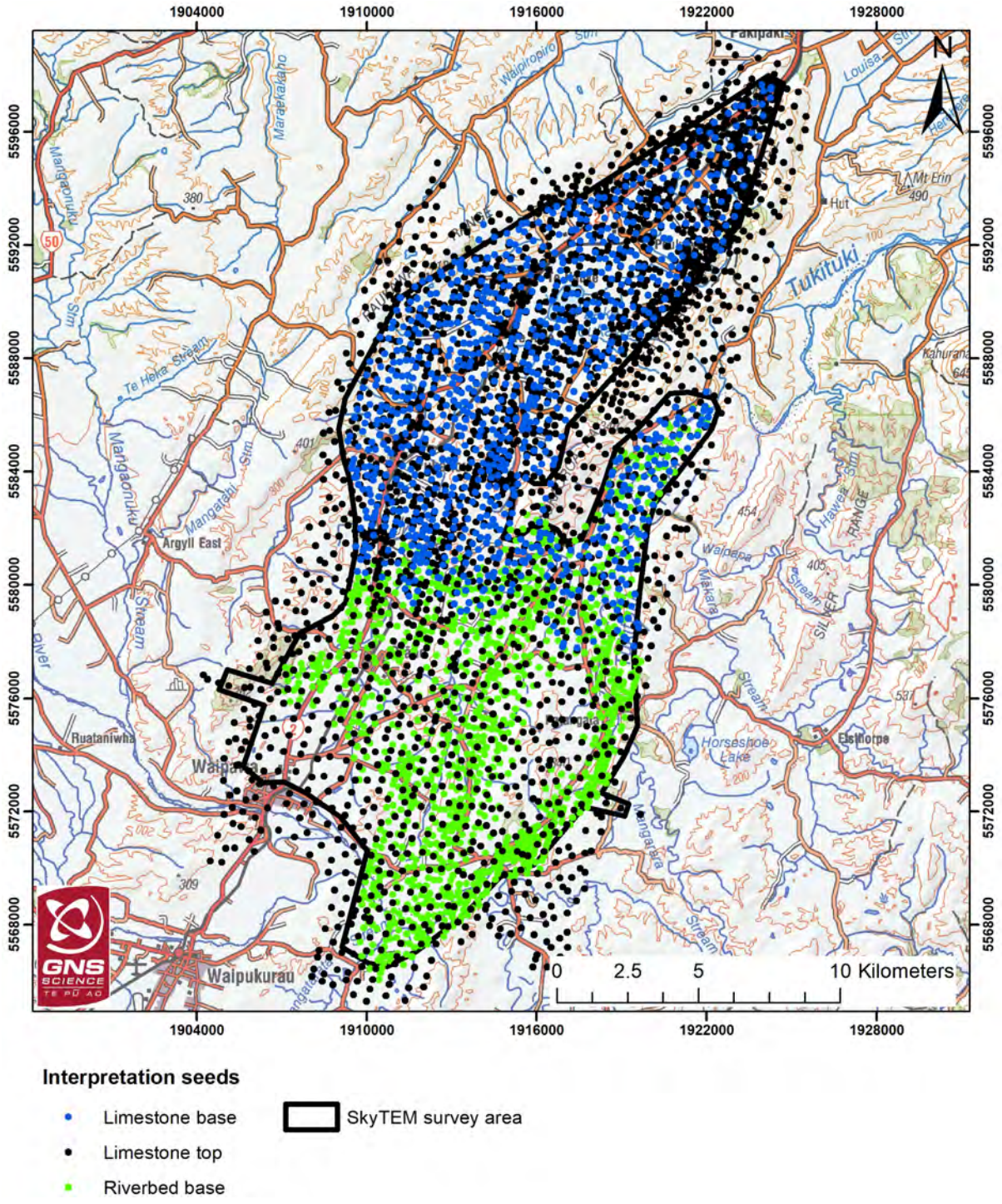

Figure 3.3 Distribution of interpretation seed points for the Limestone HU base, Limestone HU top and Riverbed HU base. Note that seed points for Limestone HU top were placed over the entire survey area in order to ensure boundary consistency with structural geology and lithological information.

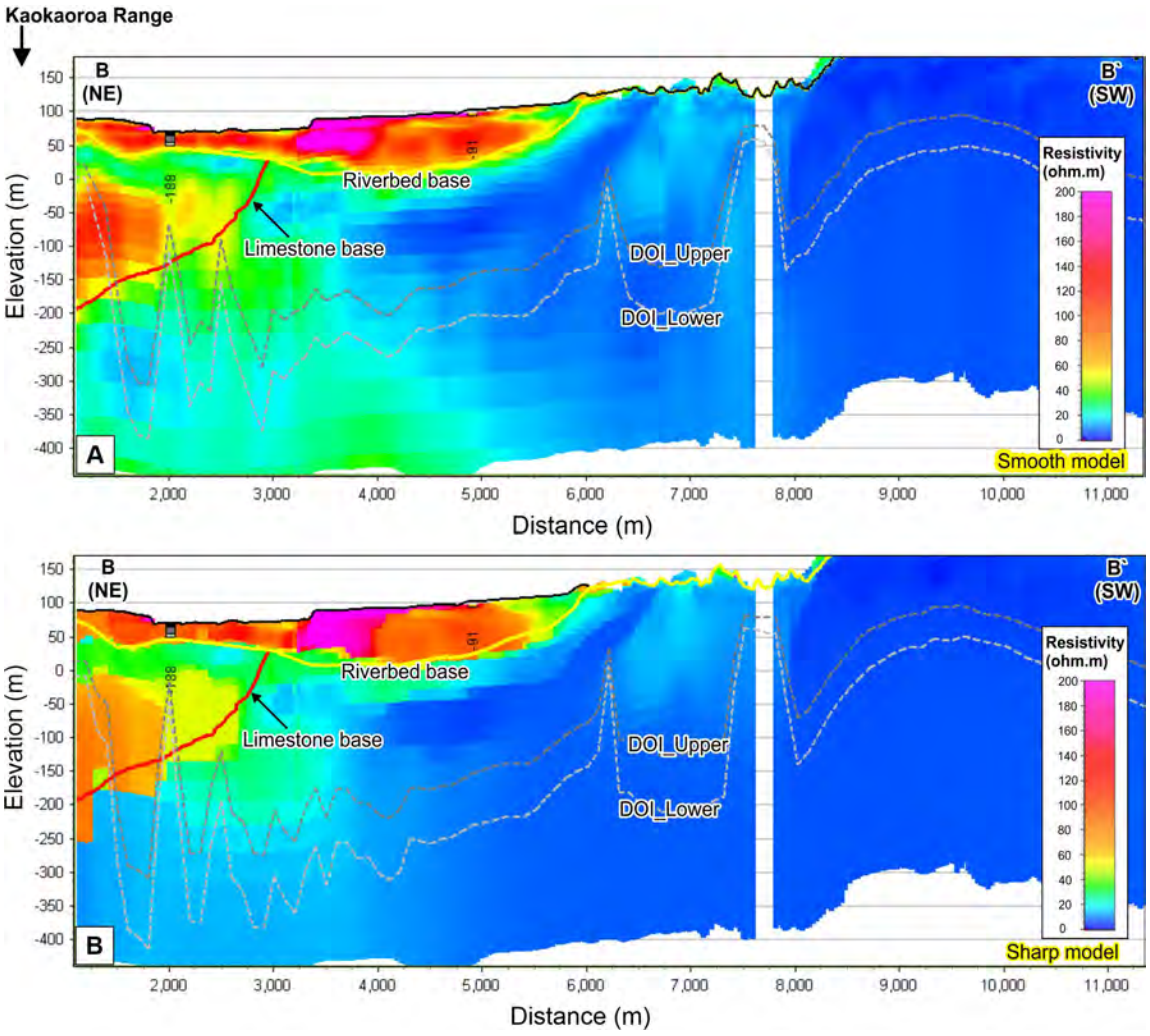

Figure 3.4 (A) An example of a smooth model resistivity profile (B–B`; see location in Figure 3.1) showing similarity of resistivity values (yellow to red colour in the left-hand side of the figure) of riverbeds and the underlying limestone. (B) Sharp resistivity model along the same B–B` profile. Note that both smooth and sharp resistivity models show similar resistivity profiles. However, some of the boundaries are clearer in the sharp model.

3.2 3D-Gridded Model Development

In this section, 3D models suitable for online visualisation were developed. A Poukawa model area was defined to more tightly enclose the SkyTEM-derived 1D resistivity models than the previous survey area polygon (Figure 3.5).

The resistivity model datasets developed by Rawlinson et al. (2021) are 1D models at SkyTEM data locations (Figure 1.2). These datasets are essentially point datasets that include gaps where electromagnetic noise was removed and where the helicopter was unable to fly due to flight-path restrictions. These datasets were interpolated to a 3D grid with horizontal cell resolution of 50 m (Figure 3.5) and vertical resolution of 2 m.

Due to the limited availability of supporting data such as lithological logs, initial testing determined that primarily data-driven methods such as spatially varying geostatistical or machine-learning methodologies were not suitable to be applied, as these methods rely on a sufficiency of high-quality data. As such, a simpler categorical threshold approach was taken. The assessments made within Section 3.1 and Appendix 1 were used to provide first estimates of thresholds. These thresholds and resultant categories were then revised through manual assessments against lithological logs within Leapfrog 3D modelling and visualisation software.

Initial testing utilised both the smooth and sharp resistivity models, but, after a comparative analysis, it was determined that the smooth resistivity model provided finer-detailed discrimination of both near-surface sediments, as well as more permeable angular structures such as potential faulting within the limestone, while the sharp resistivity model provided more guidance on larger structural changes (e.g. Section 1.2). As such, only the smooth resistivity model was utilised for the further analysis below.

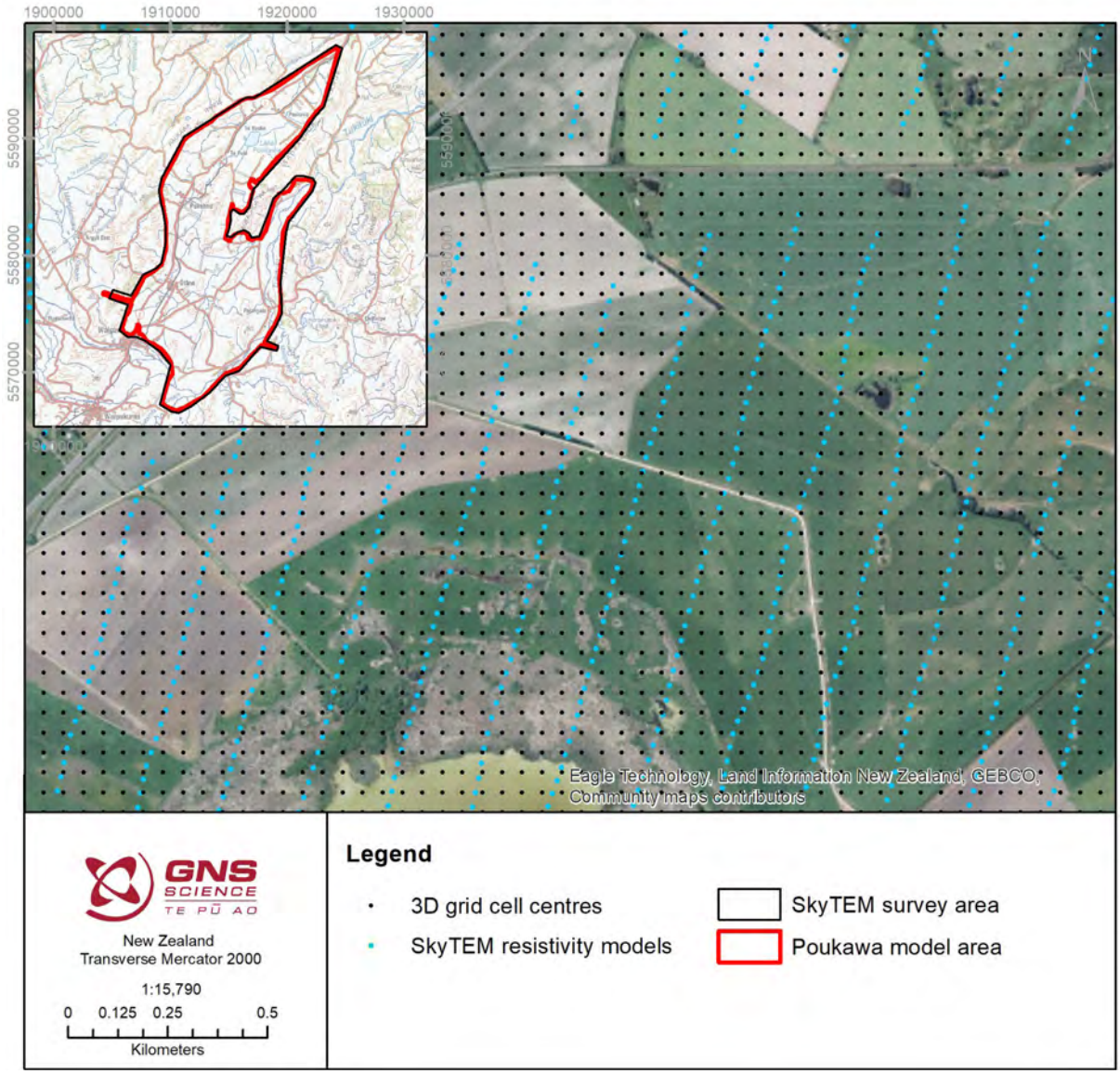

Figure 3.5 Small section of the Poukawa model area showing the difference between the original SkyTEM resistivity model locations along flight lines and the 3D uniformly gridded model locations (50 m horizontal resolution). Also shown is the minor difference between the SkyTEM survey area and the Poukawa model area.

3.2.1 Interpolated Resistivity (res) Model

To develop a more continuous 3D dataset, interpolation of the resistivity values to a uniform 3D grid was undertaken using Geoscene3D[1] software. The smooth resistivity model was chosen for this combination, as it provides finer detail than the sharp model.[2]

These data were imported into Geoscene3D as 1D geophysics models in the *.gdb* database format (*Poukawa_smooth_resistivitymodel_V1_2020.gdb*; Rawlinson et al. 2021). Kriging was selected as appropriate for interpolation, as it provides a corresponding 3D grid with an interpolation uncertainty estimate (the kriging variance), which could be utilised within subsequent applications such as numerical groundwater modelling.

A uniform 3D grid was defined with 50 x 50 m horizontal resolution and 2 m vertical resolution (cell thickness), matching the extents of the resistivity data (Table 3.1). The large memory footprint of the dataset prevented generation of a finer-resolution 3D grid at this full extent.

Geoscene3D software uses the GSLIB kriging library. Interpolation was undertaken on the $\log_{10}$-transformed resistivity data. A number of tests were performed on various smaller selections of data to check for the most appropriate kriging variables. Point Kriging was undertaken using a spherical function, sill of 0.1 and range of 2000 m. A 500 m horizontal search radius, 25 m vertical search radius and maximum of six data points in each octant were used. The horizontal and vertical search radii used impact the final coverage of the dataset.

Once interpolation was completed, null values were assigned to grid nodes outside the Poukawa model area and above the DEM (10 m resolution). The gridded resistivity model was exported as a *.csv* file, which consists of resistivity values mapped to cell nodes *X*, *Y*, *Z* and *res*. The kriging variance gridded model was similarly exported to a *.csv* file, including the following: *X*, *Y*, *Z*, *resvar*.

Table 3.1 Three-dimensional grid generated in Geoscene3D software (data mapped to cell nodes).

Corner Node Coordinates	Minimum	Maximum	Node Count	Width (m)	Node Spacing (m)
X	1904100	1924550	410	20,450	50
Y	5566400	5598000	633	31,600	50
Z	-508	332	421	840	2

3.2.2 Major Hydrogeological Unit (HU) Model

The manually delineated major hydrogeological unit (HU) surfaces from Section 3.1 were imported into Geoscene3D. To create a matching grid to the resistivity grid in Section 3.2.1, the ‘Single Floating Point Type’ 3D grid created in that section was adjusted to a ‘Word Discrete

1 https://geoscene3d.com

2 A smooth model is a many-layered model that uses a fixed layer structure (logarithmically increasing layer thicknesses), and the resistivity of each layer is solved for. The smooth regularisation scheme penalises the resistivity changes, resulting in the smoothest resistivity transitions both vertically and horizontally. A sharp model uses the same model discretisation as the smooth model, but the model regularisation scheme is different. The sharp model regularisation scheme penalises the number of resistivity changes above a certain size, instead of the absolute resistivity changes (as in the smooth model regularisation scheme). The sharp model regularisation scheme therefore results in a model with few, but relatively sharp, resistivity transitions. This allows for relative abrupt changes in resistivities while using the fixed-layer thicknesses of the smooth model (e.g. Rawlinson et al. 2021).

Value' type grid using the 'Convert Grid Value Type' in the Toolbox in Geoscene3D software, and four material categories were defined: HU1, HU2, HU3, HU4 (see Table 3.2). Geoscene3D stores information at cell node locations.

Hydrogeological units were assigned to the 3D grid (Table 3.2) using the manually delineated surfaces (Section 3.1) via the following steps:

- Assign null to all nodes.
- Assign HU3 to all nodes below Limestone HU top surface.
- Assign HU4 to all nodes below Limestone HU bottom surface.
- Assign HU1 to all nodes above Limestone HU top surface.
- Assign HU2 to all nodes above Riverbed HU bottom surface.
- Assign null to all nodes above the DEM.
- Assign null to all nodes outside the Poukawa model boundary.

After the completion of the draft version of this report, it was determined that a separation between unconsolidated and consolidated sediments would be valuable for online 3D model visualisation purposes and for simplifying aquifer potential classification (see Section 3.2.4). To achieve this, as well as some other refinements, manual adjustments were made to the model grid using Geoscene3D software's 'Profile Polygon' grid editor tool (see Table 3.2), threshold resistivity values and QMAP polygon boundaries. See Section 7 for further discussion on this.

The gridded HU model was exported as a *.csv* file where values are mapped to cell nodes *X*, *Y*, *Z* and *HU*. The exported hydrogeological unit and resistivity 3D grid files were combined into a single dataset (combined dataset), and, to assist with later calculations, the elevation (*Z*) of the top model cell mapped with HU values was also determined (*top_elev_HU*). The dataset now has the columns *X*, *Y*, *Z*, *top_elev_HU*, *res*, *resvar* and *HU*. Because the HU model utilised a continuous surface throughout the entire model area, some locations that have gaps in the *res* model have values for the HU model (Table 3.2).

Table 3.2 Definition of the hydrogeological unit (HU) model.

Hydrogeological Unit	HU Model	Description
HU1	1	Swamp and Fan HU, with manual adjustments to remove main consolidated areas and fan area in the Otane Basin.
HU2	2	Riverbed HU, with manual adjustments to add fan area in the Otane Basin and refine shallow riverbeds.
HU3	3	Limestone HU, with manual adjustments to add main consolidated area from the Swamp and Fan HU.
HU4	4	Basement HU, with manual adjustments to refine shallow riverbeds.

3.2.3 Resistivity Facies (facies) Model

As significant changes within resistivity are best assessed on a logarithmic scale, resistivity facies were defined by separating the *res* model into 12 resistivity facies classes (facies) uniformly separated on a log scale (Table 3.3; e.g. Minsley et al. 2021). These facies classes group materials that are expected to have similar hydrologic and geologic properties, based on their resistivity, to assist with easier discrimination of significant variability and similarity.

Log_{10}-transformed *res* model values were classified into uniform bins with a width of 0.15 between 1.05 and 2.55 (Table 3.3). These values were chosen based on detailed assessments of resistivity values against relevant datasets, such as lithological logs (see Appendix 1).

Resistivity values in the *res* column (interpolated resistivity model from Section 3.2.1) were converted to resistivity facies classes using the combined dataset, which now has columns *X*, *Y*, *Z*, *top_elev_HU*, *res*, *resvar*, *HU* and *facies*.

Table 3.3 Resistivity facies (facies) model definition, using resistivity values within the *res* model.

Facies	Lower-Bound Log_{10}(res)	Upper-Bound Log_{10}(res)	Lower-Bound *res* Model (ohm.m)	Upper-Bound *res* Model (ohm.m)
1	NA	1.05	NA	11
2	1.05	1.20	11	16
3	1.20	1.35	16	22
4	1.35	1.50	22	32
5	1.50	1.65	32	45
6	1.65	1.80	45	63
7	1.80	1.95	63	89
8	1.95	2.10	89	126
9	2.10	2.25	126	178
10	2.25	2.40	178	251
11	2.40	2.55	251	355
12	2.55	N/A	355	N/A

3.2.4 Aquifer Potential (AP) Model

An Aquifer Potential (AP) model was developed to separate the *facies* model into consolidated and unconsolidated sediments, while providing an indicator of the likelihood of each model cell to host aquifer-bearing material. AP classes were defined by establishing rules within the major hydrogeological units as to how each resistivity facies class maps to aquifer potential. The naming ‘aquifer potential’ refers to the likelihood that a particular cell may host aquifer-bearing material. A high AP class corresponds to a higher aquifer potential.

The primary mapping of facies to aquifer potential was undertaken by first defining resistivity thresholds upon which low, medium and high aquifer potential were defined. This separates the dataset into a simplified text category with six classes ‘aq’, mapping values to consolidated low, medium and high aquifer potential and unconsolidated low, medium and high aquifer potential (Table 3.4). Threshold values were chosen based on detailed assessments of resistivity data against relevant datasets, such as lithological logs and QMAP main rock type (see Appendix 1), as well as further manual inspections of the 3D gridded models (*res* and *HU*) against lithological logs, screen locations and consent locations using Leapfrog software.

AP classes 1–24 were defined using the combined columns *facies* and *HU*, summarised in Table 3.4. Further details are provided in Sections 3.2.4.1 and 3.2.4.2. This calculation was made on the combined dataset, which now has columns *X*, *Y*, *Z*, *top_elev_HU*, *res*, *resvar*, *HU*, *facies, AP* and *aq*.

Table 3.4 Aquifer Potential (AP) model definition, which uses the defined resistivity facies (*facies*) classes from Table 3.3 and the major hydrogeological unit (*HU*) classes from Table 3.2. Also defined is a simplified aquifer potential model with only six classes 'aq' and 'aq name'.

AP	HU	Facies	aq	aq Name	Lower-Bound Resistivity (ohm.m)	Upper-Bound Resistivity (ohm.m)
1	4	1–12	cl	Consolidated-low	N/A	N/A
2	3	1	cl	Consolidated-low	N/A	11
3	3	2	cl	Consolidated-low	11	16
4	3	3	cl	Consolidated-low	16	22
5	3	12	cl	Consolidated-low	355	N/A
6	3	11	cl	Consolidated-low	251	355
7	3	10	cl	Consolidated-low	178	251
8	3	9	cl	Consolidated-low	126	178
9	3	4	cm	Consolidated-med	22	32
10	3	5	cm	Consolidated-med	32	45
11	3	6	ch	Consolidated-high	45	63
12	3	7	ch	Consolidated-high	63	89
13	3	8	ch	Consolidated-high	89	126
14	1, 2	1	ul	Unconsolidated-low	N/A	11
15	1, 2	2	ul	Unconsolidated-low	11	16
16	1, 2	3	um	Unconsolidated-med	16	22
17	1, 2	4	um	Unconsolidated-med	22	32
18	1, 2	5	uh	Unconsolidated-high	32	45
19	1, 2	6	uh	Unconsolidated-high	45	63
20	1, 2	7	uh	Unconsolidated-high	63	89
21	1, 2	8	uh	Unconsolidated-high	89	126
22	1, 2	9	uh	Unconsolidated-high	126	178
23	1, 2	10	uh	Unconsolidated-high	178	251
24*	1, 2	11	uh	Unconsolidated-high	251	355

* Unconsolidated sediments in this area have maximum values of <300 ohm.m and therefore have no values in the facies 12 class.

3.2.4.1 Consolidated Sediments

Consolidated sediments in the area are primarily present within HU3 and HU4.

Basement (HU4) in the area was simply set to the lowest aquifer potential, AP = 1. This simplification was due to the resistivity model being gridded below the resistivity data standard DOI, resulting in some higher resistivity values at depth that are not true resistivity values. See Section 4.2.3 for further discussion about basement interpretation below the standard DOI in this study area.

The primarily limestone unit (HU3) is expected to vary based on changes from a more massive limestone to a more sandstone- and mudstone-dominated limestone. Additionally, weathering and fracturing is expected to impact resistivity. Limestone is assumed to have a mostly linear relationship with resistivity, with more massive (consolidated) limestone having higher resistivity and more permeable limestone having lower resistivity (Figure 1.3). However, there is a complication in that lower resistivity corresponds to less consolidated and/or more silt, while higher resistivity corresponds to more consolidated and/or less silt, as well as to outcropping limestone. Due to this relationship, three threshold values were required – two threshold values for splitting into medium and high potential and an additional threshold at a high resistivity value for splitting into low potential again.

Mudstone/siltstone corresponds to low permeability and low resistivity in the area (<22 ohm.m; e.g. Table 4.1). Sandstone corresponds to medium permeability and medium resistivity in the area (<45 ohm.m; e.g. Table 4.1). Appendix 1 utilised an assessment range of 100 m from datasets. Due to the limited available data, this enabled more data to be assessed; however, it also introduces more variability and error into the assessment. An initial assessment using only a range of 50 m found that screened, consented and water-bearing limestone had a maximum value of 165 ohm.m (with the highest range corresponding to a borehole with a ~50 m open-hole interval). When this assessment was increased to 100 m, the maximum value was found to be 308 ohm.m (also related to the borehole with the ~50 m open-hole interval). As this value was greater than expected, an additional manual assessment of lithological logs, screened intervals and consented intervals against the *res* model in Leapfrog software was undertaken. This assessment demonstrated that the limestone bores were particularly susceptible to errors introduced by larger assessment radii, due to their presence within areas of rapidly varying high topographic relief, and high resistivity values found in the near-surface in these locations (outcropping/weathered limestone) immediately above water-bearing intervals. This assessment confirmed that resistivity values greater than 126 ohm.m corresponded to outcropping limestone and only minimal amounts corresponded to the top of a few large open-hole intervals. This assessment also confirmed, as per Table 4.1, that water-bearing limestone intervals largely corresponded to >45 ohm.m.

Thresholds for splitting into low, medium and high aquifer potential were defined at values of 22 and 45 ohm.m, and then an upper threshold of 126 ohm.m was selected above which limestone becomes too tight and aquifer potential drops. Therefore, for HU3, facies classes 1–3 and 9–12 are defined as low aquifer potential, classes 4–5 are defined as medium aquifer potential and classes 6–8 are classified as high aquifer potential. These were mapped to the aquifer potential numbers 2–12 (Table 3.4).

3.2.4.2 Unconsolidated Sediments

Unconsolidated sediments in the area are primarily present within HU1 and HU2.

Riverbed deposits (HU2) are expected to vary between fine-grained clay and silt aquitard material to coarser-grained gravel material, as well different mixtures of these materials. In Appendix 1 (e.g. Table 4.1), the following values were assessed: clay, 6.8–29.3 ohm.m; sand, 12.7–136.6 ohm.m; and gravel, 11.4–166.5 ohm.m. Water-bearing gravel had values >16 ohm.m, with consented takes in gravel having values >32 ohm.m (Table 4.1). Consented takes in sand had values 27–28 ohm.m. Therefore, HU2 appears to exhibit the linear relationship between resistivity and permeability expected within a fluvial depositional environment, where both properties are primarily driven by clay content – less clay content correlates with both higher resistivity values and higher permeability.

Poukawa swamp deposits (HU1 – central Poukawa basin area) are expected to vary between fine-grained clay, silt and peat material, and cleaner sands, as well different mixtures of these materials – predominantly silty sand and sandy silt. Very thin gravel layers are present. Resistivity values in this area tend to be low, predominantly <22 ohm.m. The only information on the Poukawa swamp deposits is from research drilling, and the central basin material does not appear to be utilised for groundwater supplies. Numerous documented areas of drilling issues due to groundwater/gas pressures and 'heaving sand' during the research bore drilling suggest that the sands in this location have poor aquifer potential. During drilling as part of 3DAMP in the Ruataniwha Plains, 'heaving sands' were found to not be suitable aquifers and to have very low hydraulic conductivity of 0.011 m/day (Lawrence et al. 2022a; 2022b).

The previous conceptual model in Poukawa (e.g. Section 2.2.3) was based on bores in the northern part (near Te Mahanga Road).

In the east, west and northern areas of Poukawa (HU1), the lithological logs show complex thin units of limestone, shell, sand, peat, sandstone and siltstone mixed with silt and clay. It is difficult to tell from the available lithological log information whether these units are consolidated or unconsolidated. It is assumed that some of these logged units are unconsolidated derived material from the surrounding limestone and sandstone ranges. Potential inclusion of consolidated sandstone and thin limestone and shell material, as well as sparse information, complicates interpretation, and high uncertainty remains in these areas. Resistivity values in this area tend to be low, predominantly <22 ohm.m, supporting the previous assessment of this area as containing low-yielding and low-transmissivity aquifers (Dravid 1993; Section 2.2.3). However, from manual and automated assessments of values, a linear relationship between resistivity and permeability still appears to be valid.

For both HU1 and HU2, unconsolidated medium and high aquifer potential thresholds were set at 16 and 32 ohm.m, respectively, which coincide with the facies upper boundaries of classes 2 and 4. Therefore, for unconsolidated sediments, facies classes 1–2 are defined as low aquifer potential, classes 3–4 are defined as medium aquifer potential and classes 5–11 are classified as high aquifer potential (as unconsolidated sediments in this area have maximum values of <300 ohm.m, no values are present in the facies 12 class). Note that, due to the relatively low aquifer potential in this area, the concepts of 'medium' and 'high' are relative to this study area. Due to the linear relationship observed, aquifer potential in the unconsolidated sediments is expected to gradually increase as the facies classes increase in value. To develop unique aquifer potential classes, these 11 facies classes within unconsolidated sediments (HU1 and HU2) were mapped to the aquifer potential numbers 14–24 (Table 3.4).

3.2.5 Data Formats

The 3D model datasets were combined within a point *.csv* file, with x,y,z defining the centre of each grid cell. Attribute columns relate to each of the different 3D models. This format was developed for serving the data on an online webmap. The format provides quick access to all datasets for cross-section and virtual borehole visualisations, as all datasets reference the same x,y,z locations. Additionally, a selection of the 3D models was exported to individual *x,y,z,value .csv* files to enable 3D visualisation as individual block models within a Leapfrog viewer file.

A selection of the 3D models was also converted into multi-band raster files, enabling further accessibility, such as visualisation of elevation slices within GIS software. Each multi-band raster contains 421 bands in elevation order, where Band 1 = 331 mASL and Band 421 = -507 mASL, with each band consisting of a 2-m-thick vertical slice referenced to the cell centre (i.e. Band 1 = 332–330 mASL). This elevation information is included within the metadata of the files.

3.3 2D Maps

Simplifications of model information to 2D maps can assist with further hydrogeological understanding of the Poukawa Basin and Otane Basin groundwater systems.

Both the harmonic mean and geometric mean were calculated for the upper 5 m, 10 m, 15 m, 20 m, 30 m, 50 m, 75 m, 100 m and 150 m for the *res*, *facies* and *AP* models. Each dataset was converted to a raster file (e.g. Figure 4.12). The geometric mean is useful to understand average properties, while the harmonic mean highlights the influence of lower permeable material (particularly useful for understanding vertical flow properties).

4.0 RESULTS

4.1 Assessment of Resistivity Values within the Vicinity of Datasets Relevant to Hydrogeology

A summary of the assessment of resistivity values against datasets relevant to hydrogeology is provided below. Values from the smooth resistivity model and P0.1–P0.9 ranges (referring to the 10% and 90% percentiles, respectively) have been preferentially selected for the below summary.

1. Compared to the QMAP surface geological map: values <10 ohm.m are most likely to be mudstone or sandstone; values 10–30 ohm.m are most likely to be mudstone, peat, gravel or sandstone; values >30 ohm.m are most likely to be gravel or limestone (Section A1.1).
2. Groundwater levels and the lake depth are not expected to be significant features in the resistivity models (Section A1.2).
3. Compared to groundwater electrical conductivity measurements, resistivities for aquifers are expected to be approximately 8–350 ohm.m. There is expected to be a significant presence of clay within gravel sediments, and values below 8.53 ohm.m are likely to be influenced by clay minerals enhancing conductivity (Section A1.5).
4. Compared to measured peat depths, peat is expected to have a resistivity range of 8.3–67.8 ohm.m (Section A1.3).

A simplified summary of the smooth model and 80% threshold values is presented for the main lithologies in the area in Table 4.1 (Sections A1.4–A1.7). A further discussion of the limestone values is provided in Section 3.2.4.1, where it was found through manual inspections that greater than 126 ohm.m corresponded to outcropping/weathered limestone.

Table 4.1 Summary of values from smooth model and 80% threshold.

Lithology	Details*	P0.1	P0.9	Expected Character
Limestone	Water bearing	49.0	165.7	Aquifer
	Consented	43.1	307.8	Aquifer
	Screened	15.5	222.1	Aquifer
	Unknown	21.4	303.4	Variable
Gravel	Water bearing	15.7	161.7	Aquifer
	Consented	31.5	72.2	Aquifer
	Screened	11.4	94.1	Aquifer
	Unknown	17.2	166.5	Aquifer
Sand	Consented	27.4	28.2	Aquifer
	Screened	12.9	28.0	Aquifer
	Unknown	12.7	136.6	Aquifer
Sandstone	Consented	34.2	44.7	Aquifer
	Screened	14.7	35.8	Aquifer
	Unknown	11.7	46.3	Variable
Silt	Unknown*	11.6	23.2	Aquitard
Peat	Unknown	7.9	34.0	Aquitard

Lithology	Details*	P0.1	P0.9	Expected Character
Clay – no major limestone influence	Unknown*	6.8	29.3	Aquitard
Siltstone	Unknown*	6.0	43.3	Aquitard
Mudstone/shale	Unknown*	7.0	22.0	Aquitard

* Screened assessments did not require an 80% threshold on lithology volume, so have been lumped with 'unknown' where screened assessments covered a wider range than the lithological assessments.

4.2 Manual Delineation of Major Hydrogeological Boundaries

Three boundaries were manually delineated:

1. Riverbed HU base boundary.
2. Limestone HU top boundary.
3. Limestone HU base boundary.

As can be seen in Figure 3.3 by the distribution of limestone base and riverbed base seed points, the Basement HU primarily underlies the Riverbed HU, and the Limestone HU primarily underlies the Swamp and Fan HU. However, in the centre of the study area near the boundary between the Poukawa Basin and the Otane Basin, the Limestone HU also underlies the Riverbed HU, further complicating interpretation through this area.

For the depth and thickness maps presented in this section, the Riverbed HU base boundary was used to define the entirety of the base for the Riverbed HU, as well as a portion of the top of the Basement HU (where the Basement HU underlies the Riverbed HU). The Limestone HU top boundary was used to define the entirety of the base of the overlying Swamp and Fan HU. The Limestone HU top boundary and Limestone HU base boundary were used to define the entirely of the Limestone HU (except where the Limestone HU outcrops). The Limestone HU base boundary was used to define a portion of the top of the Basement HU (where the Basement HU underlies the Limestone HU). A 10 m DEM surface was also used to delineate the top of all HU where they were at the ground surface, and to derive thickness and depth maps.

4.2.1 Delineation of the Riverbed HU Base Boundary

There are several rivers and streams running through Otane Basin (Figure 2.4). Borehole data suggest that the Riverbed HU is primarily composed of gravels, sands, silts, clay and limestone clasts.

In the resistivity models, Riverbed HU deposits show a relatively high resistivity (Figure 3.2) compared to the underlying mudstone and sandstone lithologies of Whangai and Waipawa formations (Late Cretaceous to Paleocene) and Tolaga Group (Miocene). In general, Riverbed HU deposits show resistivity values >10 ohm.m (Figure 3.4), which is consistent with the base cut-off value of gravel found in the Otane area, as well as the QMAP assessment against mudstone (Appendix 1). The Riverbed HU base horizon was mapped in the resistivity model taking this resistivity cut-off value. In some areas (e.g. a few areas along the Tukituki River and close to the hills; Figure 4.1), the difference in resistivity between the riverbed and underlying lithology is very low. This could be related to the presence of a thin riverbed deposit that may not be resolved by the SkyTEM system. It could also be related to the similar lithological composition of the riverbed and underlying bed. Therefore, the uncertainty in interpretation in these areas is higher. In this study, a minimum bed thickness of 10 m has been taken as a mappable riverbed unit.

Interpretation of the entire resistivity model shows that Riverbed HU deposits are primarily distributed over an area of about 80 km^2 in the southern part of the SkyTEM survey area (Otane Basin; Figure 4.1), with a maximum thickness up to ~190 m. A thick (up to ~190 m) area of the Riverbed HU deposits was identified in the resistivity model along a paleochannel of the Waipawa River (underlying Papanui Stream) from south to north in the survey area (Figure 4.1). The resistive unit (Riverbed HU) along the current Tukituki River is interpreted to be thin (<20 m) in most of the portions of the river in the survey area. However, the Riverbed HU thickness is slightly greater in the southern and northern portions of the river, where the current Waipawa River and Papanui Stream, respectively, merge with the Tukituki River (Figure 4.1).

Riverbed HU deposits show a vertical and lateral variation in resistivity. In general, the older Riverbed HU deposits (paleo-Waipawa River) and the northern area of the Tukituki River (north of the convergence of the Papanui Stream) have higher resistivity values (up to >200 ohm.m) compared to more recent Riverbed HU deposits in the south-eastern part of the area (<30 ohm.m). This resistivity variation may be related to the type of lithology present in the Riverbed HU. Logged lithology shows that the paleo-Waipawa riverbed primarily consists of gravel, sand and silt with minor mud and clay. However, more recent riverbed deposits in the south consist of mainly clay, mud and silt with minor sand and gravel. Recent riverbed deposits in the northern portion of Tukituki River include gravel. This variation is likely associated with the current variable fluvial depositional environment, as the southern portion of the river is narrow, whereas to the north it fans out to a wider area. The northern area is also surrounded by limestone hills (Mangaheia Group, Late Pliocene) that could provide sediments to the riverbed and hence provide higher resistivity values. There are several thin, patchy, low resistivity (<10 ohm.m) layers observed within this broad Riverbed HU. These low resistive layers are dominated by clay-rich units that may act as aquitards.

The uncertainty in the interpretation of the Riverbed HU at the northern portion of the Tukituki River is larger because the riverbed deposits and the underlying limestone show a similar resistivity character (Figure 3.4). The limited borehole data available in that area provided limited assistance with mapping the Riverbed HU base horizon.

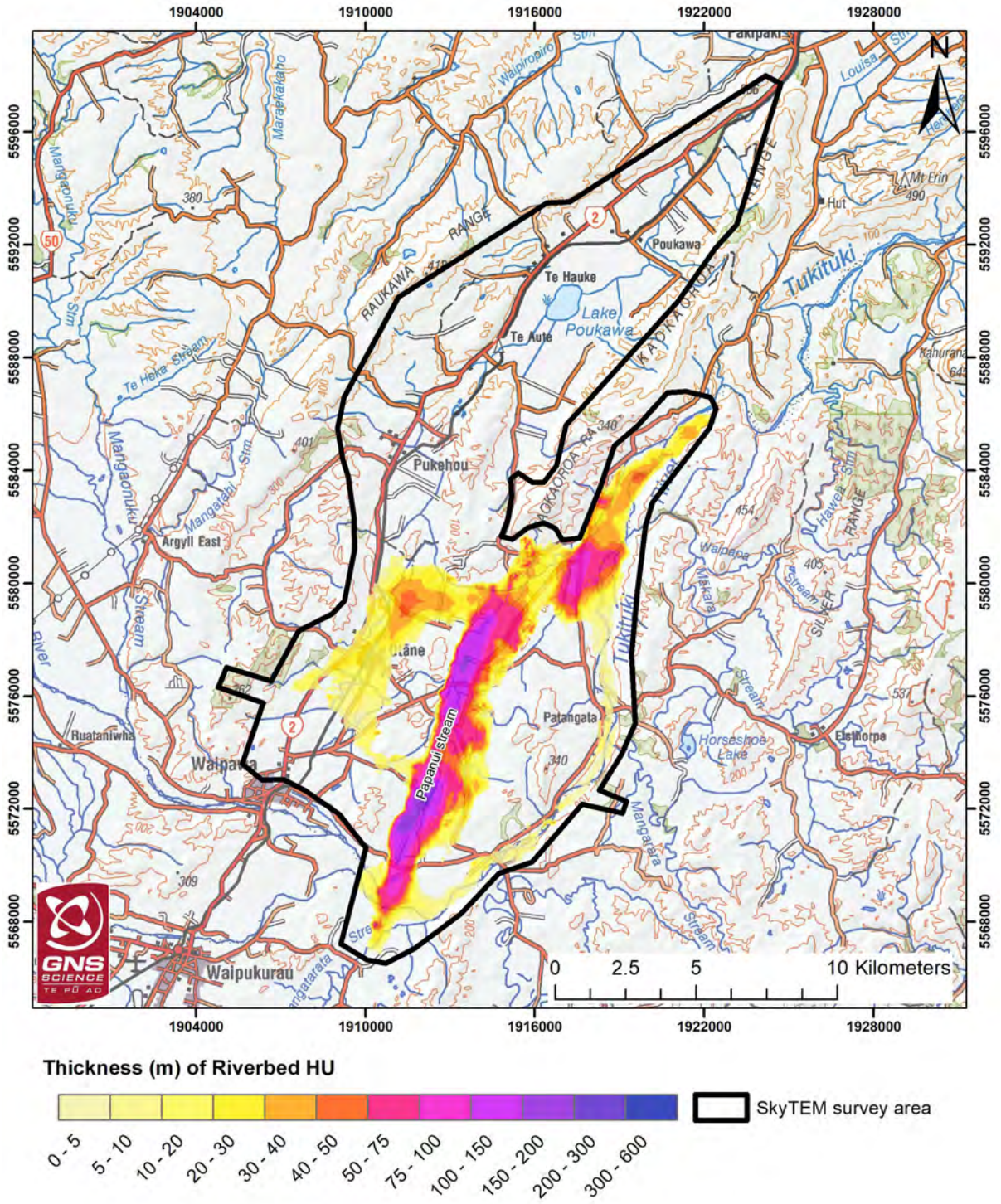

Figure 4.1 Thickness map of the Riverbed HU.

4.2.2 Delineation of the Limestone HU Top Boundary

Throughout most of the study area, the Limestone HU top horizon delineates the base of the overlying Swamp and Fan HU.

The Limestone HU top boundary was mapped using a horizon picked on a sharp increase in resistivity (to approximately >20 ohm.m) from the overlying Swamp and Fan HU (Figure 3.2). In general, Swamp and Fan HU deposits mostly show resistivity values <50 ohm.m. Borehole data suggest that the swamp and fan deposits are composed of primarily sand, silt, clay and gravel (derived from limestone, sandstone and mudstone), as well as organic mud and peat. However, in some areas (close to the hills), fan deposits show higher resistivity values. Boreholes in this region describe the presence of thin layers (<10 m) of limestones within this Swamp and Fan HU, which could contribute to the higher resistivity. It is likely that these limestone intervals are sediments derived from surrounding limestone hills.

The Limestone HU top and DEM were used to derive a map of depth to limestone. Depth to the Limestone HU is shown in Figure 4.2. Structural lows are present immediately around Lake Poukawa and some regions to the north and west of the lake. These structural lows provided accommodation space for the deposition of swamp and fan deposits.

Swamp and Fan HU deposits cover an area of ~75 km^2 and are distributed in the northern parts of the study area (Figure 4.3), which are surrounded by hills composed of limestone, sandstone and siltstone of the Late Pliocene Mangaheia Group. A thickness map of these deposits (Figure 4.3) suggests that Lake Poukawa was much bigger in size in the past, consistent with previous work in this area (Section 2.2).

In the north and west of the area, the classification is complicated by the presence of sandstone overlying limestone. Boreholes also show thin units of limestone, shell, sand, peat, sandstone and siltstone mixed with silt and clay. It is difficult to tell from the available lithological log information whether these units are consolidated or unconsolidated. It is assumed that some of these logged units are unconsolidated derived material from the surrounding limestone and sandstone ranges. Potential inclusion of consolidated sandstone and thin limestone and shell material, as well as sparse information, complicates interpretation, and high uncertainty remains in these areas. Due to the primary objective of delineating the depth to limestone, where limestone was distinguishable in the resistivity data, the sandstone was included within the Swamp and Fan HU. Additionally, within the deepest part of the basin, there is no clear resistivity contrast, increasing uncertainty here. As discussed in Section 4.2.1, uncertainty is also high at the northern portion of the Tukituki River, where riverbed deposits overlie limestone, because the riverbed deposits and underlying limestone show a similar resistivity character.

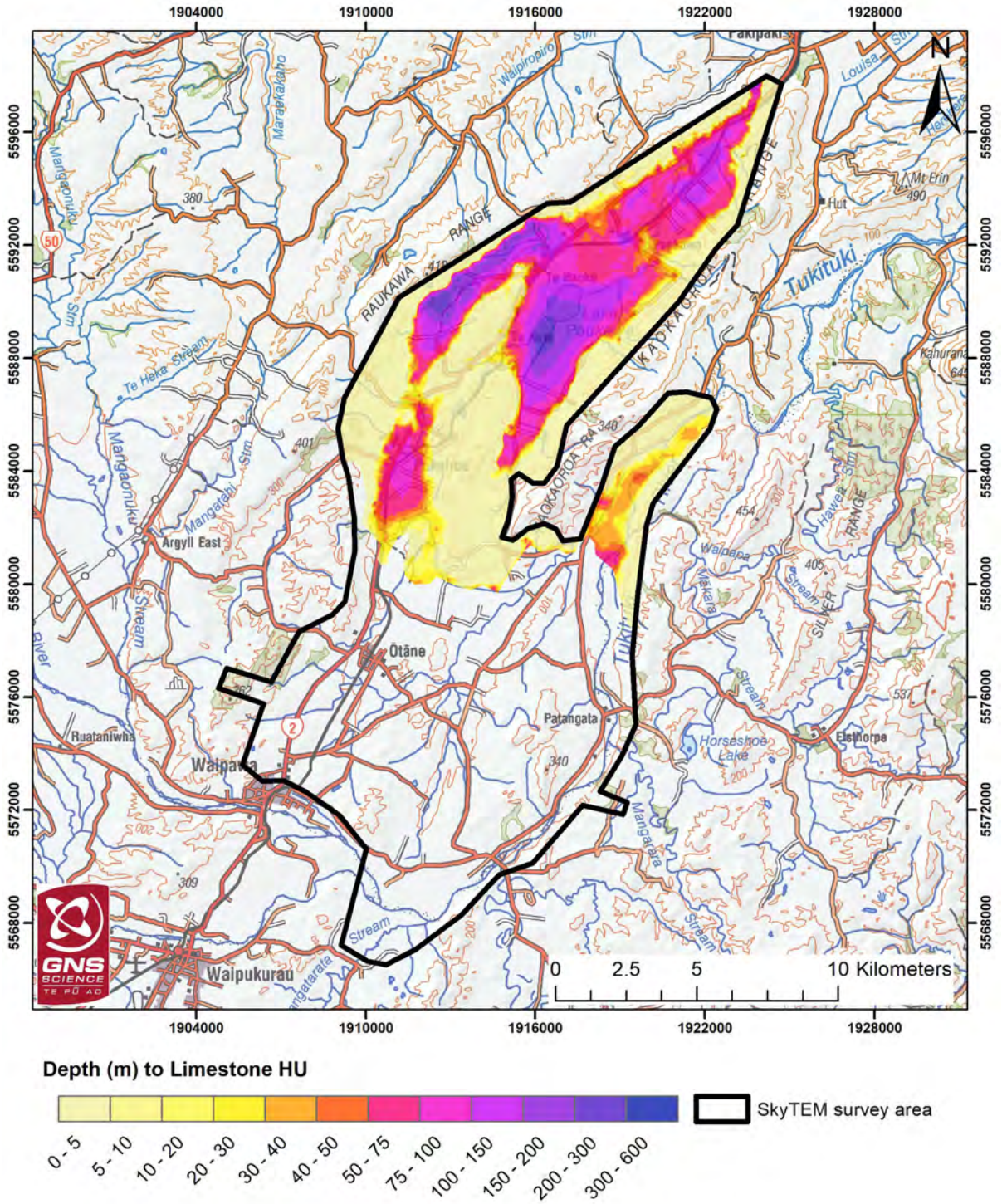

Figure 4.2 Map showing the depth to Limestone HU.

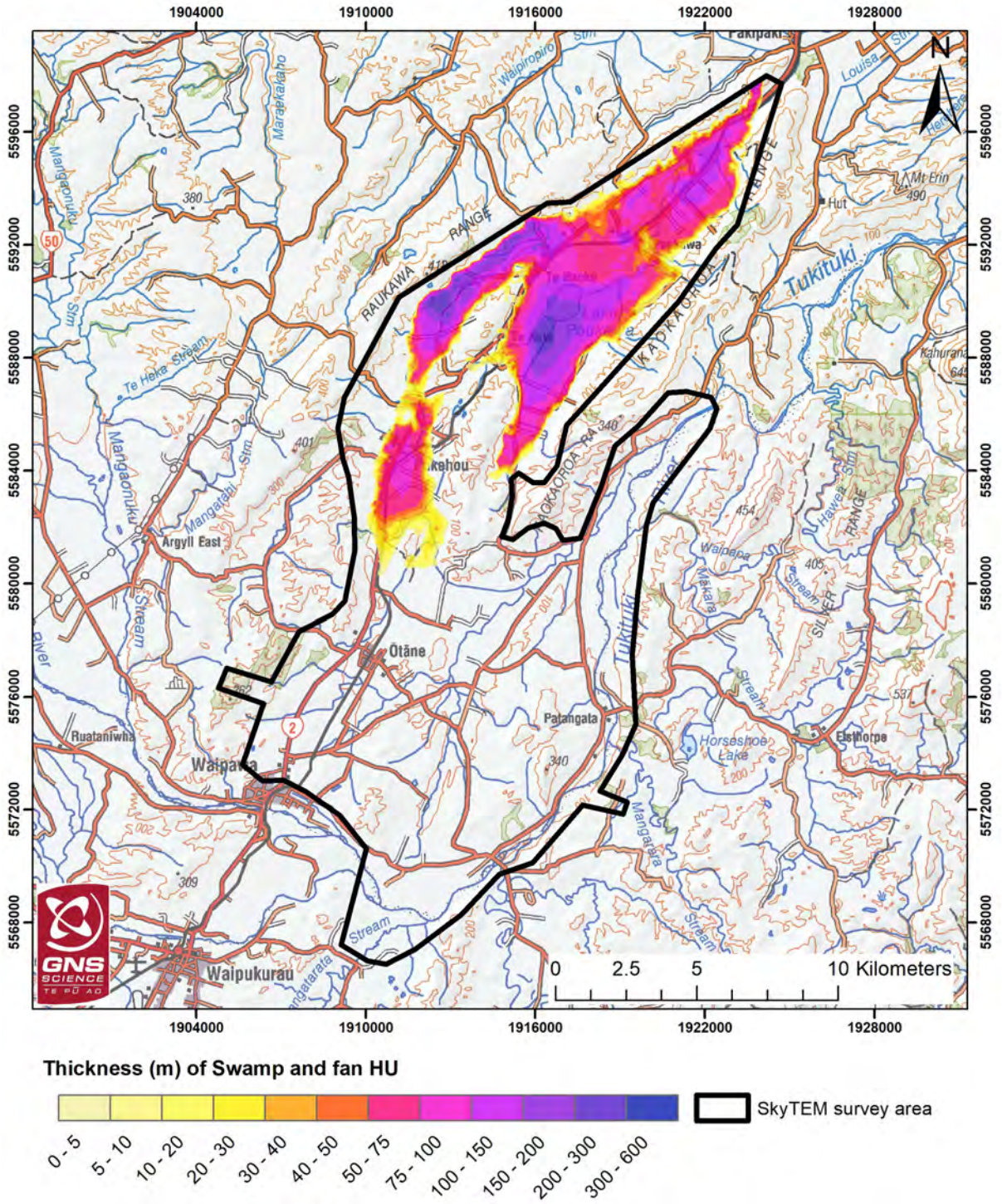

Figure 4.3 Thickness map of the Swamp and Fan HU.

4.2.3 Delineation of the Limestone HU Base Boundary

Throughout the study area, limestone typically has resistivity values >20 ohm.m. In a similar approach used to map the Limestone HU top horizon, the Limestone HU base horizon was delineated using a sharp change in resistivity from the overlying limestone to the underlying sandstone and mudstone units of Whangai and Waipawa formations (Figure 3.2). However, the uncertainty in the interpretation of the Limestone HU base is higher compared to the interpretation of upper horizons. This increase in uncertainty is because, in many areas, the base of the Limestone HU is located below DOI Lower and DOI Upper (Figure 3.2). The SkyTEM data quality is poor below these DOIs and the base of the Limestone HU may not have been imaged properly. Because of this, we suggest that the Limestone HU base horizon (Figure 4.4) in this study provides a minimum lower boundary of the limestone. The Limestone HU base also represents the top of the Basement HU (i.e. top of the Whangai and Waipawa formations). To the south, where the Limestone HU is not present (Figure 4.5), the Riverbed HU base represents the top of the Basement HU. The Limestone HU and Riverbed HU base horizons were merged to calculate a depth to Basement HU across the entire survey area (Figure 4.6).

The Limestone HU is distributed in the northern part of the SkyTEM survey region and covers an area around 130 km^2 (Figure 4.5). The maximum thickness of the Limestone HU mapped by the resistivity model is approximately 590 m. However, this thickness provides a minimum value, as limestone is subject to erosion and there is higher uncertainty in mapping the base of the limestone. Additional information about the base of the Limestone HU is presented in the next section.

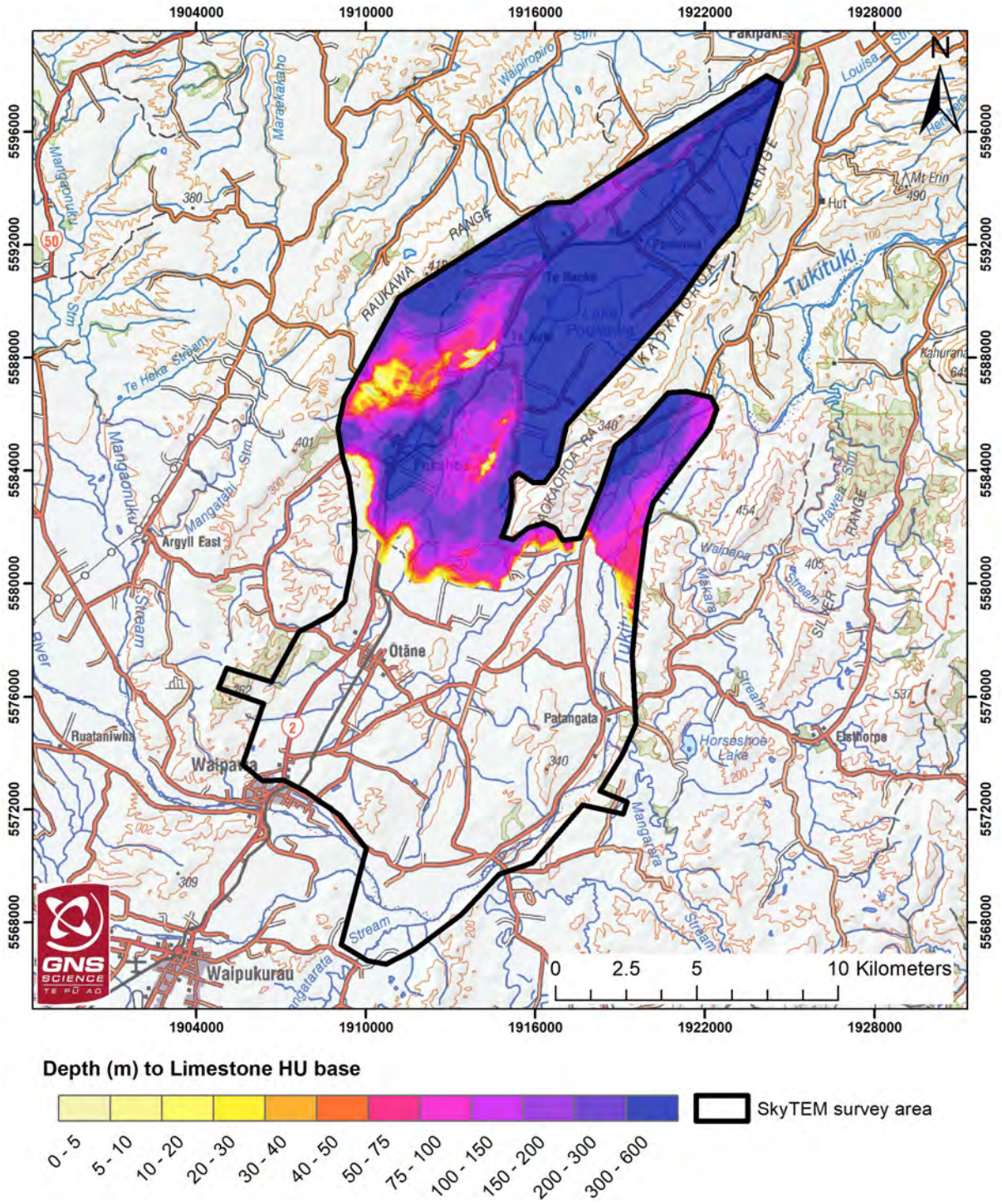

Figure 4.4 Depth to base of the Limestone HU. Note: The depth here represents the minimum lower boundary as per Section 4.2.3.

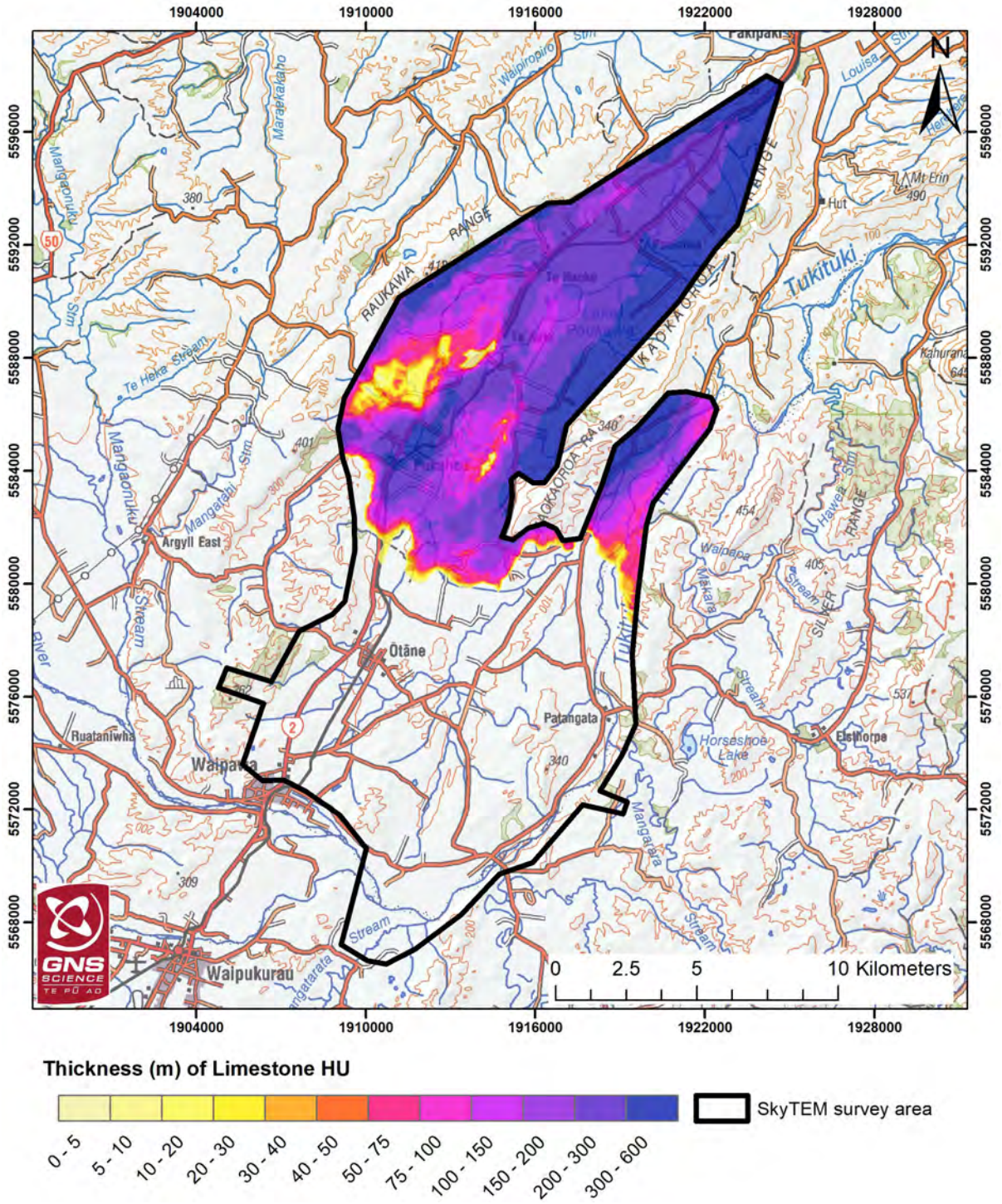

Figure 4.5 Thickness map of the Limestone HU.

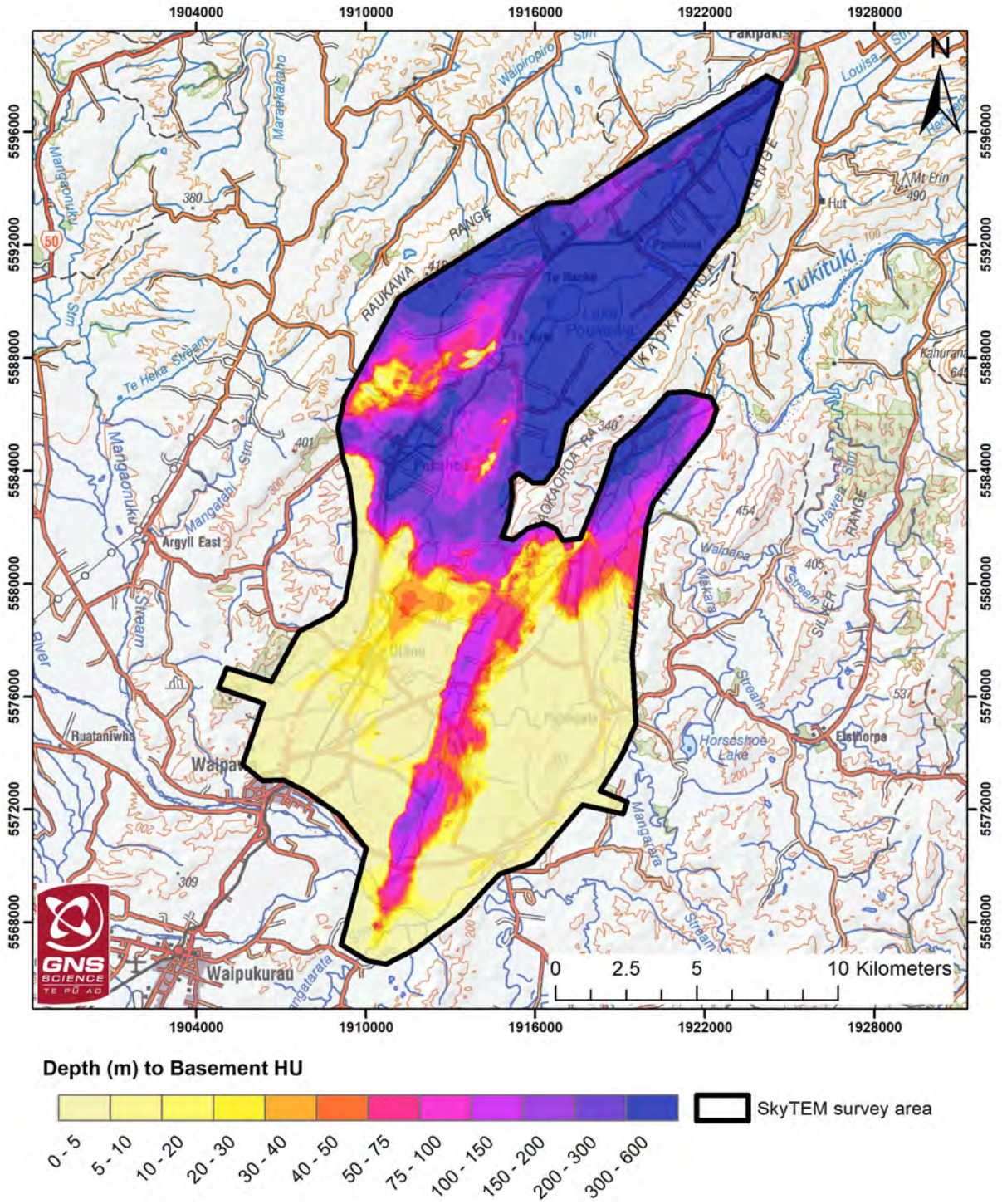

Figure 4.6 Depth to Basement HU (top of the Whangai and Waipawa formations).

4.2.3.1 Deep Resistivity Models

There are no petroleum exploration wells within the Poukawa and Otane basins that could provide some deeper estimate of the electrical resistivity of the sediments from geophysical logs. The closest wells are Mason Ridge-1 (15 km northwest of Lake Poukawa) and Ongaonga-1 (18 km southwest of Lake Poukawa). Neither well can be easily correlated to the geology in the top 500 m of the Poukawa Basin, so they do not provide any constraints on the SkyTEM inversions.

Some information about the bulk electrical properties is available from regional magnetotelluric soundings that have been conducted by GNS Science and partners as part of a study of the Hikurangi Subduction zone (Heise et al. 2019). Five soundings are located within the limits of the SkyTEM survey in the Poukawa and Otane basins. The spacing between soundings is 7–8 km.

Magnetotellurics (MT) is a frequency-domain electromagnetic method that exploits naturally occurring fields (magnetic storms and ionospheric activity) to produce models of the electrical resistivity from depths of 0.5 km to 100 km. The depth of investigation is dependent on the bulk resistivity of earth and the frequencies used in the study. Heise et al. (2019) utilised a broad-band instrument (384–0.01 Hz) that is sensitive to changes in resistivity in the top 1 km in low-resistivity sedimentary basins. In most cases, the resistivity structure identified by the MT soundings is strongly three-dimensional because of the volume of investigation and the complexity of the regional resistivity structure. However, in the centre of the Poukawa Basin, one of the soundings (Site MT 513) provides a reliable 1D model of the top 500 m of the basin.

Figure 4.7 shows the location of the five sites within the Poukawa and Otane basins and highlights the location of site MT513. The inversion approach is similar to the SkyTEM smooth inversion, in that the layering is fixed, and the resistivity of each layer changes gradually with depth. MT data are particularly sensitive to the presence of low-resistivity layers due to the nature of the diffusion of electrical and magnetic fields in the earth. The resistivity properties derived should be comparable to the SkyTEM models, except that the layers will be thicker and the sensitivity to subtle changes in resistivity will be lower.

The sharp and smooth SkyTEM models from the closest point to the MT sounding have been extracted from the SkyTEM dataset and are plotted alongside the MT model, as well as the interpreted top and base of the Limestone HU for comparison (Figure 4.8). The smooth 1D inversion models agree very closely with the MT model, showing a low-resistivity layer of 10 ohm.m at a depth of 60–100 m, underlaid by a thicker resistive layer to a depth of 400–500 m. The peak resistivity of this layer is 50 ohm.m, compared to a value of 60 ohm.m estimated by the SkyTEM inversion. The base of the Limestone HU is close to the DOI for the SkyTEM data but will be reasonably well resolved by the MT. The interpreted top and base of the Limestone HU correlate well with the MT model, but, as there is no sudden drop in resistivity, the base of the limestone could be as deep as 450 m (currently 338 m). There are significant uncertainties included in the MT data analysis and modelling, but the level of agreement with the SkyTEM models provides some support to the interpretation of the deeper layers in the SkyTEM data.

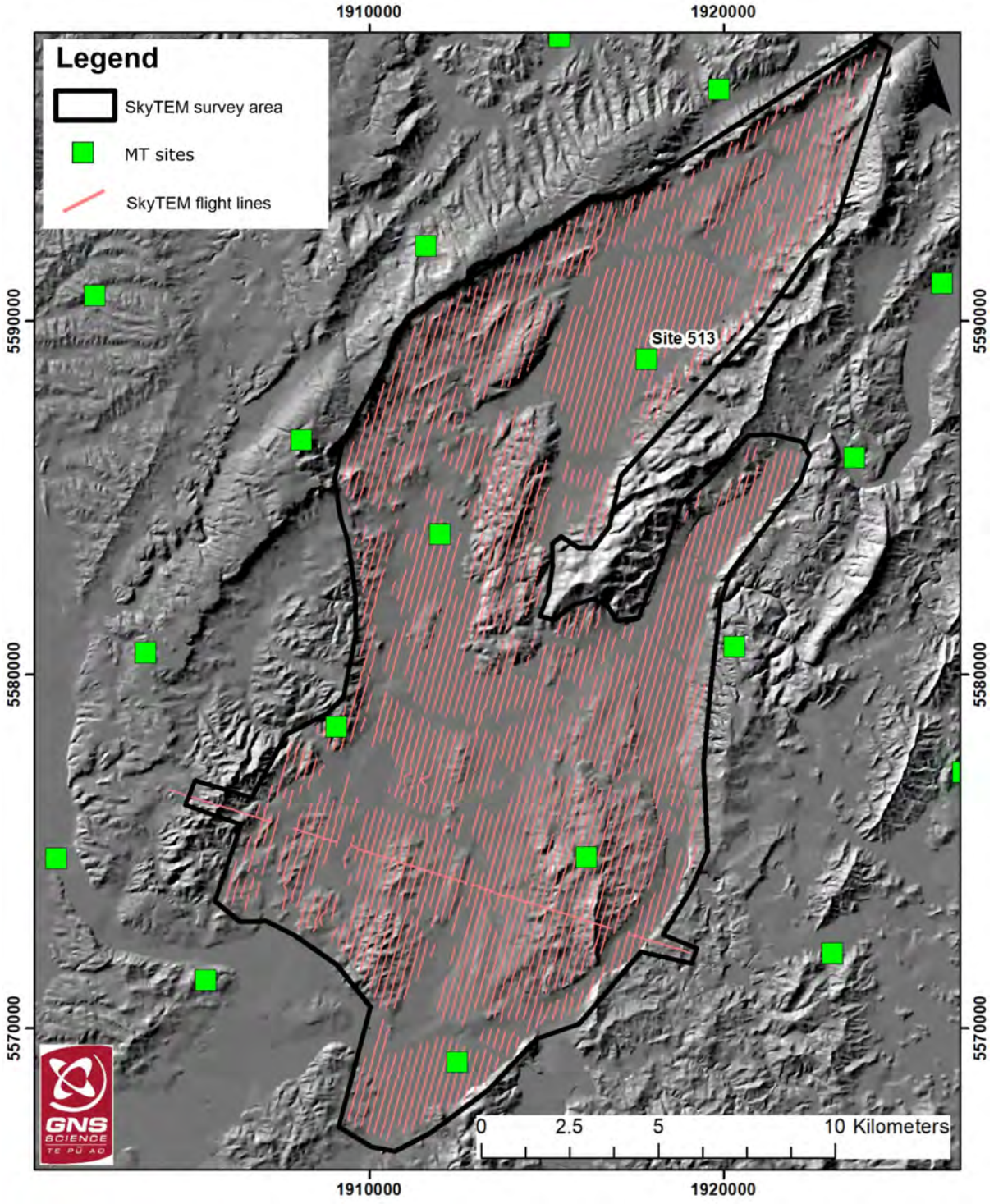

Figure 4.7 Map of the Poukawa and Otane basins showing the locations of the regional magnetotelluric (MT) sites and the SkyTEM flight lines. Site 513 lies in the centre of the Poukawa Basin close to Lake Poukawa.

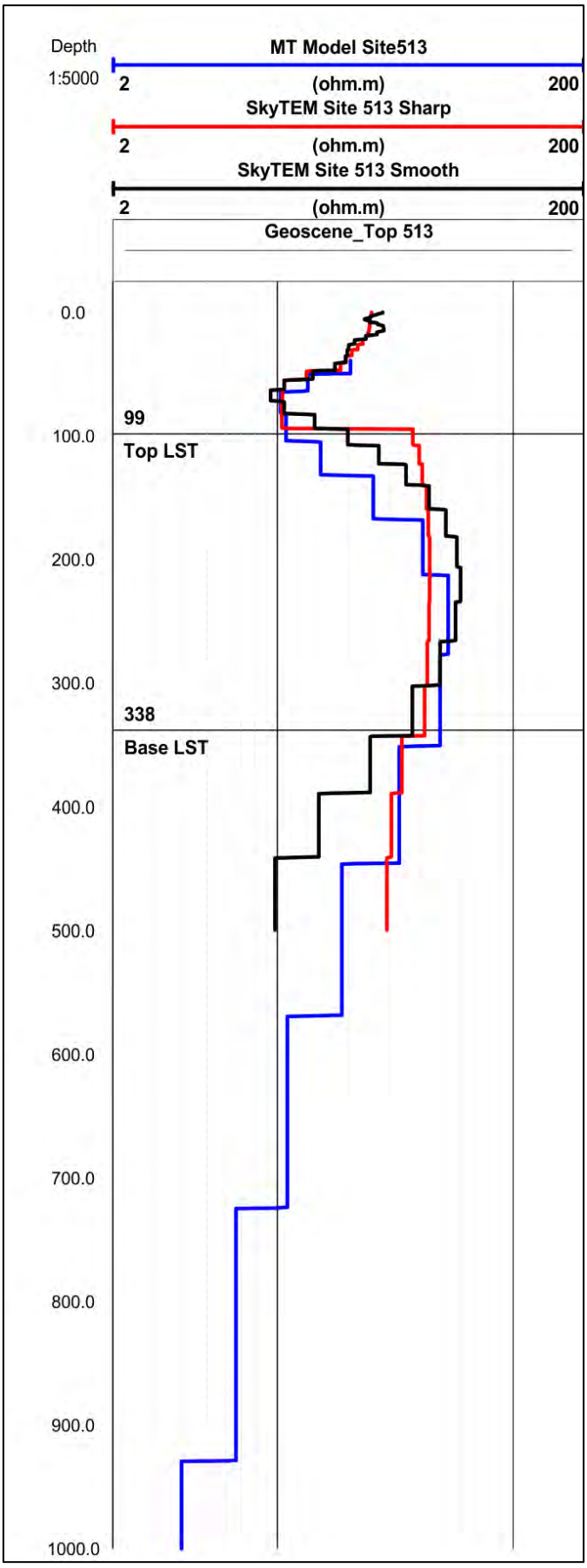

Figure 4.8 Model from a 1D inversion of magnetotelluric (MT) data (blue) and comparison to SkyTEM models at the same location (red and black). The top and base of the Limestone HU (Top LST and Base LST) are from the manual interpretation of the SkyTEM resistivity model (Sections 4.2.2 and 4.2.3).

4.3 3D-Gridded Model Development

Three-dimensional model datasets were combined within a *.csv* file, with x,y,z defining the centre of each grid cell and including the following parameters: *X*, *Y*, *Z, top_elev_HU*, *res*, *resvar*, *HU*, *facies*, *AP* and *aq* (Table 4.2; Figures 4.9 and 4.10). A selection of these models was converted to multi-band raster format, enabling further accessibility, such as visualisation of elevation slices within GIS software.

The 3D models utilise 50 x 50 m grid cells horizontally and 2-m-thick grid cells vertically. Grid cells are defined in elevation (relative to mean sea level) rather than depth (relative to the ground surface), so exact clipping at the surface varies based on the grid location versus DEM location. A 10 m resolution DEM was used for surface clipping.

A summary of the developed models is provided below:

- An interpolated resistivity (*res*) model, which interpolated the SkyTEM-derived smooth resistivity model to the regular grid. Model gaps remain at distances greater than 500 m from any resistivity data.
- A major Hydrogeological Unit (*HU*) model, which utilised the previously developed manually delineated major hydrogeological unit surface to split the 3D grid into four HU units (HU1–HU4), as well as additional manual adjustments to the subsequent grid to improve separation between consolidated and unconsolidated sediments and overcome some resolution limitations of the manually delineated surfaces (see Table 3.2). The surfaces were developed using interpolation, which fills any gaps in the resistivity data. Due to the approach taken for the manual adjustments, some sharp discontinuous features appear in the model.
- A resistivity facies (*facies*) model, which separated the *res* model into 12 $\log_{10}$-based uniform intervals to group materials that are expected to have similar hydrologic and geologic properties based on their resistivity (to assist with easier discrimination of significant variability and similarity). Model gaps are the same as in the *res* model.
- An Aquifer Potential (*AP*) model, which has 24 classes and utilised the *HU* and *facies* models to separate the model into likely consolidated sediments (HU3–HU4; 13 classes) and likely unconsolidated sediments (HU1–HU2; 11 classes), while providing an indicator of the likelihood of each model cell to host aquifer-bearing material (after assessments against other datasets, such as lithological logs). This model utilised the same relationships between resistivity and permeability across the entire study area. Model gaps are the same as in the *res* model.

The models developed are limited by the supporting datasets available, such as lithological logs. Uncertainty increases with increased distance from such supporting datasets.

Table 4.2 Summary of 3D model output file.

Attribute	Description	Type	Comments
X	Easting in NZTM of the centre of the model cell	Numerical	50 m horizontal cell resolution
Y	Northing in NZTM of the centre of the model cell	Numerical	50 m horizontal cell resolution
Z	Elevation (m ASL) in NZVD2016 of the centre of the model cell	Numerical	2 m vertical cell resolution
top_elev_HU	Elevation (m ASL) in NZVD2016 of the centre of the highest Z cell at this X,Y location that has HU data	Numerical	See Section 3.2.2
res	Resistivity (ohm.m)	Numerical	See Section 3.2.1
resvar	Kriging variance of the resistivity model	Numerical	See Section 3.2.1
HU	Major hydrogeological units	Categorical: 1–4	See Section 3.2.2
facies	Resistivity facies model	Categorical: 1–12	See Section 3.2.3
AP	Aquifer potential model	Categorical: 1–24	See Section 3.2.4
aq	Simplified aquifer potential model	Categorical: cl, cm, ch, ul, um, uh	See Section 3.2.4

This page left intentionally blank.

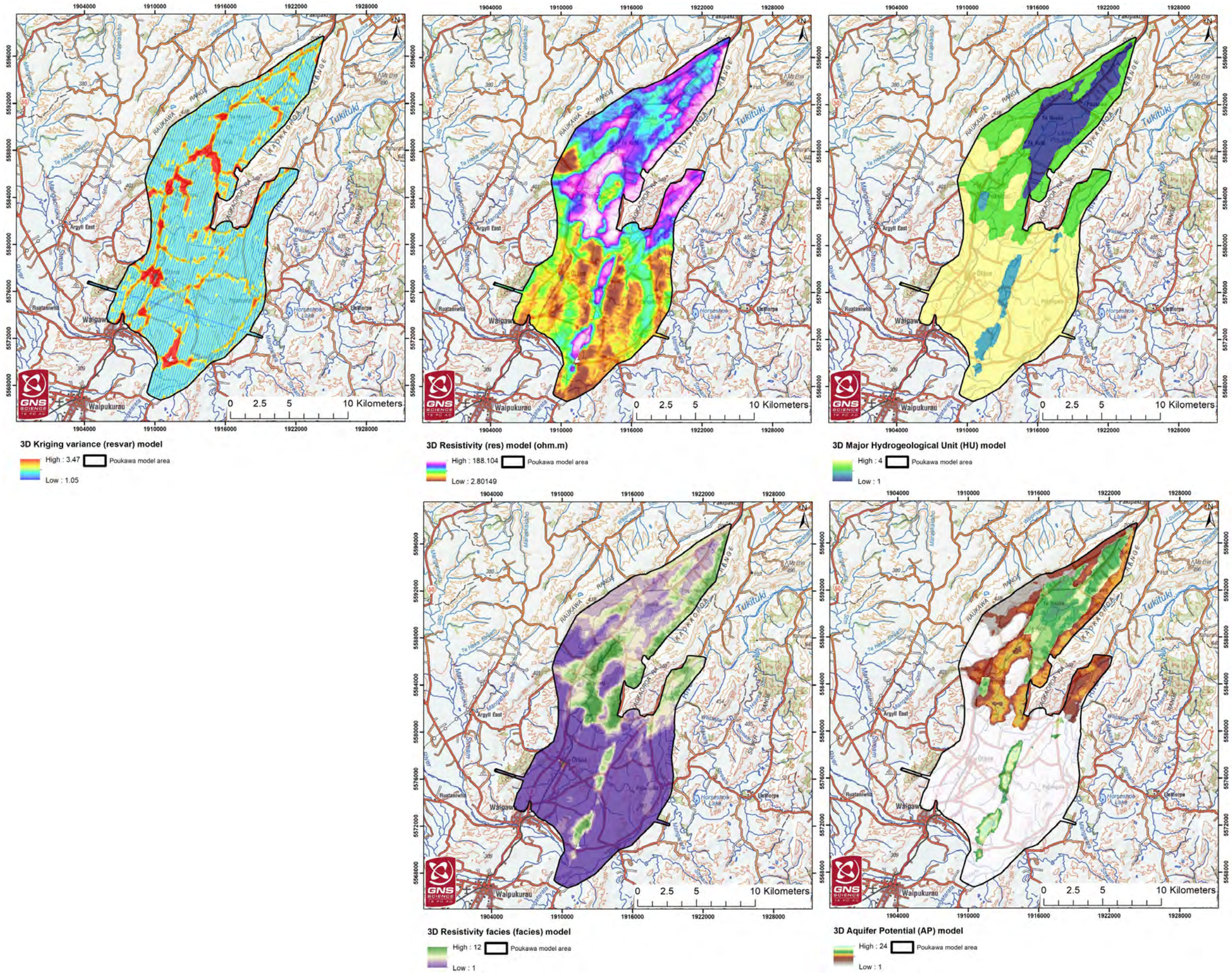

Figure 4.9 Three-dimensional models, map view at 0 mASL. See Section 3.2 for model details.

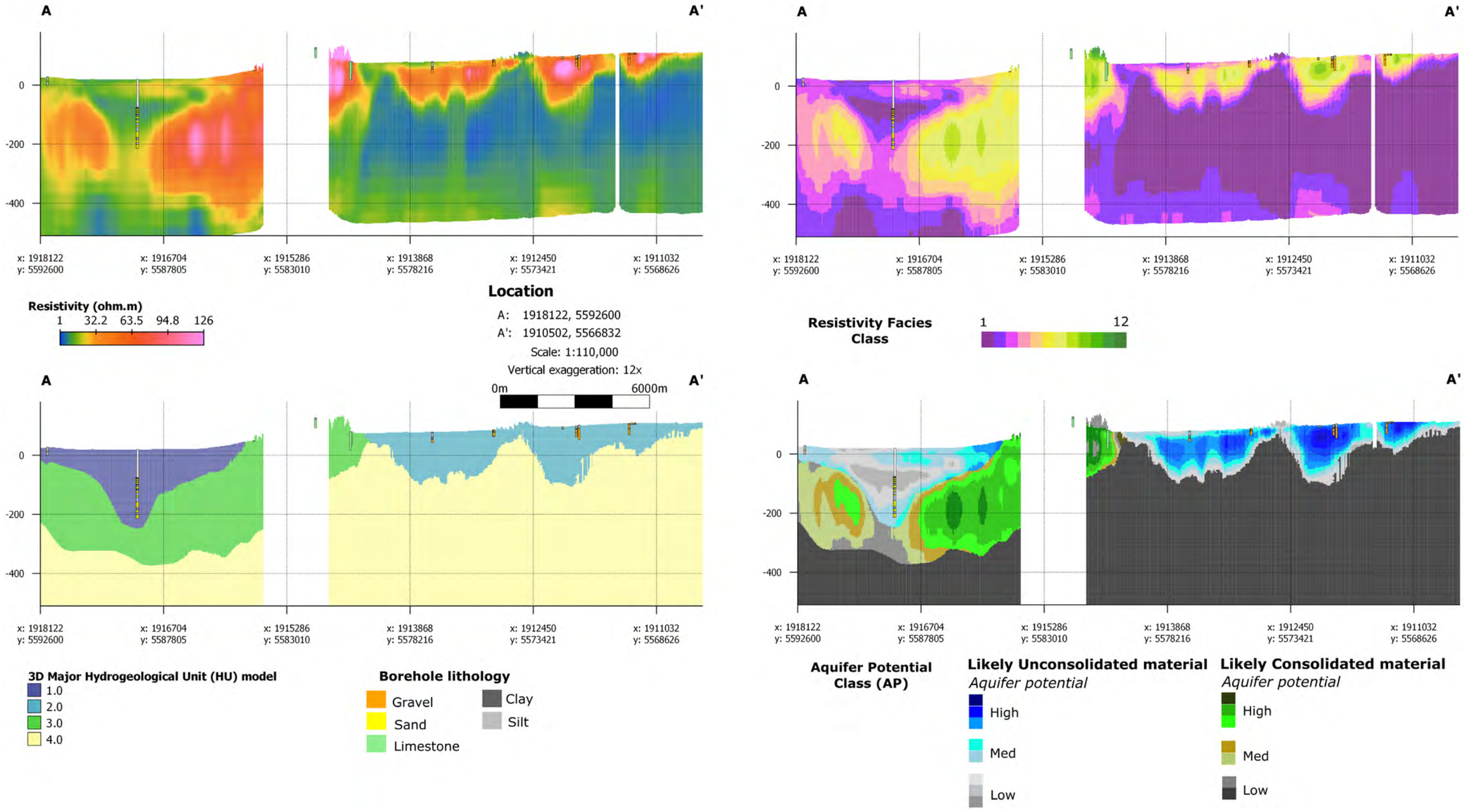

Figure 4.10 Three-dimensional models shown across profile A–A'. Cross-section location is shown in Figure 3.1. See Section 3.2 for model details.

4.4 2D Maps

Simplifications of the 3D models to 2D maps can assist with more readily investigating various aspects of the Poukawa Basin and Otane Basin groundwater systems. Near-surface properties (*res, facies* and *AP*; Figure 4.12) for the upper 5 m, 10 m, 15 m, 20 m, 30 m, 50 m, 75 m, 100 m and 150 m were created using geometric and harmonic means.

There are no large volumes of unconsolidated sediments within the study area. The 2D maps highlight two locations near Otane likely to contain the greatest volume of readily extractable groundwater from unconsolidated sediments (Figure 4.11).

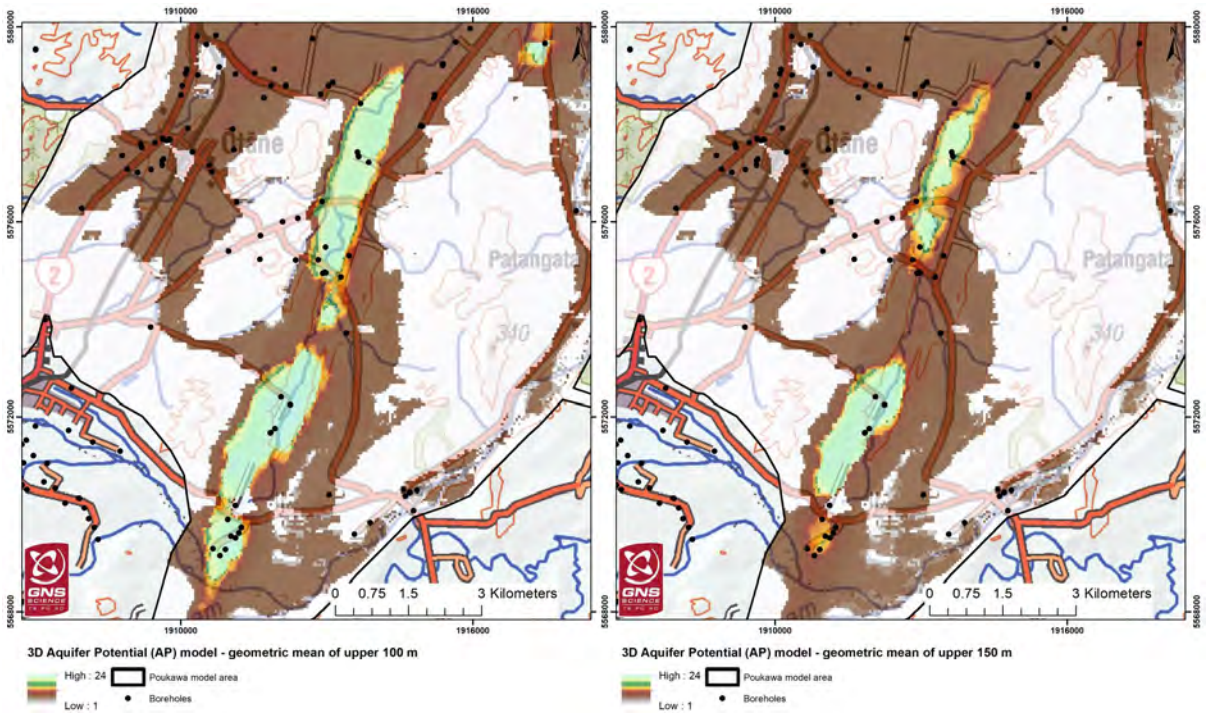

Figure 4.11 Zoom-in of the Aquifer Potential (AP) model, showing two locations (light blue areas) near Otane likely to contain the greatest volume of readily extractable groundwater from unconsolidated sediments in the study area. (Left) Geometric mean of the upper 100 m; (right) geometric mean of the upper 150 m.

This page left intentionally blank.

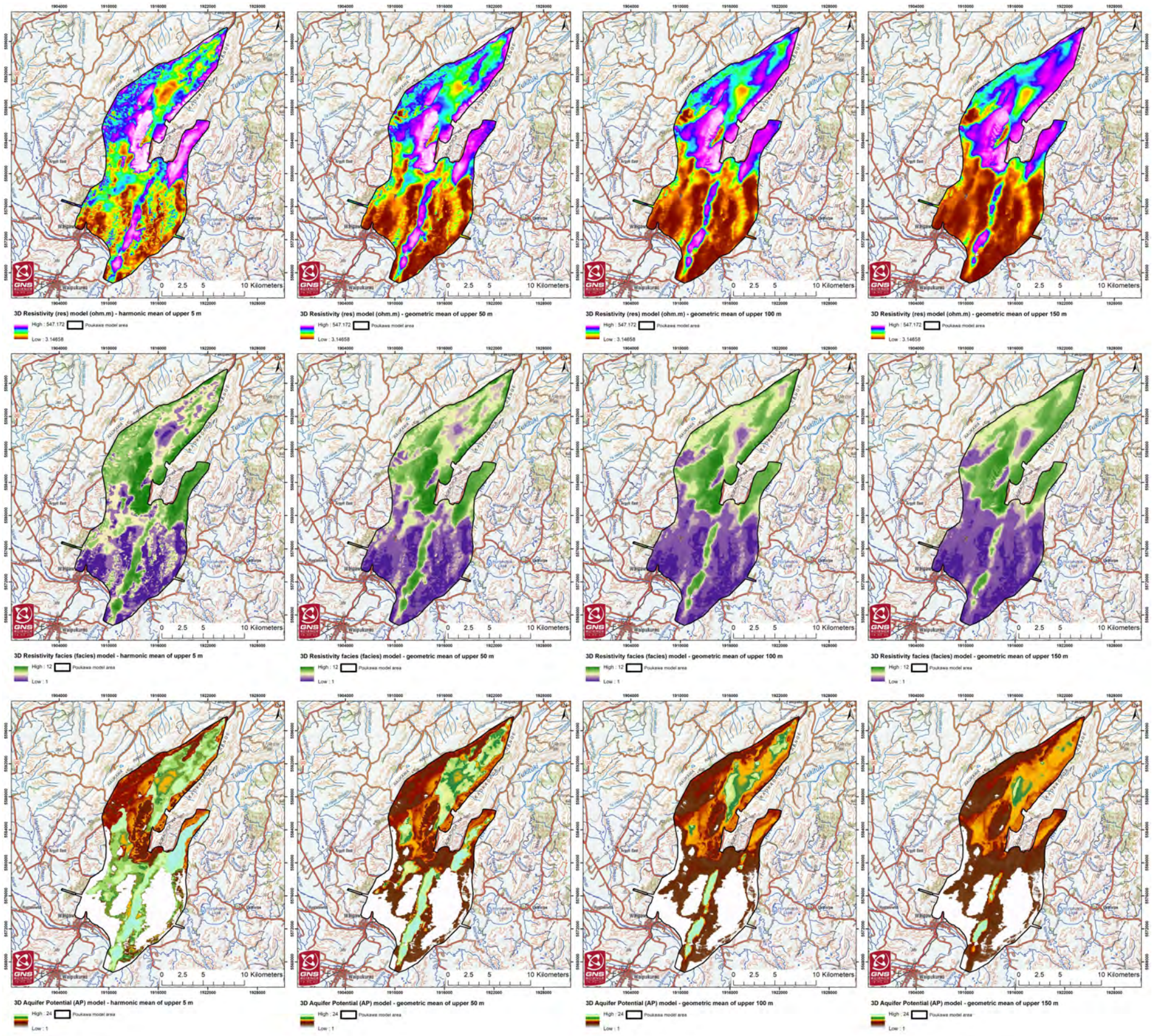

Figure 4.12 A selection of near-surface property estimates. Rows from top to bottom: (top row) resistivity (ohm.m); (middle row) resistivity facies; (bottom row) AP model. Columns from left to right: (first) harmonic mean of upper 5 m; (second) geometric mean of upper 50 m; (third) geometric mean of upper 100 m; (fourth) geometric mean of upper 150 m.

This page left intentionally blank.

5.0 SUMMARY OF RESULTS RELATED TO OBJECTIVES

The objectives of this interpretation work were to assess the following in the Poukawa and Otane area, as achievable within the scope of this project:

1. The 3D lithological structure of relevance to groundwater:
    a. Waipawa and Papanui Stream riverbed delineation.
    b. Depth to limestone (Mangaheia Group).
    c. Base of limestone (Mangaheia Group).
    d. Thickness of any unconfined layer in the Poukawa area.
    e. Any differences within the limestone, e.g. permeability/fracture zones.
    f. Peat thickness.
2. Connection to the Heretaunga Plains.
3. Delineation of main faults.

An additional objective included the development of 3D datasets suitable for display within an online 3D visualisation tool. The online visualisation tool was developed after the completion of the draft version of this report, with the draft datasets and models utilised for iterative testing. It was determined during this testing that a separation between consolidated and unconsolidated sediments was useful for simplified visualisation and understanding. This timeline impacted some of the methodological approach taken. To preserve results related to objective 1b (depth to limestone), adjustments to improve the separation of consolidated and unconsolidated sediments were only undertaken on the gridded 3D models.

SkyTEM data were used in this study to address items 1a–e from the objectives. Further information was made available to inform items 2 and 3, but additional detailed studies are needed to address these further; and item 1f was assessed and considered to be outside the resolution of the data (see further details below).

Item 1, the 3D lithological structure of relevance to groundwater, was assessed throughout this report. Items 1a, 1b and 1c were manually delineated using Geoscene3D software. Items 1d, 1e and 1f were assessed using threshold values and associated categories. Item 1f is considered to be outside the resolution of the dataset.

Items 2 and 3 were not addressed in detail but are discussed below.

5.1 Waipawa and Papanui Stream Riverbed Delineation

Manual delineation of the base of the Riverbed HU, which includes the Waipawa and Papanui Stream riverbeds, was undertaken in Geoscene3D software with a minimum bed thickness of 10 m required for a mappable riverbed unit. In general, Riverbed HU deposits show resistivity values >10 ohm.m, and the Riverbed HU base horizon was mapped in the resistivity model taking this resistivity cut-off value. The uncertainty in the interpretation of the Riverbed HU at the northern portion of the Tukituki River is larger because the riverbed deposits and underlying limestone show a similar resistivity character.

Within the developed 3D models, the Riverbed HU was manually adjusted to HU2 (see Table 3.2). These deposits appear to exhibit the linear relationship between resistivity and permeability expected within a fluvial depositional environment, where both properties are primarily driven by clay content – less clay content correlates with both higher resistivity values and higher

permeability. An aquifer potential classification was applied to further split this unit into categories with similar hydrogeological properties. The results display a good correlation between logged gravel and clay material, as well as expectations from existing information.

In summary:

- Spread across an area ~80 km^2 in the Otane area.
- Up to ~190 m thick.
- Thickest area is a paleochannel of the Waipawa River.
- Strong linear relationship between resistivity and permeability.

2D and 3D digital datasets have been provided that describe these deposits.

5.2 Limestone HU

In summary:

- Distributed in the north (within the Poukawa Catchment) and covers an area ~130 km^2.
- Up to ~590 m thick.
- Thickest area is along the eastern ranges.

Assumed linear relationship between resistivity and permeability, although this is complicated by lower resistivity corresponding to more porous and/or more silt, while higher resistivity corresponds to more massive and/or less silt, as well as to outcropping limestone.

5.2.1 Depth to Limestone HU (Mangaheia Group)

Manual delineation of the top of the Limestone HU was undertaken in Geoscene3D software using a horizon picked on a sharp increase in resistivity from the overlying Swamp and Fan HU. In the north and west of the area, in the Poukawa Catchment, the classification is complicated by the presence of sandstone overlying limestone. In some cases, sandstone was included in the Swamp and Fan HU, while, in other cases, the sharp resistivity change coincided with the top of the sandstone and is mapped within the Limestone HU. Uncertainties in the depth to limestone are considered to be highest in the north and west, where sandstone units complicate the interpretation of the resistivity. It is difficult to tell from the available lithological log information whether thin logged units are consolidated or unconsolidated. It is assumed that some of these logged units are unconsolidated derived material from the surrounding limestone and sandstone ranges. Potential inclusion of consolidated sandstone and thin limestone and shell material, as well as sparse information, complicates interpretation, and there remains high uncertainty in these areas. Additionally, within the deepest part of the basin, there is no clear resistivity contrast to identify changes in lithology and therefore the uncertainty in interpretation of the top of Limestone HU is high here; however, deep borehole information assists with providing a minimum depth to limestone.

2D digital datasets have been provided that describe the depth to the Limestone HU.

5.2.2 Base of Limestone HU (Mangaheia Group)

Manual delineation of the base of the Limestone HU was undertaken in Geoscene3D software. The Limestone HU base horizon was mapped using a sharp change in resistivity from the overlying limestone to the underlying sandstone and mudstone of the Whangai and Waipawa formations. The uncertainty in the interpretation of the Limestone HU base is high because, in many areas, the base of the Limestone HU is located below the DOI Lower and DOI Upper, where the resistivity data has a significantly higher uncertainty. A comparison to existing MT data supported the interpretation of the base of the Limestone HU and verified that the Limestone HU thickness should be considered to provide a minimum value.

The maximum thickness of the Limestone HU mapped by the resistivity model is approximately 590 m. The previously estimated limestone thickness was between approximately 150 and 450 m (see Section 2.2).

2D digital datasets have been provided that describe the base of the Limestone HU.

5.2.3 Any Differences within the Limestone, e.g. Permeability/Fracture Zones

Borehole data suggest that the thickness of limestone varies laterally. Some areas show thick blocky limestones, whereas other areas show alternations of limestone, sandstone and mudstone beds. The resistivity response within limestone appears to be a function of the thickness of the limestone bed, overall lithological composition and structural complexity. Thickness of limestone is less at structural highs, as it is prone to erosion. Thicker limestones show high resistivity compared to areas with thinner limestones. Limestone shows slightly lower resistivity (in contrast to thick limestone) close to structural highs (Figures 5.1 and 5.2). Near structural highs, lower resistivity may be related to the presence of fractures in the limestone bed. However, high resistivity tends to be found in outcropping limestone at the location of structural highs. In the regions close to the structural highs, lower resistivity may be related to the presence of thin layers of transported limestone that were amalgamated with other fan deposits. The western hills (Figure 1.4 and Figure 5.1) show a lithological composition of alternating limestone, sandstone and mudstone. Hence, it has a lower resistive character compared to the thicker blocky limestone units to the east.

Within the developed 3D models, the Limestone HU was manually adjusted to HU3 (see Table 3.2). HU3 was assumed to have a mostly linear relationship with resistivity, with more massive (consolidated) limestone having higher resistivity and more permeable limestone having lower resistivity. However, there is a complication in that lower resistivity corresponds to more porous and/or more silt, while higher resistivity corresponds to more massive and/or less silt, as well as to outcropping limestone. As such, three threshold values were utilised to define an aquifer potential classification. The results largely show a higher aquifer potential in the eastern ranges than the western ranges, associated with the facies change across this area. Water resources will not be continuous throughout this consolidated unit.

3D digital datasets have been provided that describe these variations. See Section 5.2.4 for a further discussion on faulting.

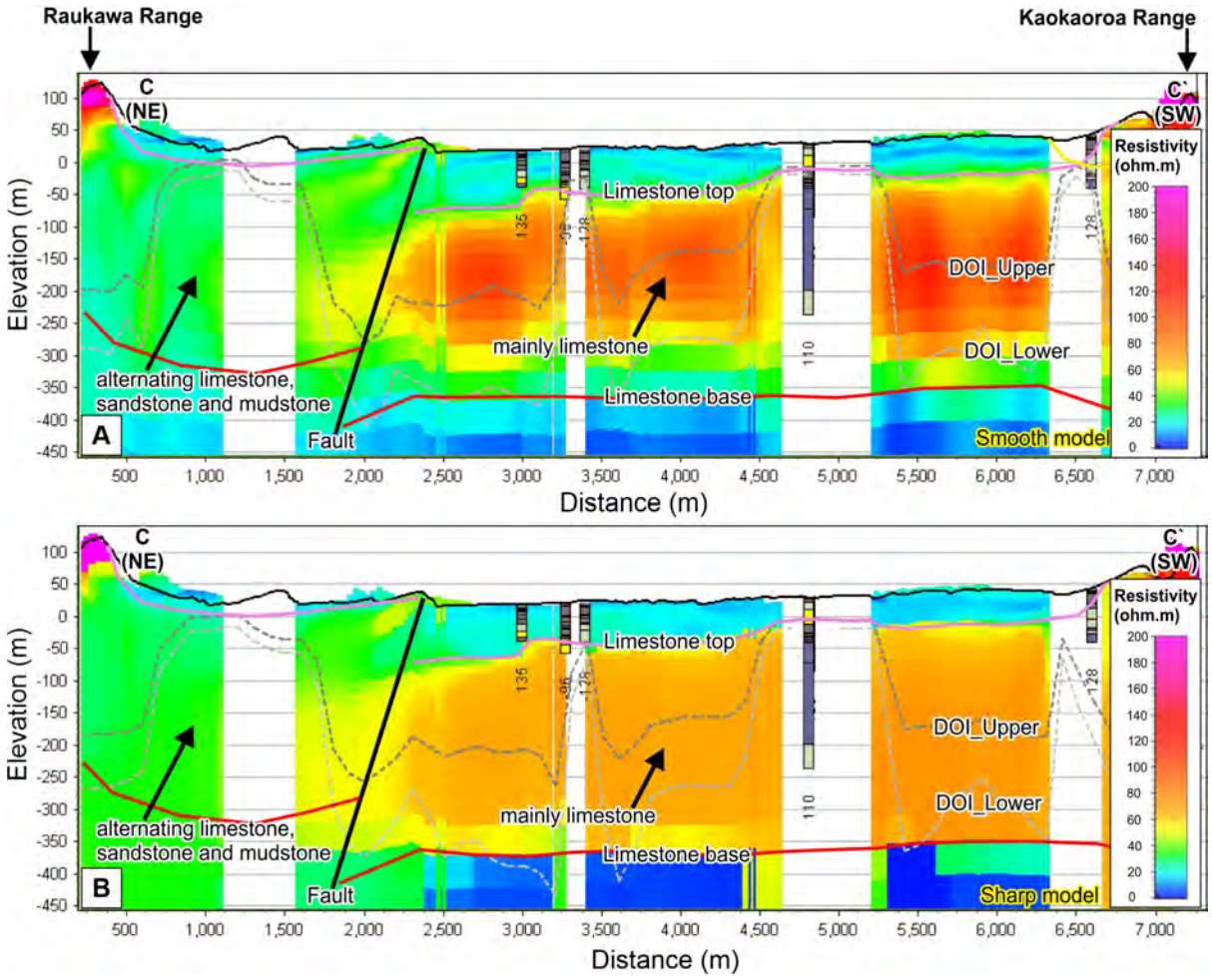

Figure 5.1 An example of a N–S profile showing resistivity variation within the Limestone HU in smooth and sharp resistivity models. See location of the profile C–C` in Figure 3.1.

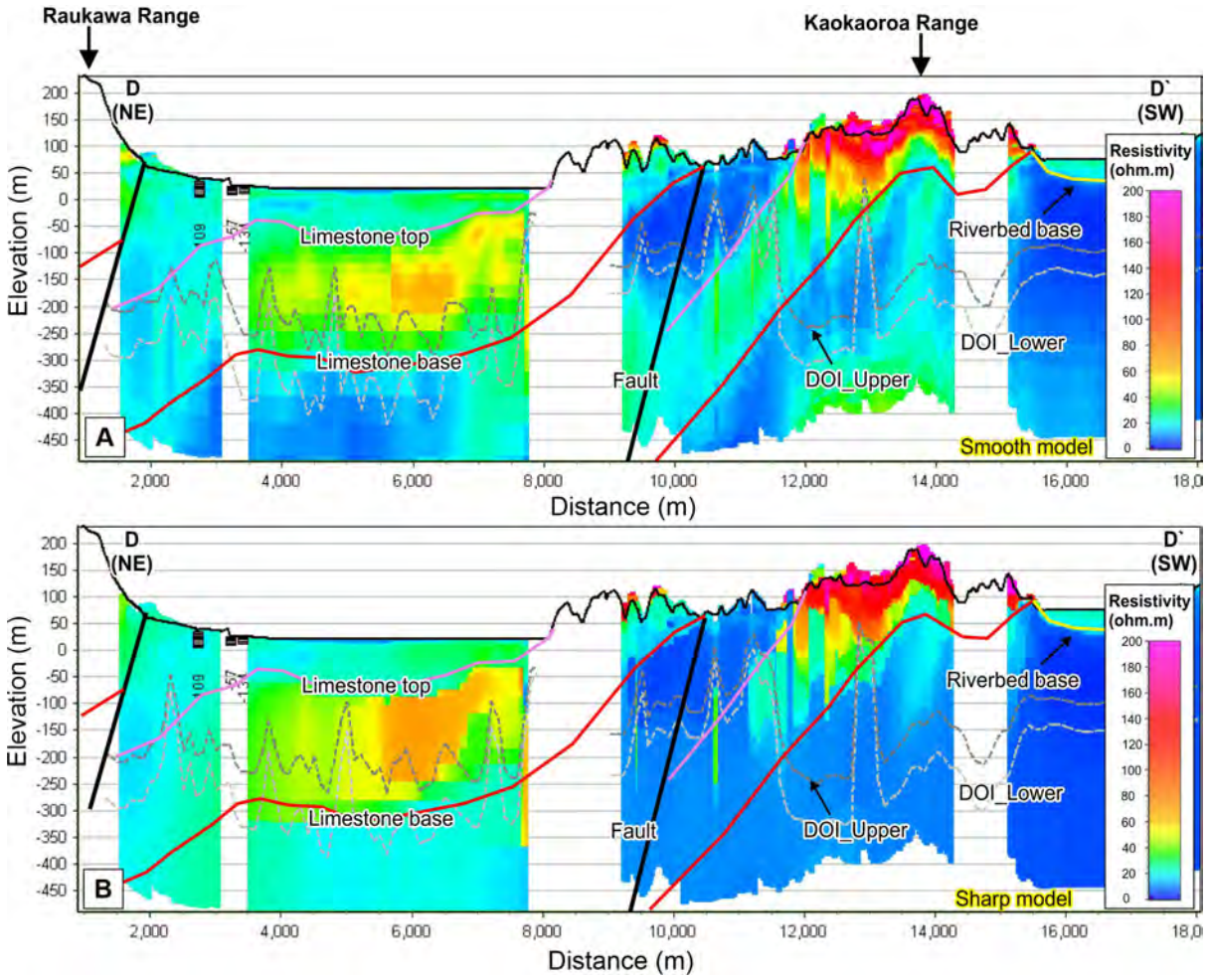

Figure 5.2 An example of the resistivity profiles showing identification of faults in the SkyTEM resistivity models. Sharp model shows a distinct resistivity contrast at the Limestone HU top compared to the smooth model. See location of the profile D–D` in Figure 3.1.

5.2.4 Delineation of Main Faults

Approximate positions of the faults are mapped on some of the resistivity profiles based on QMAP surface geology, shape of the terrain and distribution of the resistive units (Figure 3.2, Figures 5.1–5.3). Sharp resistivity models sometimes help to visualise sharp changes in resistivity and hence facilitates the mapping of the faults, while the smooth models can sometimes visualise the inclined changes better (Figure 5.3).

Faults observed in the dataset are reverse faults. In many cases, the resistivity models do not show a sharp depth shift of resistive units (representative of fault throw) along the fault zone. This could be related to the resolution of the SkyTEM data; structural complexity close to the faults, and hence variations in porosity and permeability within the limestone; and/or compositional variation within the limestone. Faults are better imaged close to the surface and become more difficult to discern with depth, probably due to the SkyTEM data resolution (e.g. Figure 5.3). Fault throw varies, and some of the mapped fault throws are up to 400 m.

Faults were not delineated as part of this work (due to scope); however, the observations above suggest that manual interpretation of faults could be used to assist with improving understanding of faults in the area.

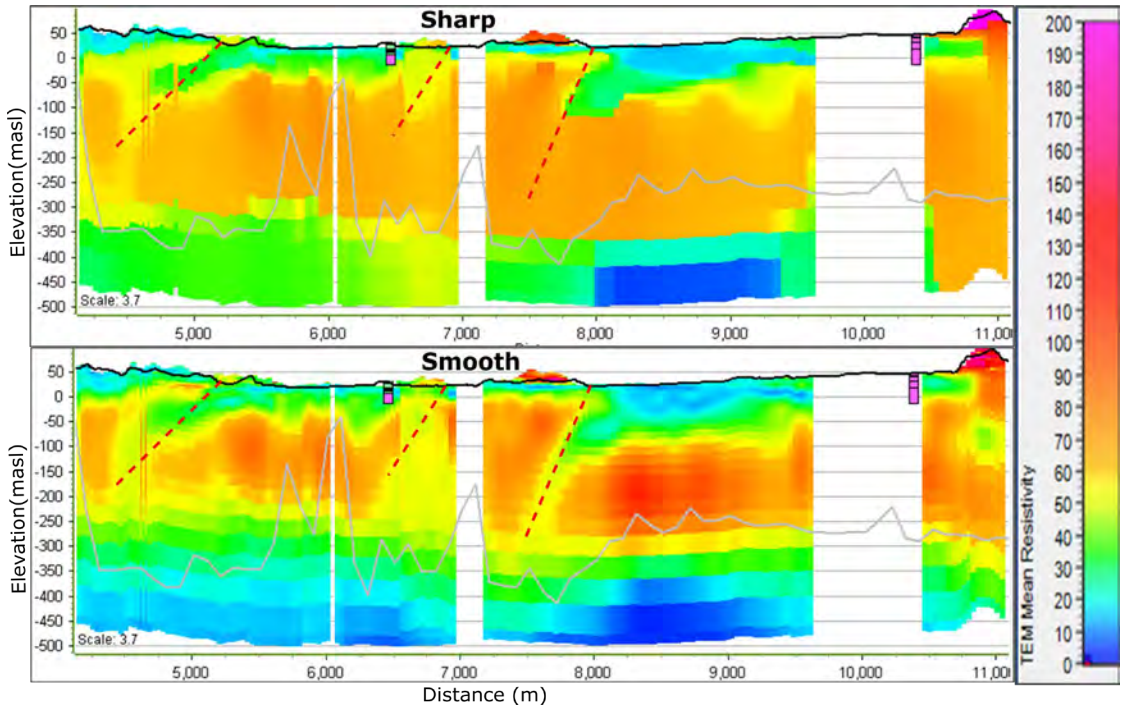

Figure 5.3 Profile examples of a sharp and smooth inversion of the same SkyTEM dataset showing resistivity in ohm.m. The grey line shows the depth of investigation. Dipping faults (approximate locations shown by the red dashed lines) are displayed in different ways by the smooth and sharp models. Figure from Rawlinson et al. (2021).

5.3 Poukawa Area

5.3.1 Thickness of Peat Layer

An assessment in Appendix 1 provided resistivity values for peat of 8.4–25.4 ohm.m (P0.1–P0.9, depth to peat) and 8.0–17.3 ohm.m (P0.1–P0.9, research lithological log, 80% threshold, smooth model). A visual inspection in Leapfrog software suggests that, where peat is reasonably thick, it appears to be well mapped by resistivity values <10 ohm.m. However, these resistivity ranges overlap too much with other units such as clay, so peat is not a distinct signal.

5.3.2 Connection to Heretaunga Plains

Previous groundwater modelling (Cameron et al. 2011) assumed that groundwater in the Poukawa Basin discharged into the Heretaunga Plains system near Pakipaki, following the Poukawa Stream. It was also considered possible that groundwater discharges from the basin at depth via the underlying sandstone or limestone (Cameron et al. 2011).

Resistivity data is limited near this northern outlet of the basin due to data removal associated with electromagnetic noise along SH 2 and the railway line. Additionally, interpretation of the hydrogeological unit in this area is complicated by the resistivity nature of the local sandstone- and limestone-derived sediments and complex relationships of logged lithological units (see Section 3.2.4.2). Both consolidated and unconsolidated sediments are classified here as having predominantly medium aquifer potential (see Section 3.2.4).

Connection to the Heretaunga Plains is considered likely through the sandstone and limestone. More detailed local studies in this area are recommended to unravel the complicated relationship of resistivity with the sandstone, limestone, sand, peat and siltstone logged materials in this area to better understand the near-surface materials.

5.3.3 Thickness of Any Unconfined Layer in the Poukawa Area

As discussed in Sections 3.2.4.2 and 5.3.2, this area has generally low resistivity values, and previous studies have suggested low-yielding and low-transmissivity aquifers. Additionally, lithological log descriptions consist of complex and discontinuous successions of thin intervals of sediments for which it is unclear whether they correspond to consolidated or unconsolidated sediments (described as, for example, limestone and sandstone). Neither the lithological logs nor the resistivity data indicate a significant unconfined aquifer, with most of the area classified as low to medium aquifer potential.

6.0 DIGITAL DELIVERABLES

All digital maps and data are geo-referenced to coordinate system New Zealand Transverse Mercator (NZTM 2000) and New Zealand Vertical Datum 2020 (NZVD2016).

6.1 3D-Gridded Products

A *.csv* file with all 3D models (see Table 4.2):

- *3D\Poukawa_SkyTEM_3Dmodels_V1_2024.csv*

Multi-band raster files for a selection of the 3D models, for numerical groundwater modelling and viewing in GIS. Each multi-band raster contains 421 bands in elevation order, where Band 1 = 331 mASL and Band 421 = -507 mASL, with each band consisting of a 2-m-thick vertical slice referenced to the cell centre. This elevation data is included within the metadata of the files:

- *3D\Poukawa_SkyTEM_res_V1_2024.tif*
- *3D\Poukawa_SkyTEM_resvar_V1_2024.tif*
- *3D\Poukawa_SkyTEM_HU_V1_2024.tif*
- *3D\Poukawa_SkyTEM_AP_V1_2024.tif*
- *3D\Poukawa_SkyTEM_facies_V1_2024.tif*

6.2 2D Maps

2D map products provided in raster and GIS polygon formats.

Boundary surfaces, which are delivered in the readily accessible ascii grid format (with 10 m resolution):

- *2D\Lst_top_V1_2024.asc*
- *2D\Lst_base_V1_2024.asc*
- *2D\Riverbed_base_V1_2024.asc*

Depth and thickness maps, derived from the boundary surfaces:

- *2D\RiverbedHU_thickness_V1_2024.asc*
- *2D\SwampFanHU_thickness_V1_2024.asc*
- *2D\LimestoneHU_thickness_V1_2024.asc*
- *2D\DepthtoLimestoneHU_V1_2024.asc*
- *2D\DepthtoBasementHU_V1_2024.asc*

Model area:

- *2D\Poukawa_SkyTEM_modelarea.shp*

Near-surface properties – '*' corresponds to one of *res, facies* and *AP.* Values are provided for both the harmonic mean (*hmean*) and the geometric mean (*gmean*):

- *2D\Poukawa_SkyTEM_upper5m_hmean_*_V1_2024.tif*
- *2D\Poukawa_SkyTEM_upper10m_hmean_*_V1_2024.tif*
- *2D\Poukawa_SkyTEM_upper15m_hmean_*_V1_2024.tif*

- *2D\Poukawa_SkyTEM_upper20m_hmean_*_V1_2024.tif*
- *2D\Poukawa_SkyTEM_upper30m_hmean_*_V1_2024.tif*
- *2D\Poukawa_SkyTEM_upper50m_hmean_*_V1_2023.tif*
- *2D\Poukawa_SkyTEM_upper75m_hmean_*_V1_2023.tif*
- *2D\Poukawa_SkyTEM_upper100m_hmean_*_V1_2024.tif*
- *2D\Poukawa_SkyTEM_upper150m_hmean_*_V1_2023.tif*

6.3 Supporting Datasets

A 10 m DEM used for 3D model clipping at the ground surface:

- *Supporting\PoukawaSkyTEM_DEM_10m.asc*

Manual interpretation points that were used to generate the boundary surfaces are provided as x,y,z *.csv files:

- *Supporting\Lst_top_points_V1_2024.csv*
- *Supporting\Lst_base_points_V1_2024.csv*
- *Supporting\Riverbed_base_points_V1_2024.csv*

A Leapfrog viewer file containing the DEM, lithological logs and a selection of the 3D models as block models:

- *Supporting\PoukawaSkyTEM_LeapfrogViewer.lfview*

A colour reference file for webmap display:

- *Supporting\Poukawa_webmap_colours.csv*

7.0 CONCLUSIONS AND RECOMMENDATIONS

Three manually delineated surfaces were utilised to separate the study area into major hydrogeological units and to delineate limestone. 3D model datasets were combined within a *.csv* file, with x,y,z defining the centre of each grid cell and including the following parameters: *X*, *Y*, *Z*, *top_elev_HU*, *res*, *resvar*, *HU*, *facies*, *AP*, *aq*. Models were defined through interpolation and using an automated thresholding approach. A selection of these models was converted to multi-band raster format. The 3D models utilise 50 x 50 m grid cells horizontally and 2-m-thick grid cells vertically.

The combined approach of manual delineation and automated thresholding was considered an effective way to deal with a resistivity dataset that displayed many overlapping values from different lithological units, limited supporting datasets and non-linear relationships between resistivity and permeability in some areas.

After the completion of the draft version of this report, it was determined that a separation between unconsolidated and consolidated sediments would be valuable for online 3D model visualisation purposes. To preserve results related to the objective of mapping depth to limestone, adjustments to improve the separation of consolidated and unconsolidated sediments were only undertaken on the gridded 3D models. This results in some differences between the HU 3D model and the manual surfaces.

Uncertainties are present in the resistivity models, the manually delineated major hydrogeological units, and the categories defined within each hydrogeological unit. However, the datasets enable a 3D view of the subsurface geology and hydrogeology not previously possible, providing refinement of the existing understanding of groundwater resources in the Poukawa and Otane basins. Additionally, simplifications of the 3D models to 2D maps can assist with more readily investigating various aspects of the groundwater systems. The models can also support a greater understanding of other datasets and could be used to guide additional data collection with greater precision.

Recommendations

- Additional drilling would be advantageous to refine interpretations in the future, particularly in the sandstone-dominated northern part of the Poukawa Basin.
- Additional electromagnetic measurements on local material would be advantageous to refine material ranges, using, for example, ground TEM, direct-current resistivity (on material samples or 2D surveys) or borehole resistivity logging.
- Smaller areas could be studied in more detail to undertake fault delineation and refine relationships between the resistivity values and the local materials.
- Additional information that would be of value to improving the quality of modelling includes GPS-located borehole information with high-quality lithological logs and screen location information.
- Additional manual revisions to the HU 3D model could be undertaken for refinements.

8.0 ACKNOWLEDGEMENTS

This work has been jointly funded by the New Zealand Government's Provincial Growth Fund, Hawke's Bay Regional Council and GNS Science's Strategic Science Investment Fund (Ministry of Business, Innovation & Employment).

Thank you to Simon Harper and Tim Farrier (digital elevation model) of Hawke's Bay Regional Council, as well as Jeff Smith (previously at Hawke's Bay Regional Council) for their contributions to this project. Thank you to Amanda Langley of Project Haus for project management support.

Thank you to Chris Worts for business partnerships support. Thank you to Jesper Pedersen and Nikolaj Foged of Aarhus University for reviewing an early draft of this report. Thank you to Conny Tschritter and Rogier Westerhoff for providing report reviews, and to Angela Griffin and Maïwenn Herpe for contributions to preparation of the research lithological log descriptions and figures.

9.0 REFERENCES

Archie GE. 1942. The electrical resistivity log as an aid in determining some reservoir characteristics. *Transactions of the AIME*. 146(1):54–62. https://doi.org/10.2118/942054-g

Auken E, Christiansen AV, Westergaard JH, Kirkegaard C, Foged N, Viezzoli A. 2009. An integrated processing scheme for high-resolution airborne electromagnetic surveys, the SkyTEM system. *Exploration Geophysics*. 40(2):184–192. https://doi.org/10.1071/EG08128

Barber J. 2019. Papanui catchment groundwater study: dissolved reactive phosphorus. Napier (NZ): Hawke's Bay Regional Council. 33 p. Report 5397-RM19-244.

Beu AG. 1995. Pliocene limestones and their scallops: lithostratigraphy, pectinid biostratigraphy and paleogeography of eastern North Island Late Neogene limestone. Lower Hutt (NZ): Institute of Geological & Nuclear Sciences. 243 p. (Institute of Geological & Nuclear Sciences monograph; 10).

Beanland S, Melhuish A, Nicol A, Ravens J. 1998. Structure and deformational history of the inner forearc region, Hikurangi subduction margin, New Zealand. *New Zealand Journal of Geology and Geophysics*. 41(4):325–342. https://doi.org/10.1080/00288306.1998.9514814

Brown LJ, Cameron SG, Morgenstern U. 1998. Availability of a sustainable groundwater resource in the Poukawa Basin, Hawke's Bay. [Lower Hutt (NZ)]: Institute of Geological & Nuclear Sciences. Client Report 53853C.12.

Cameron SG. 2002. Assessment of effects of pumping groundwater from bore 4683 on Lake Poukawa, Hawke's Bay. Wairakei (NZ): Institute of Geological & Nuclear Sciences. 31 p. Client Report 2002/16. Prepared for Trevor Good.

Cameron SG, Gusyev MA. 2011a. Assessment of effects of pumping Brownrigg Agriculture wells on the Poukawa Basin using a pseudo-transient groundwater-surface water interaction model. Wairakei (NZ): GNS Science. 19 p. Consultancy Report 2011/309. Prepared for Brownrigg Agriculture.

Cameron SG, Gusyev MA. 2011b. Poukawa Basin groundwater model pumping scenarios. Wairakei (NZ): GNS Science. 42 p. Consultancy Report 2011/226. Prepared for Hawke's Bay Regional Council.

Cameron SG, Minni G. 2009. Modelled cumulative affects of pumping Brownrigg Agriculture wells on groundwater and surface resources in the Poukawa basin. Wairakei (NZ): GNS Science. 15 p. Consultancy Report 2009/335. Prepared for Brownrigg Agriculture.

Cameron SG, Reeves RR. 2004. Predicted cumulative affects of pumping Brownrigg Agriculture bores on spring and stream flow, and Lake Poukawa inflow and outflow. Wairakei (NZ): Institute of Geological & Nuclear Sciences. 19 p. Client Report 2004/05. Prepared for Brownrigg Agriculture.

Cameron SG, White PA. 1999. Assessment of effects of pumping groundwater on Lake Poukawa, Hawke's Bay. Wairakei (NZ): Institute of Geological & Nuclear Sciences. 54 p. + appendices. Client Report 1999/114. Prepared for Brownrigg Agriculture.

Cameron SG, White PA. 2001. Brownrigg Agriculture bore 4667: assessment of effects of pumping groundwater on Lake Poukawa, Hawke's Bay. Wairakei (NZ): Institute of Geological & Nuclear Sciences. 45 p. Client Report 2001/119. Prepared for: Brownrigg Agriculture.

Cameron SG, Gusyev MA, Meilhac C, Minni G, Zemansky GM. 2011. Pseudo-transient groundwater-stream interaction model for determination of the effect of groundwater abstraction on spring-fed stream flow in the Poukawa basin, Hawke's Bay. Lower Hutt (NZ): GNS Science. 76 p. (GNS Science report; 2011/07).

Cashman SM, Kelsey HM. 1990. Forearc uplift and extension, southern Hawke's Bay, New Zealand: mid-Pleistocene to present. *Tectonics*. 9(1):23–44. https://doi.org/10.1029/TC009i001p00023

Dravid D. 1993. Geology and groundwater conditions around Lake Poukawa, southern Hawke’s Bay. Napier (NZ): Hawke’s Bay Regional Council. Brief Report.

Farrier T. 2020. 3D Aquifier Mapping Project DEM Version 2. Napier (NZ): Hawke’s Bay Regional Council.

Fellows DL. 1984. Lake Poukawa drilling project. Located at: GNS Science, Lower Hutt, NZ; New Zealand Geological Survey Immediate Report EDS 84/14. 14 p.

Glover PWJ. 2016. Archie's law – a reappraisal. *Solid Earth*. 7(4):1157–1169. https://doi.org/10.5194/se-7-1157-2016

Harper MA, Howorth R, McLeod M. 1986. Late Holocene diatoms in Lake Poukawa: effects of airfall tephra and changes in depth. *New Zealand Journal of Marine and Freshwater Research*. 20(1):107–118. https://doi.org/10.1080/00288330.1986.9516135

Harper S. 2012. Tukituki catchment groundwater resources. Napier (NZ): Hawke’s Bay Regional Council. 27 p. Technical report EMT 13/01.

Harper S. 2019. Personal communication: HBRC datasets [provided 2019 Dec]. Senior Scientist, Environmental Science; Hawke’s Bay Regional Council, Napier, NZ.

Heise W, Ogawa Y, Bertrand EA, Caldwell TG, Yoshimura R, Ichihara H, Bennie SL, Seki K, Saito Z, Matsunaga Y, et al. 2019. Electrical resistivity imaging of the inter-plate coupling transition at the Hikurangi subduction margin, New Zealand. *Earth and Planetary Science Letters*. 524:115710. https://doi.org/10.1016/j.epsl.2019.115710

Heron DW, custodian. 2020. Geological map of New Zealand. 3rd ed. Lower Hutt (NZ): GNS Science. 1 USB, scale 1:250,000. (Institute of Geological & Nuclear Sciences 1:250,000 geological map; 1).

Hill R, Borman D, Singleton P. 2020. Hawke’s Bay peatland survey 2018. Napier (NZ): Hawke’s Bay Regional Council. 47 p. Publication 5356.

Howorth R, Froggatt PC, Robertson SM. 1980. Late Quaternary volcanic ash stratigraphy of the Poukawa area, Central Hawke's Bay, New Zealand. *New Zealand Journal of Geology and Geophysics*. 23(4):487–491. https://doi.org/10.1080/00288306.1980.10424119

Hull AG. 1990. Tectonics of the 1931 Hawke's Bay earthquake. *New Zealand Journal of Geology and Geophysics*. 33(2):309–320. https://doi.org/10.1080/00288306.1990.10425689

Jellyman D, Sykes J. 2009. The eel (tuna) stocks of Lake Poukawa, Hawkes Bay. Christchurch (NZ): National Institute of Water & Atmospheric Research. 37 p. Client Report CHC2009-172. Prepared for Te Ohu Kai Moana Poukawa 13B Trust.

Kelsey HM, Erdman CF, Cashman SM. 1993. Geology of southern Hawkes Bay from the Maraetotara Plateau and Waipawa westward to the Wakarara Range and the Ohara Depression. Lower Hutt (NZ): Institute of Geological & Nuclear Sciences. 17 p. (Institute of Geological & Nuclear Sciences science report; 93/02).

Kelsey HM, Hull AG, Cashman SM, Berryman KR, Cashman PH, Trexler JH, Jr., Begg JG. 1998. Paleoseismology of an active reverse fault in a forearc setting: the Poukawa fault zone, Hikurangi forearc, New Zealand. *GSA Bulletin*. 110(9):1123–1148. https://doi.org/10.1130/0016-7606(1998)110<1123:Poaarf>2.3.Co;2

Kingma JT. 1971. Geology of the Te Aute subdivision. Lower Hutt (NZ): New Zealand Geological Survey. 173 p. (New Zealand Geological Survey bulletin; 70).

Lawrence MJF, Herpe M, Kellett RL, Pradel GJ, Sanders F, Coup L, Rawlinson ZJ, Reeves RR, Brakenrig T, Cameron SG, et al. 2022a. Hawke's Bay 3D Aquifer Mapping Project: drilling completion report for borehole 17136 (3DAMP_Well1), Ongaonga-Waipukurau Road, Ruataniwha Plains. Lower Hutt (NZ): GNS Science. 156 p. Consultancy Report 2022/31. Prepared for Hawke's Bay Regional Council.

Lawrence MJF, Herpe M, Pradel GJ, Kellett RL, Coup L, Sanders F, Rawlinson ZJ, Reeves RR, Brakenrig T, Cameron SG, et al. 2022b. Hawke's Bay 3D Aquifer Mapping Project: drilling completion report for borehole 17164 (3DAMP_Well3), Burnside Road, Ruataniwha Plains. Lower Hutt (NZ): GNS Science. 76 p. Consultancy Report 2022/15. Prepared for Hawke's Bay Regional Council.

Lee JM, Bland KJ, Townsend DB, Kamp PJJ, compilers. 2011. Geology of the Hawke's Bay area [map]. Lower Hutt (NZ): GNS Science. 1 folded map + 93 p., scale 1:250,000. (Institute of Geological & Nuclear Sciences 1:250,000 geological map; 8).

Lowrie W. 2006. Fundamentals of geophysics. 7th ed. Cambridge (GB): Cambridge University Press. 354 p.

Madarasz-Smith A, Wade O, Wade H, Hicks A. 2016. The estuaries of the TANK catchments: Ahuriri and Waitangi estuaries, values, state and trends. Napier (NZ): Hawke's Bay Regional Council. 118 p. HBRC Report RM 16-20.

Minsley BJ, Rigby JR, James SR, Burton BL, Knierim KJ, Pace MDM, Bedrosian PA, Kress WH. 2021. Airborne geophysical surveys of the lower Mississippi Valley demonstrate system-scale mapping of subsurface architecture. *Communications Earth & Environment*. 2(1):131. https://doi.org/10.1038/s43247-021-00200-z

Morgenstern U, Gordon D. 2017. Water and nutrient flow pathways in the Papanui Catchment: source, mean residence time, and connection between ground- and surface-water. Lower Hutt (NZ): GNS Science. 27 p. (GNS Science report; 2017/08). https://doi.org/10.21420/G2KG6G

Rattenbury MS, Heron DW. 1997. Revised procedures and specifications for the QMAP GIS. Lower Hutt (NZ): Institute of Geological and Nuclear Sciences. 52 p. (Institute of Geological & Nuclear Sciences science report; 97/03).

Rawlinson Z. 2013. A review of the most effectual and economical geophysical techniques for characterising groundwater within New Zealand. Lower Hutt (NZ): GNS Science. 90 p. (GNS Science report; 2013/38).

Rawlinson Z. 2023. Hawke's Bay 3D Aquifer Mapping Project: 3D hydrogeological models from SkyTEM data in the Heretaunga Plains. Wairakei (NZ): GNS Science. 69 p. Consultancy Report 2023/57. Prepared for Hawke's Bay Regional Council.

Rawlinson Z. 2024. Hawke's Bay 3D Aquifer Mapping Project: 3D hydrogeological models from SkyTEM data in the Ruataniwha Plains. Wairakei (NZ): GNS Science. 62 p. Consultancy Report 2023/117. Prepared for Hawke's Bay Regional Council.

Rawlinson ZJ, Westerhoff RS, Kellett RL, Pederson JB, Maurya PK, Foged N. 2021. Hawke's Bay 3D Aquifer Mapping Project: Poukawa and Otane Basin SkyTEM data processing and resistivity models. Wairakei (NZ): GNS Science. 76 p. Consultancy Report 2020/138. Prepared for Hawke's Bay Regional Council.

Rissmann C, Lovett AP. 2016. Hydrochemical analysis for the Otane Waste Water Treatment Plant. Lower Hutt (NZ): GNS Science. 27 p. Consultancy Report 2016/83. Prepared for Hawke's Bay Regional Council.

Robertson SM. 1978. Study of the Late Quaternary history of Poukawa Basin. [MSc thesis]. Wellington (NZ): Victoria University of Wellington. 178 p.

Robertson SM, Howorth R. 1980. Core descriptions for three stratigraphic holes drilled near Lake Poukawa, Hawke's Bay, New Zealand. Wellington (NZ): Victoria University of Wellington. 19 p. (Publication of Geology Department, Victoria University of Wellington; 19).

Robinson PH, Hull AG, Jaegers A. 1984. The lithologic log of Lake Poukawa drilling project hole 5 (LPDP-5) Central Hawkes Bay, New Zealand. Lower Hutt (NZ): New Zealand Geological Survey. 25 p. Report G 92.

Shane P, Lian OB, Augustinus P, Chisari R, Heijnis H. 2002. Tephrostratigraphy and geochronology of a ca. 120 ka terrestrial record at Lake Poukawa, North Island, New Zealand. *Global and Planetary Change*. 33(3–4):221–242. https://doi.org/10.1016/S0921-8181(02)00079-6

Shulmeister J, Dickinson W, Dolan J, Jahnke M, Langdale S, Shaw S. 1998. Graphical log, photographs and background information for Lake Poukawa core 97-1, Hawke's Bay, New Zealand. Wellington (NZ): Victoria University of Wellington. 86 p. (Geology Board of Studies Publication; no. 20).

SkyTEM Australia Pty Ltd. [2020]. Acquisition and processing report: SkyTEM helicopter EM survey, Hawkes Bay, NZ. Malaga (AU): SkyTEM Australia Pty Ltd. 33 p. Report AUS 10056. Prepared for Hawke's Bay Regional Council.

Sørensen KI, Auken E. 2004. SkyTEM – a new high-resolution helicopter transient electromagnetic system. *Exploration Geophysics*. 35(3):194–202. https://doi.org/10.1071/EG04194

APPENDICES

This page left intentionally blank.

APPENDIX 1 ASSESSMENT OF RESISTIVITY VALUES WITHIN THE VICINITY OF DATASETS RELEVANT TO HYDROGEOLOGY

Datasets were compared to resistivity values to assess relationships between them of relevance to hydrogeological interpretation. The following datasets were considered:

- Surface geological map (QMAP)
- Water levels
- Measured groundwater electrical conductivity
- Peat depths
- Water takes
- Research lithological logs
- Hawke's Bay Regional Council (HBRC) Well database.

Data manipulation for this assessment utilised a combination of ArcGIS software and Python scripts. Unless specified otherwise, the resistivity data files *Poukawa_smooth_resistivitymodel_V1_2020_inv.xyz* and *Poukawa_sharp_resistivitymodel_V1_2020_inv.xyz* (Rawlinson et al. 2021) were imported into Python as 'pandas' DataFrames for assessment (pandas is a Python library for data analysis). Where required, other datasets were prepared in ArcGIS software before being exported as *.csv* files. As for the resistivity data files, these *.csv* files were imported into Python as pandas DataFrames for assessment. Throughout the following text, P0.1 and P0.9 refer to the 10% and 90% percentiles.

Values from both the smooth and sharp resistivity models were analysed together initially. After a comparative analysis, it was determined that the smooth resistivity model provided finer-detailed discrimination (also expected based on the different algorithms used to derive these models), so an additional assessment of just values from the smooth resistivity model was also performed.

A1.1 Surface Geological Map (QMAP)

Surface geological (QMAP) information (Heron 2020) was assessed to provide information on likely resistivity ranges for geological and lithological units. Due to the spatial uncertainty of mapped QMAP units (250 m; Rattenbury and Heron 1997), QMAP polygons were utilised to create smaller polygons (boundary – 250 m inner buffer) within ArcGIS. A point shapefile of the resistivity model locations was created and, within ArcGIS, the 'Extract values to points' tool was used to assign QMAP information to the point shape file. The full surface resistivity dataset consisted of 26,449 points but, by limiting the selection to greater than 250 m from a QMAP polygon boundary, the dataset was reduced to 10,613 points.

QMAP 'mainrock' information was used to assign lithologies to the resistivity dataset, except, where 'mainrock' was limestone and 'subrocks' were sandstone, this was classed as sandstone; and where 'mainrock' was claystone, this was classed as mudstone (Figures A1.1 and A1.2). In total, five main lithologies were utilised: limestone, sandstone, mudstone, gravel and peat.

Based on the surface-geological nature of QMAP (mapped surface geology is expected to correspond to the dominant geological unit in the top 10 m; Rattenbury and Heron 1997), approximately the top 10 m of data was used for this assessment (resistivity model layers 1–7). Additionally, a deeper assessment of approximately the top 50 m was used (resistivity

model layers 1–17) to allow an assessment of non-weathered material within the consolidated rock units (e.g. limestone, sandstone, mudstone). Statistical results and histograms of the results are shown in Figures A1.3 and A1.4 and Table A1.1.

Unfortunately, the QMAP main rock lithologies are not end members. Areas with a main rock type of gravel have a longer description of alluvial gravel, sand and mud; or lacustrine and fluvial sediments (sandstone, mudstone, tephra, silt, lignite); or moderately weathered gravel (with sand, silt, pumice and clay). Additionally, mapped mainrock type sandstone has subrocks of mudstone, siltstone, limestone and shell beds; and mapped mainrock type mudstone has subrocks of sandstone, limestone and marl. This ambiguity of the geological map can be seen particularly in the overlap of values between peat, gravel, mudstone, limestone and sandstone in the 0–30 ohm.m range:

- Mudstone ranges from 7.1 to 22.6 ohm.m (Table A1.1; *Mudstone_50m*, P0.1–P0.9).
- Peat ranges from 9.6 to 24.8 ohm.m (Table A1.1; *Peat_10m*, P0.1–P0.9).
- Gravel ranges from 9.9 to 103.3 ohm.m (Table A1.1; *Gravel_10m*, P0.1–P0.9).
- Sandstone ranges from 5.5 to 30.6 ohm.m (Table A1.1; *Sandstone_50m*, P0.1–P0.9).
- Limestone ranges from 26.4 to 238.5 ohm.m (Table A1.1; *Limestone_50m*, P0.1–P0.9).

Due to the expected continuity of geological material, consolidated rock units were summarised using resistivity data from the top 50 m, whereas softer unconsolidated units were summarised using resistivity data from the top 10 m. An analysis of resistivity values only within the smooth model provided only very minor differences in value ranges. Some preliminary simplified expectations can be set by this assessment:

- Values <10 ohm.m are most likely to be mudstone or sandstone.
- Values 10–30 ohm.m are most likely to be mudstone, peat, gravel or sandstone.
- Values >30 ohm.m are most likely to be gravel or limestone.

These values are consistent with the typical ranges seen in Figure 1.3 for peat (lignite) sandstone, mudstone (shale) and limestone (porous). The lower-end values for gravel are much lower than the ranges seen in Figure 1.3 but compare well to the ranges for silty sand and saturated silt and clay. The higher-end values for gravel are consistent with saturated gravel in Figure 1.3. This is consistent with the view that the QMAP gravel main rock type is likely to be a significant over-simplification in this area due to the depositional environment.

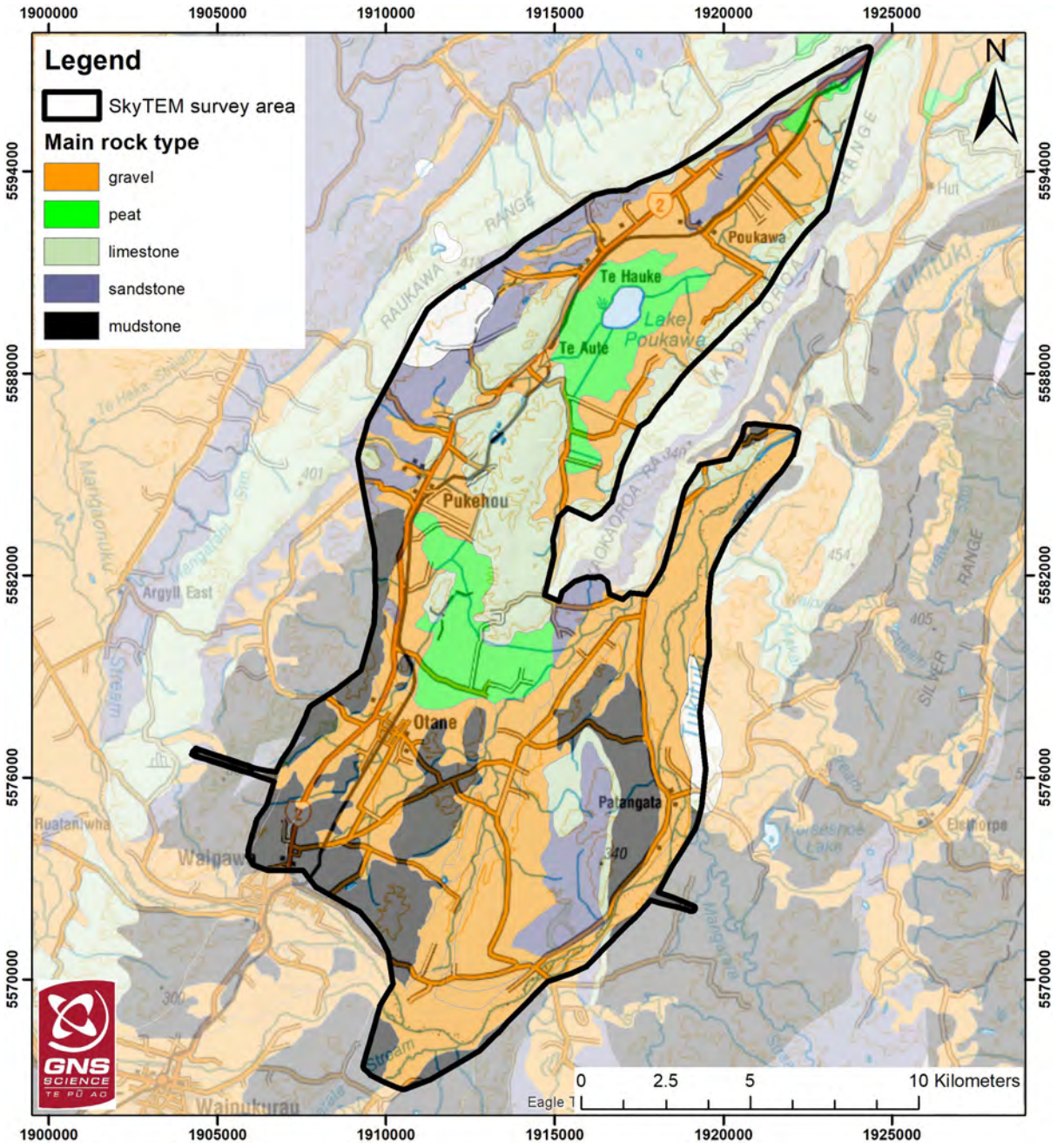

Figure A1.1 QMAP surface geological map simplified to main rock type.

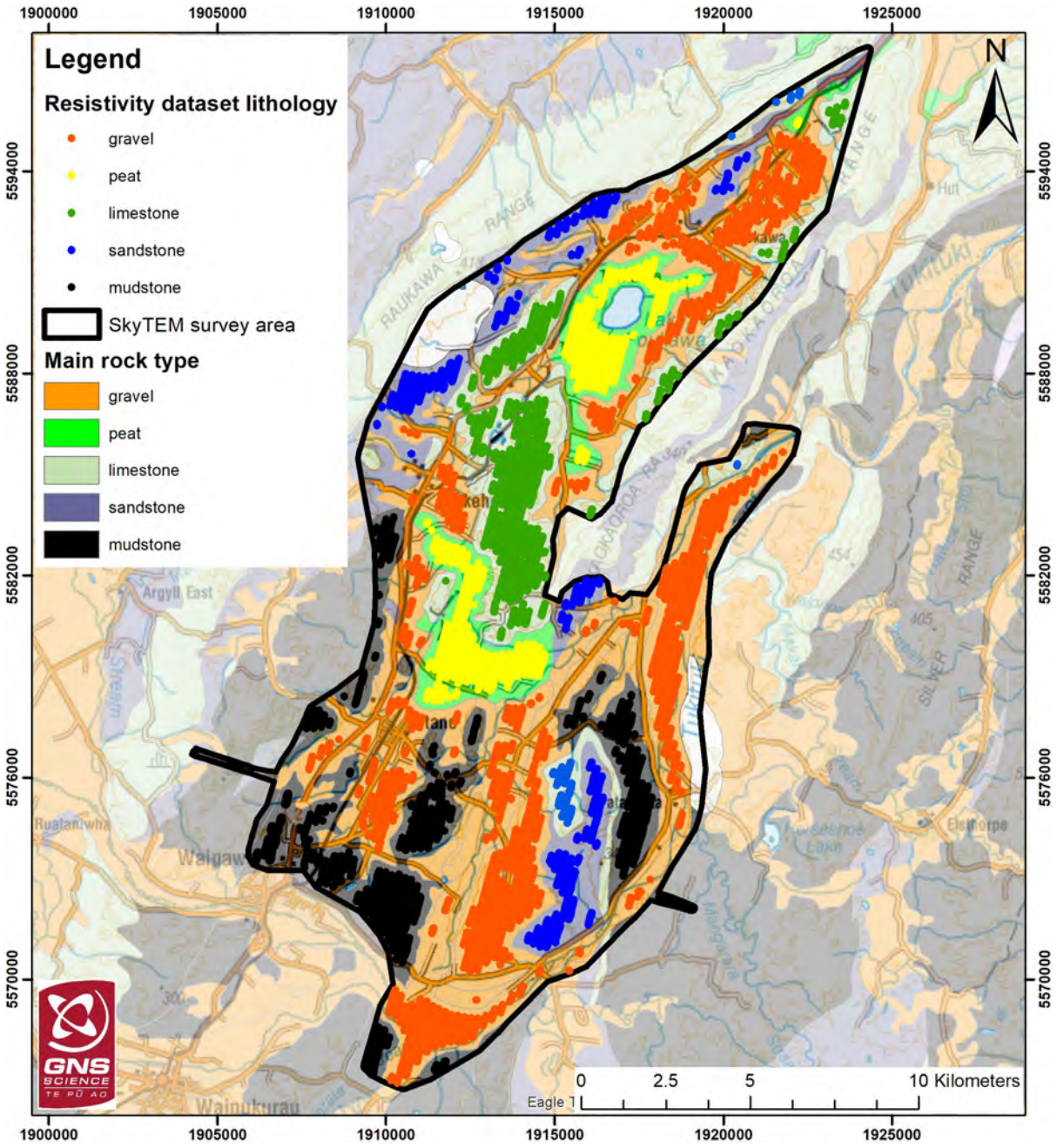

Figure A1.2 Resistivity model points within QMAP polygons (>250 m from polygon boundaries), assigned lithology type.

Table A1.1 QMAP lithological unit resistivity statistics in ohm.m for resistivity layers down to approximately 10 m (*_10m*) and 50 m (*_50m*). P0.1 and P0.9 refer to the 10% and 90% percentiles. Rows are coloured by main rock type to match Figures A1.3 and A1.4. STD = standard deviation. MAD = mean absolute deviation.

Lithology	Min.	Max.	P0.1	P0.9	Mean	STD	Median	MAD	N
Peat_10m	4.4	45.1	9.6	24.8	16.9	5.9	16.7	4.8	13,755
Peat_ 50m	3.4	125.1	10.7	28.4	20.6	10.0	19.8	6.4	33,405
Gravel_10m	2.8	311.0	9.9	103.3	37.8	41.0	20.2	29.8	42,336
Gravel_50m	2.7	311.0	6.3	79.2	31.0	35.5	18.7	23.7	102,816
Limestone_10m	7.6	1873.0	29.2	254.8	144.2	112.2	135.4	80.7	15,085
Limestone_50m	5.7	1873.0	26.4	238.5	135.3	102.0	128.8	76.0	36,635
Mudstone_10m	1.3	551.9	8.8	30.4	19.9	27.0	15.4	9.6	18,872
Mudstone_50m	1.3	551.9	7.1	22.6	15.3	18.5	12.9	6.4	45,832
Sandstone_10m	2.3	752.7	7.3	32.8	22.4	34.8	17.4	12.7	9,660
Sandstone_50m	2.3	752.7	5.5	30.6	19.4	34.1	13.1	12.7	23,460

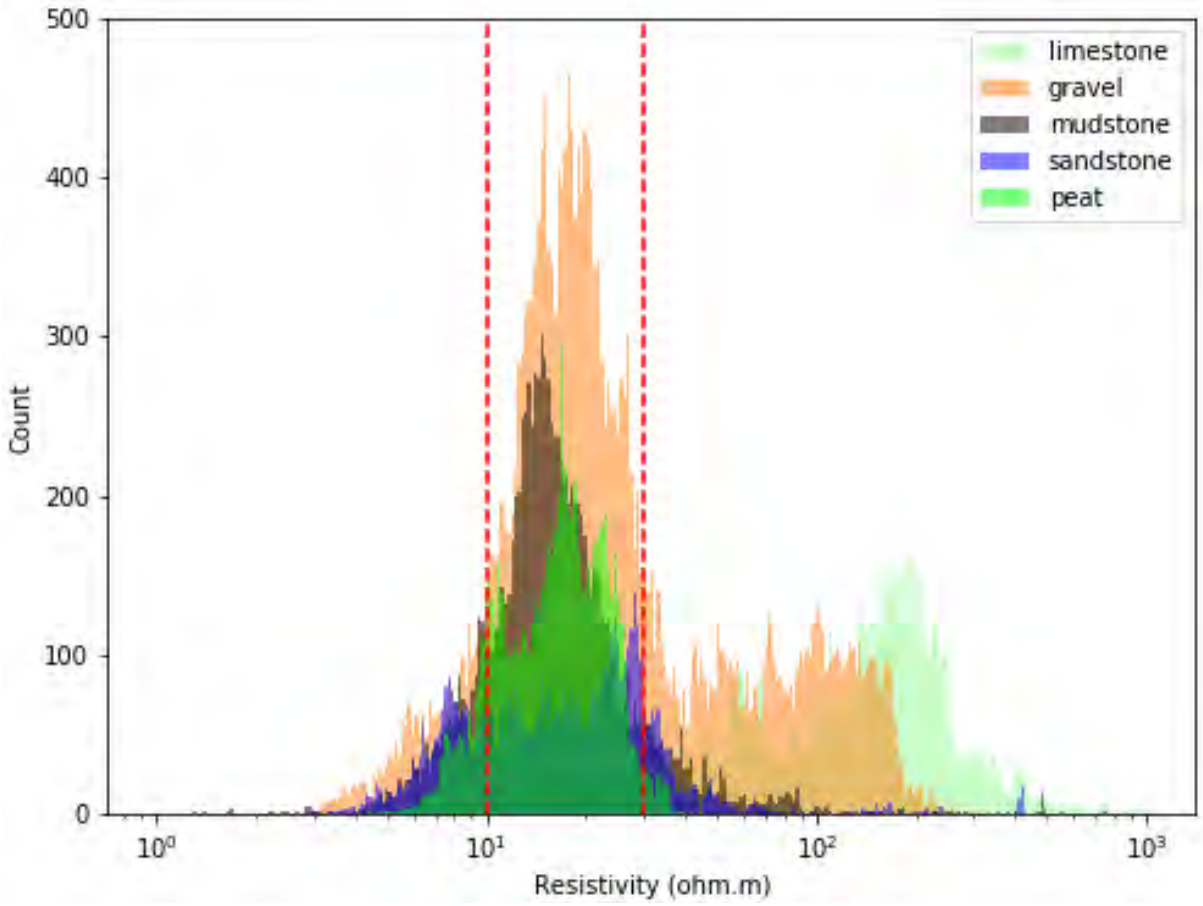

Figure A1.3 Top 10 m of resistivity values for mapped QMAP lithologies. The range from 1 to 1000 is binned for histograms into 300 bins. For reference, red dashed lines are placed at 10 and 30 ohm.m.

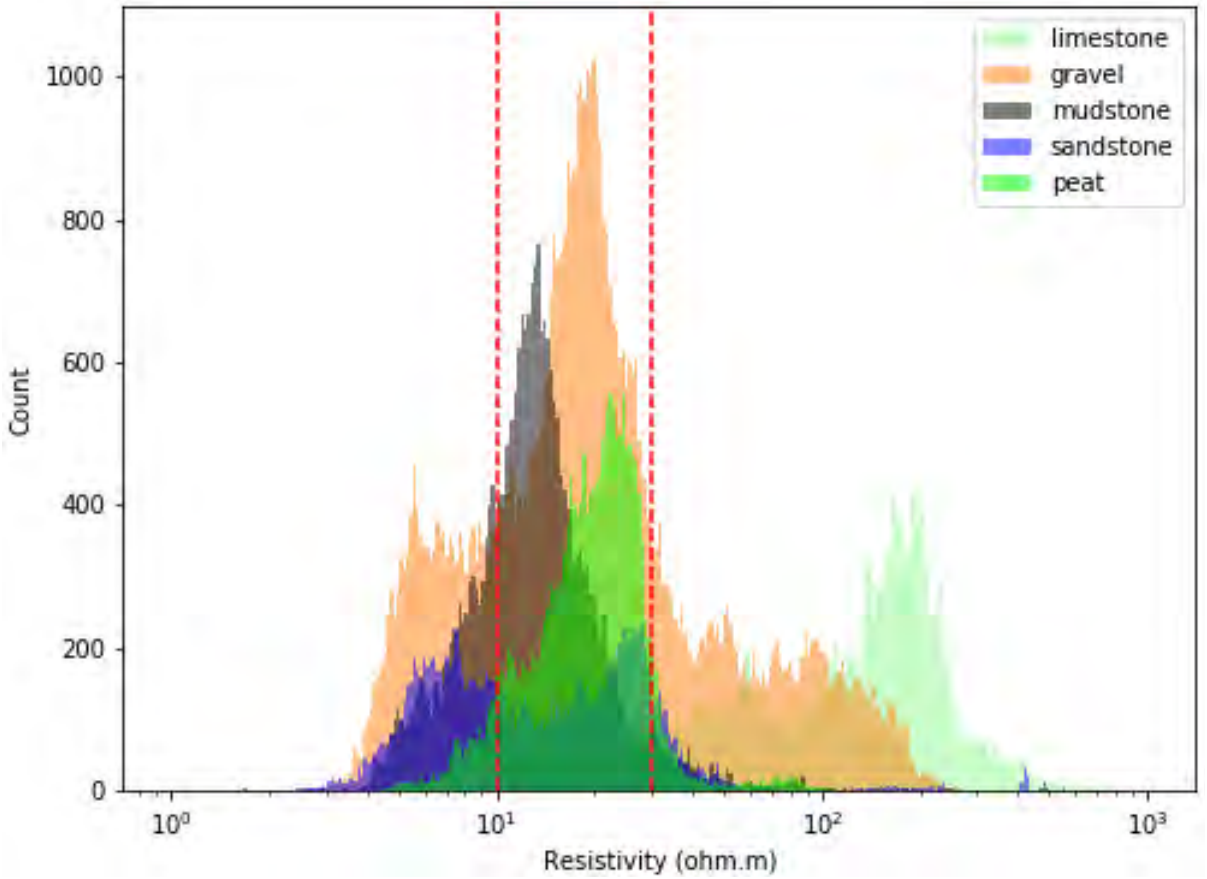

Figure A1.4 Top 50 m of resistivity values for mapped QMAP lithologies. The range from 1 to 1000 is binned for histograms into 300 bins. For reference, red dashed lines are placed at 10 and 30 ohm.m.

A1.2 Water Levels

Due to the shallow lake depth (see Section 2.2), Lake Poukawa is not expected to have a significant impact on the resistivity model. No groundwater-level measurements are available for the unconfined aquifer system (only piezometric measurements are available from the limestone aquifer; Cameron et al. 2011) but, due to the expected thinness of this layer (~10 m), connection to Lake Poukawa and the flat topographic elevation in this area, the water table is not expected to be deep.

One well (5006; screened at ~29 m depth) in the Otane area has had groundwater levels monitored since 2003. These levels exhibit seasonality and range between approximately 0.5 and 2.5 m below ground level (Harper 2012).

Gravels are mapped as a mainrock type through much of the study area. Dry gravels in the near-surface can create very high resistivity values (~1000–10,000 ohm.m); however, such values were not encountered in the assessment of near surface resistivity layers (Section A1.1).

The water table can create a significant resistivity contrast; however, in this case, it is not expected to appear as a key feature within the resistivity models.

A1.3 Peat Depths

Locations of measured peat depths (Hill et al. 2020) were assessed to provide information on likely resistivity ranges for peat. Hill et al. (2020) measured depth to the mineral subsurface base using a sectional fiberglass probe with an 18 mm drill at its tip. For sites where peat thickness was less than 1 m, a standard 6 cm diameter Edelman soil auger was used to determine peat depth (Hill et al. 2020). The deepest measured peat in the survey area was 8.84 m below ground level.

All resistivity data within 50 m of the measured peat locations was extracted. This process reduced the dataset to nine peat samples. The closest resistivity sounding for each peat sample was then selected. In all cases, data was found at distances of less than 10 m. From the closest resistivity sounding, all resistivity layers from both the smooth and sharp resistivity models with a bottom depth shallower than the measured peat depth were selected for assessment.

The six peat samples in the Poukawa area had resistivity values that ranged from 8.4 to 25.7 ohm.m (minimum to maximum), 9.3 to 25.4 ohm.m (P0.1–P0.9) and had a mean of 13.7 ohm.m and standard deviation of 5.5 ohm.m. The three peat samples in the Te Aute area (Otane Basin) had resistivity values that ranged from 6.9 to 69.5 ohm.m (minimum to maximum), 8.3 to 67.8 ohm.m (P0.1–P0.9) and had a mean of 29.1 ohm.m and standard deviation of 23.3 ohm.m.

One peat sample from the Otane area (TA51) had resistivity information greater than 9 m away and had much higher resistivity values than the rest of the dataset. As such, it was considered an outlier due to its proximity to surficially mapped limestone (within 250 m). The remaining eight samples had resistivity values that ranged from 6.8 to 29.3 ohm.m (minimum to maximum), 8.4 to 25.4 ohm.m (P0.1–P0.9) and had a mean of 13.7 ohm.m and standard deviation of 6.1 ohm.m (Figure A1.5).

An analysis of resistivity values within only the smooth model provided only very minor differences in value ranges.

Peat has a high organic content and high porosity, so the resistivity will be dominated by the saturation of the samples. Here, peats are present in low-lying areas and are typically saturated. A bulk resistivity of 14 +/- 6 ohm.m is at the lower end of the typical lignites but is mid-range for fresh water (Figure 1.3) and consistent with measured groundwater electrical conductivity (Section A1.5).

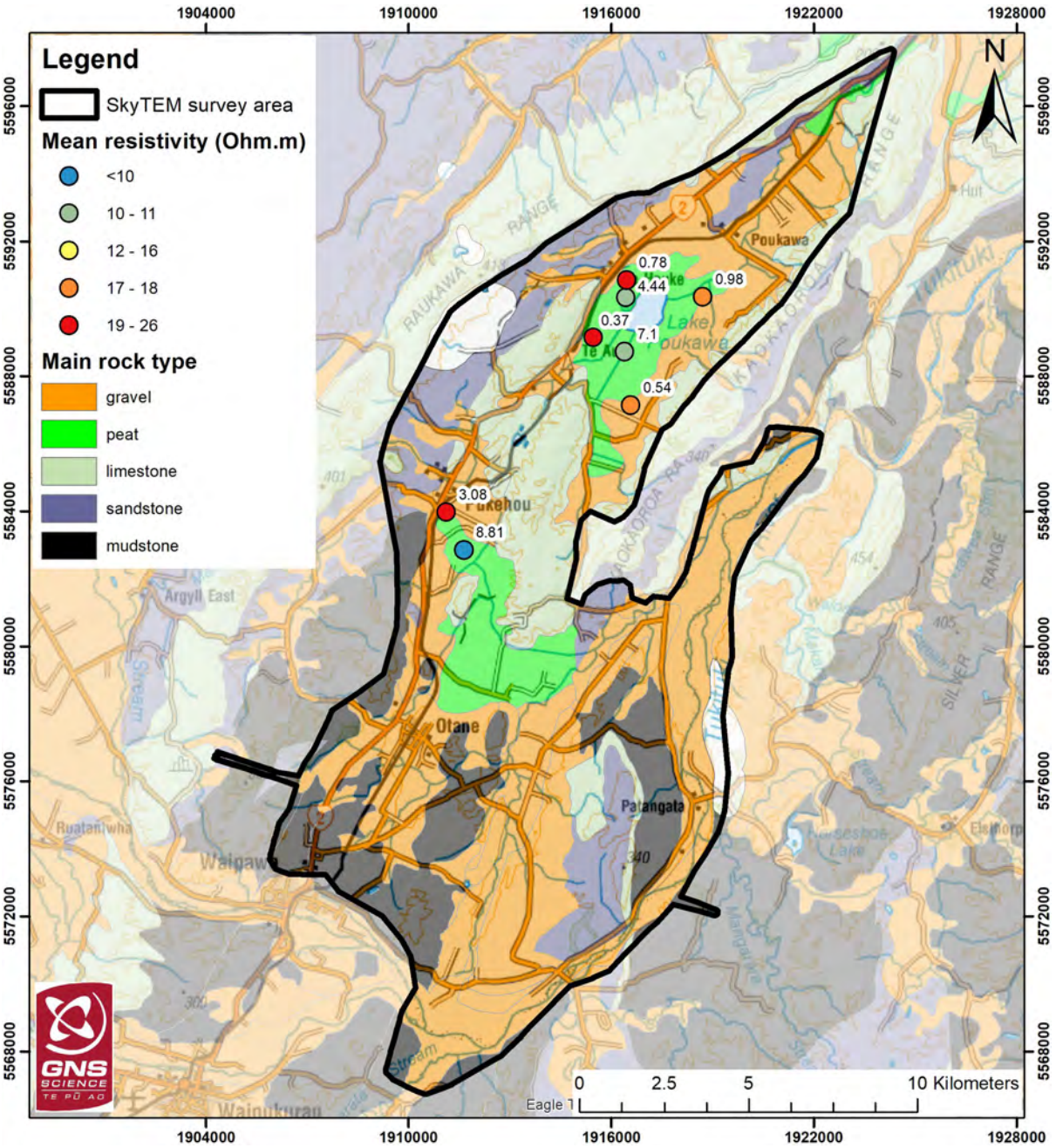

Figure A1.5 Peat samples within 50 m of resistivity data, labelled by depth of measured peat in metres and coloured by mean resistivity.

A1.4 Water Takes

A1.4.1 Water-Bearing Intervals and Lithologies

Construction information from the HBRC well database (Harper 2019) was utilised to assess water-bearing intervals. Bores with contiguous screen and open-hole depth intervals were converted to a single interval. Where both top and bottom screen and top and bottom open hole attributes contained no information (had values of ‘nan’ or ‘0’), the screen was selected to start from 5 m above the bore depth (5 m being the median screen length in the area). Where only bore depth information is available, and no screen or open-hole information, bores with bore depth ≤5 m were removed. Manual checks were undertaken to make further adjustments where needed based on comments in the construction information; for example, bores with comments of ‘dry’, ‘abandoned’, ‘exploratory’, ‘map reference / ref not accurate’, ‘too saline’ and ‘no water’ were discarded, and bores with additional casing, screen, pump-test or open-hole information in the comments were sense-checked against the lithological logs and this information utilised to adjust the water-bearing interval information. This resulted in 143 quality-checked water-bearing intervals. For each water-bearing interval, the dominant lithology within the interval was selected (with gravel, sand, limestone and sandstone given preference where they were present within the screened interval). The results are shown within Figure A1.6, with the 143 intervals corresponding to lithology as follows: gravel 43; limestone 40; sand 17; clay 15; sandstone 14; siltstone 8; mudstone 4; ash/pumice 1; shale 1.

Sixty-eight bores with water-bearing interval information were within 100 m of resistivity values (Figure A1.7). All resistivity information that fell within 100 m of a bore was selected, and resistivity values were subsequently selected that fell within the documented water-bearing interval. An assessment was undertaken for each lithology type using both the smooth and sharp models (Table A1.2). The bores classified as ‘sand’ lithology include one bore with a main lithology of ash/pumice but with sand and shell in the full description. Relatively minor differences were found between the smooth and sharp model assessments.

Due to the selection of all information within a fairly wide radius (100 m), and the different algorithms used by the smooth and sharp model inversions, the P0.1 and P0.9 smooth model estimates are considered most representative of the true range related to the water-bearing lithology. The bores screened in limestone range between 15.5 and 222.1 ohm.m, which corresponds to the entire porous limestone range in Figure 1.3. The bores screened in gravel range from 11.4 to 94.1 ohm.m, which is consistent with water-saturated sand, silt and clay, as well as gravel and alluvium in Figure 1.3. All other screened intervals have resistivity values consistent with Figure 1.3.

Screened intervals should correspond to water-bearing units. However, it is known from experience that significant errors can exist within the HBRC wells database regarding screen locations (from close inspection of lithological logs, recorded screened intervals and discussions with well owners). Given the wide range of screened lithologies and corresponding resistivity values, assumptions of water-bearing units should be considered with caution.

Table A1.2 Resistivity statistics in ohm.m for resistivity layers within a screened interval. P0.1 and P0.9 refer to the 10% and 90% percentiles; N refers to the number of bores.

Model	Lithology	Maximum Distance (m)	N	Minimum	Maximum	P0.1	P0.9	Mean
Sharp	All	100	68	5.2	620.1	9.4	84.8	46.0
Smooth	All	100	68	5.6	650.1	9.9	93.7	45.9
Sharp	Gravel	100	21	5.6	168.1	9.7	106.5	43.7
Sharp	Limestone	100	16	10.7	620.1	14.7	152.5	90.6
Sharp	Sand	100	10	13.1	68.8	14.7	25.6	21.2
Sharp	Clay	100	9	6.6	50.4	6.8	26.8	14.6
Sharp	Sandstone	100	7	11.4	92.0	15.8	32.1	26.5
Sharp	Siltstone	100	4	7.3	71.3	8.9	38.9	25.8
Sharp	Mudstone	100	1	5.2	19.4	5.7	17.8	13.7
Smooth	Gravel	100	21	7.3	203.8	11.4	94.1	44.0
Smooth	Limestone	100	16	10.2	650.1	15.5	222.1	91.1
Smooth	Sand	100	10	9.9	58.6	12.9	28.0	20.4
Smooth	Clay	100	9	5.6	32.4	6.8	27.4	14.2
Smooth	Sandstone	100	7	10.8	61.4	14.7	35.8	26.7
Smooth	Siltstone	100	4	7.0	66.4	10.0	43.3	25.2
Smooth	Mudstone	100	1	5.9	19.2	7.5	16.9	12.5

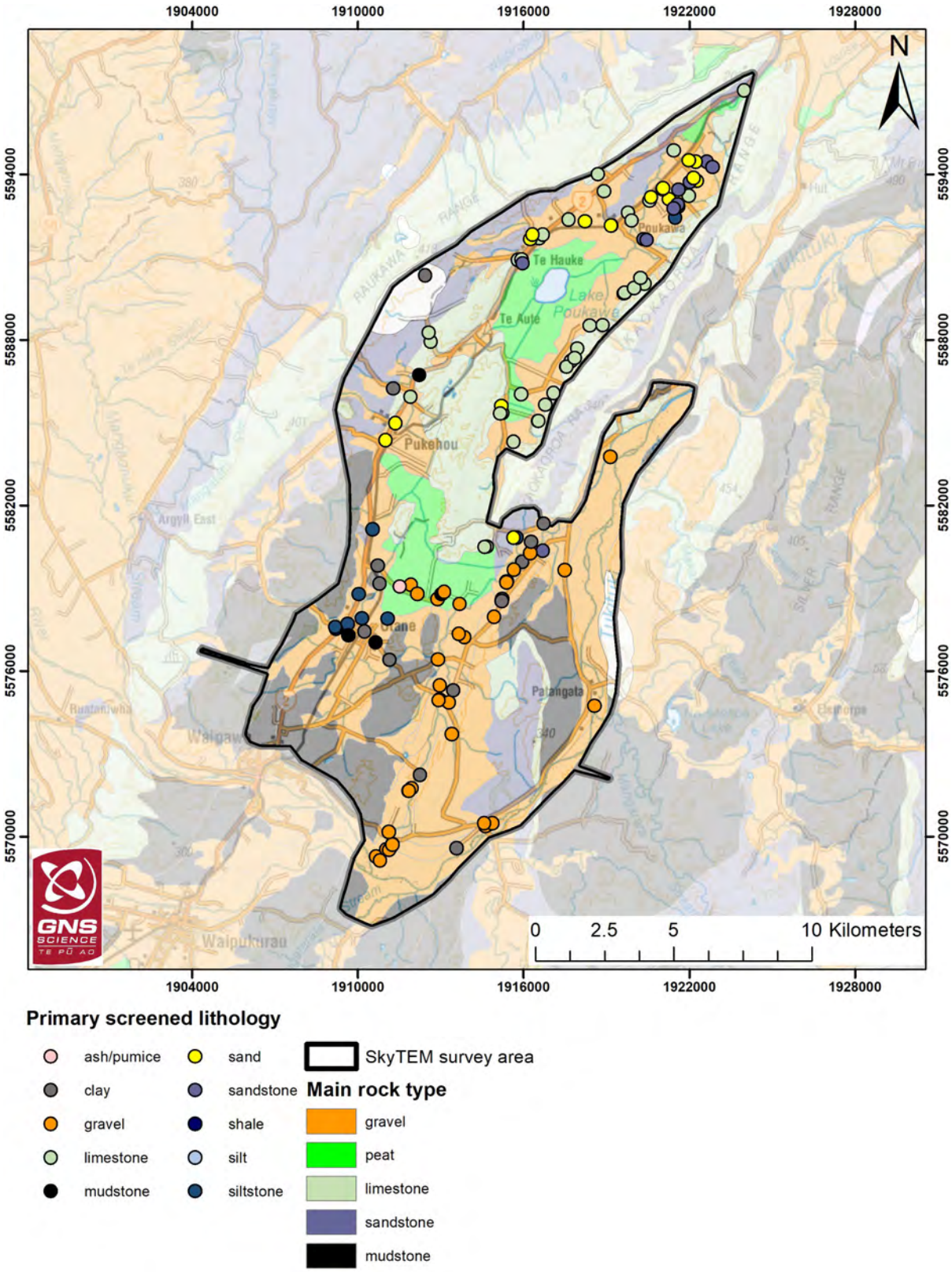

Figure A1.6 Main lithology recorded within screened interval.

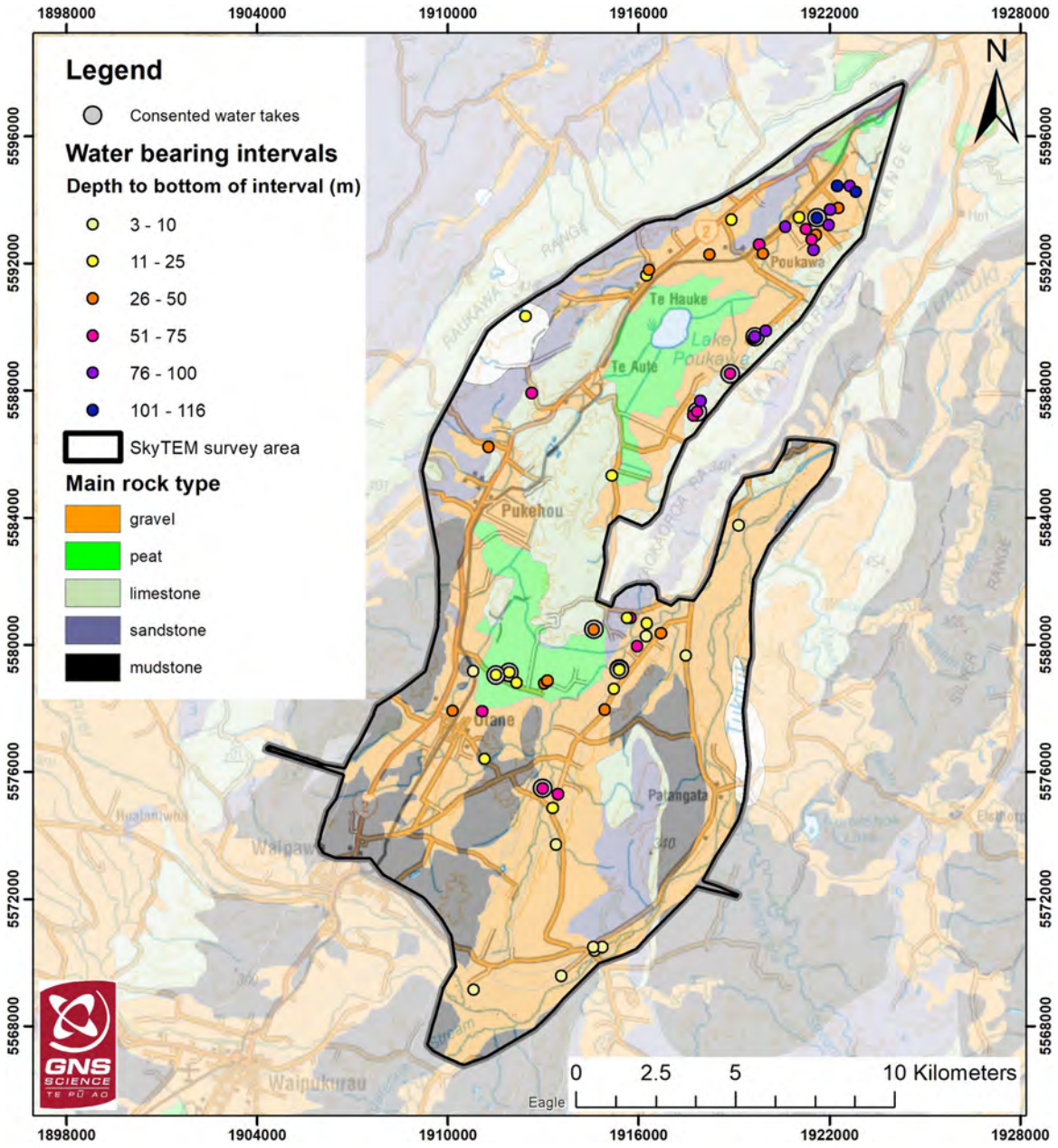

Figure A1.7 Bore depth information in metres for consented takes and boreholes with screen information within 100 m of resistivity data.

A1.4.2 Larger Water Takes (Consented)

Ten consented takes with water-bearing interval information (Section A1.4.1; Harper 2019) were within 100 m of resistivity values (Figure A1.7). All resistivity information within 100 m of each consented take that fell within the water-bearing interval was assessed from both the sharp and smooth models (Table A1.3). A more detailed assessment of only the smooth model values was also performed (Table A1.3).

The bores with water-bearing intervals in limestone cover a wide range, 43.1–307.8 ohm.m (P0.1–P0.9), but, because these are all open-hole over large intervals (36–80 m), it is unclear what portion of this range corresponds to the water-bearing part of the limestone. In Figure 1.3, this corresponds to the entire porous limestone range and the lower end of the massive limestone range. The bores screened in gravel have quite low resistivity values and correspond to water-saturated sand, silt and clay in Figure 1.3. The resistivity values suggest that the deeper gravels have a lower porosity or more clay than the shallower gravels.

Table A1.3 Resistivity statistics in ohm.m for resistivity layers within the screened interval of a consented take. P0.1 and P0.9 refer to the 10% and 90% percentiles. 'Smooth' refers to resistivity values obtained from the smooth model and 'sharp' refers to resistivity values obtained from the sharp model.

Assessment	Bores	Minimum	Maximum	P0.1	P0.9	Mean
Smooth	1828, 5950, 4373, 3159, 15039, 4176, 3528, 4667, 16693, 4840	17.4	650.1	27.0	174.1	110.0
Sharp	1828, 5950, 4373, 3159, 15039, 4176, 3528, 4667, 16693, 4840	14.3	620.1	27.0	174.1	108.7
Smooth limestone	5950, 4373, 4176, 4667	17.4	650.1	43.1	307.8	164.7
Smooth all gravel	3159, 15039, 3528, 4840	27.7	78.5	31.5	72.2	52.3
Smooth model shallow gravel	3528, 15039, 3159	27.7	78.5	31.7	75.2	55.6
Smooth model deeper gravel	4840	28.9	42.1	29.6	39.2	34.8
Smooth sandstone	1828	34.2	44.7	34.2	44.7	39.5
Smooth ash/pumice with sand and shell	16693	27.2	28.4	27.4	28.2	27.8

A1.5 Measured Groundwater Electrical Conductivity

State of the Environment (SOE) groundwater quality information for the area was provided by HBRC (Harper 2019). This dataset was assessed to extract electrical conductivity information within the study area. Additionally, one site from the National Groundwater Monitoring Programme (NGMP) falls within the study area and relevant groundwater quality information was extracted from the online Geothermal and Groundwater database.[3]

To best inform this assessment, the measurements would ideally be available from the time that the SkyTEM data were collected (January/February 2020). Electrical conductivity over time showed some significant seasonal trends; therefore, where feasible, the December–March time period was selected as the time period closest to the SkyTEM survey time (January/February 2020) when hydrogeological conditions are expected to be comparable. SOE sampling is typically undertaken quarterly; therefore, for these datasets, the December 2019 and March 2020 samples were averaged. Only samples from June and October 1994 were available for the NGMP site, therefore, the October measurement was selected as most representative. In total, eight different sites had available groundwater electrical conductivity information, which were converted into resistivity values (Figure A1.8; Table A1.4).

Groundwater acts as an electrolyte (Lowrie 2006) and so increases the conductivity of water-bearing lithologies. This conductivity increase depends on the volume of water as well as the chemical composition of the water. Freshwater is resistive, but suspended or dissolved solids such as clays and/or salt will increase its conductivity. Lower resistivity values indicate longer groundwater residence times (longer time for dissolved solids to accumulate). The New Zealand drinking water standards[4] have a guideline value for total dissolved solids of 1000 mg/L but comment that taste may become unacceptable from 600 to 1200 mg/L.

3 https://ggw.gns.cri.nz/ggwdata/listAnalysisResults.jsp?FEATURE=5013

4 https://gazette.govt.nz/notice/id/2022-sl2379

This lower bound of 600 mg/L corresponds to a resistivity value of approximately 11 ohm.m, and the guideline value corresponds to a resistivity value of approximately 6.6 ohm.m. Within the Venice system for the classification of marine waters, brackish water is classified as 0.2–8.3 ohm.m and freshwater as >8.3 ohm.m (e.g. Madarasz-Smith et al. 2016).

Groundwater resistivity values in our study area range from 8.64 to 54.20 ohm.m (Figure A1.8; Table A1.4) and so fall within the range for freshwater. The lowest recorded value of 8.53 ohm.m was measured at site 5006 (1173 μS/cm), and the highest recorded value of 54.64 ohm.m was measured at site 16208 (183 μS/cm). The variability in these values is not considered of significance for the hydrogeological interpretation of the resistivity model (as would be the case if there were a mix of fresh and saline water in the area). These measurements are representative of the shallow groundwater system (<61 m deep). If the lowest value measured is assumed to be representative of groundwater in the area, then this suggests that any resistivity values within the resistivity models below 8.53 ohm.m are likely to be influenced by clay minerals, enhancing conductivity.

The relationship between rock resistivity and water resistivity has been evaluated in a formula called Archie's law (Archie 1942). As Archie's law is only valid for material without conductive material in the matrix (e.g. clay), the apparent formation factor (F) can be defined as $F = R_O/R_W$, where R_W is the resistivity of the water, and R_O is the bulk or saturated resistivity of rock. Corrections exist to account for the presence of conductive minerals, but these require additional information and assumptions (e.g. Glover 2016). F is a function of the type of matrix and porosity of the material, where a lower F corresponds to higher porosity ($F = a/\phi^m$, where a is the tortuosity factor representing pore shape, m is the cementation exponent and ϕ is the porosity). If the bulk resistivity of the sample is the same as the resistivity of the pore fluids, then the porosity must be high. In the presence of no conductive minerals, $F = 1$ would correspond to 100% porosity. However, where F is close to 1 in this study area, this instead suggests the presence of conductive minerals (e.g. clay) and the breakdown of Archie's law (based on local lithological information describing the presence of conductive minerals).

The location and depth information of the groundwater electrical conductivity measurements were used to extract smooth model resistivity information within a 200 m radius and at a matching depth interval (Table A1.5). Using this information, apparent formation factors (F) were calculated, which range between 0.9 and 6.4 (Table A1.5). Assuming that these apparent formation factors and measured R_W values are representative of the area, resistivities for aquifers are expected to be approximately 8–350 ohm.m. From Figure 1.3, this is consistent with freshwater saturated silt and clay, silty sand, sand, sand/gravel, gravel and porous limestone. The low apparent formation factor values calculated for many of the wells suggests the presence of clay, which is confirmed by the lithological log description for well 16256 (Table A1.5).

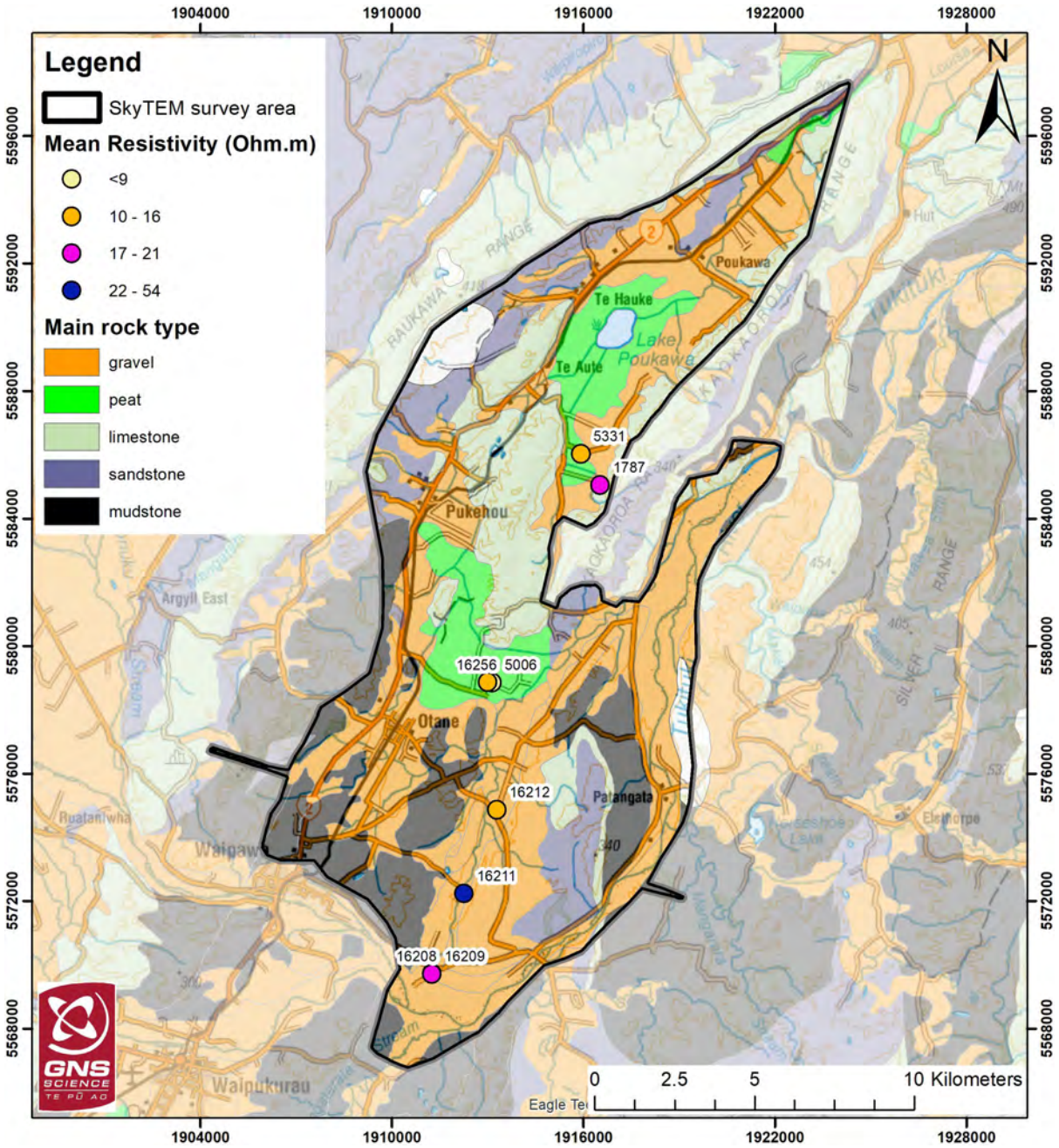

Figure A1.8 Groundwater electrical conductivity measurement locations. Locations are labelled by bore number to enable comparison with Table A1.4 and are coloured by mean resistivity.

Table A1.4 Summary of groundwater electrical conductivity measurements.

Bore No.	Lithology	Electrical Conductivity (μS/cm) (Mean)	Comment	Resistivity (ohm.m) (Mean)
5006	Gravel	1157.50	Specific Conductivity – Lab	8.64
5331	Limestone with sand	732.00	Specific Conductivity – Lab	13.66
16208	Gravel	184.50	Specific Conductivity – Lab	54.20
16209	Gravel	478.00	Specific Conductivity – Lab	20.92
16211	Gravel	195.50	Specific Conductivity – Lab	51.15
16212	Gravel	641.00	Specific Conductivity – Lab	15.60
16256	Gravel with clay/limestone	637.00	Specific Conductivity – Lab	15.70
1787	Sandstone	540.00	NGMP; total solids (electrical conductivity) μS/cm at 25°C	18.52

Table A1.5 Calculation of apparent formation factor (F) for sites with groundwater electrical conductivity measurements (Table A1.4). R_W is the resistivity of the water and R_O is the bulk or saturated resistivity of rock. P0.1 and P0.9 refer to the 10% and 90% percentiles.

Bore No.	Lithology	R_W (ohm.m)	R_O P0.1 (ohm.m)	R_O P0.9 (ohm.m)	F	Distance between R_W and Nearest R_O (m)
5006	Gravel	8.64	7.6	16.6	0.9–1.9	58
5331	Limestone with sand	13.66	N/A	N/A	N/A	>200
16208	Gravel	54.20	N/A	N/A	N/A	>200
16209	Gravel	20.92	N/A	N/A	N/A	>200
16211	Gravel	51.15	63.7	131.1	1.2–2.6	155
16212	Gravel	15.60	75.6	100.2	4.8–6.4	75
16256	Gravel with clay/limestone	15.70	16.7	25.2	1.1–1.6	40
1787	Sandstone	18.52	58.4	75.7	3.2–4.1	106

A1.6 Research Lithological Logs

The highest quality lithological logs in the area were drilled for research purposes during the Lake Poukawa Drilling Project (LPDP), from 1976 to 1984, and the Victoria University of Wellington paleoclimate study in 1996. The boreholes have highly detailed logs. These logs were digitised from their associated reports: LPDP 1–3 (Robertson and Howorth 1980), LPDP 4 (Fellows 1984), LPDP 5 (Robinson et al. 1984) and Poukawa 97-1 (Shulmeister et al. 1998). The drilling projects located the wells on topographical maps and aerial photos, and the reports provide some coordinates and a base map. There is some disagreement in the coordinates of the wells compared to the maps across the various reports. For this report, their locations were obtained by georeferencing the map of bore locations shown in Figure 1 of Shulmeister et al. (1998). Therefore, there is a greater uncertainty in the location of these wells than the groundwater wells that have been located with GPS. The closest resistivity data was selected for each well (Table A1.6; Figure A1.9) and manually assessed against the lithology (e.g. Figures A1.10–A1.13).

The lithological logs have been presented using a consistent lithological code in strip logs in Figures A1.10–A1.13. No geophysical logs were collected in the research boreholes. In the Victoria University of Wellington borehole Poukawa 97-1, magnetic susceptibility data were measured on the core at 5 cm intervals. The raw data are presented in Shulmeister et al. (1998) and show dramatic increases in magnetic susceptibility across the tephra layers. The smoothed data have been digitised and presented in Figure A1.13. The magnetic susceptibility data respond to the magnetic mineral content of the sediments, primarily the input of volcanic-derived sediment into the basin by re-working of ash deposits on the surrounding land. There are 4–5 cycles of sediment input identified in the magnetic susceptibility data that correlate with units of higher sand content (higher susceptibility) and lower silt content (lower susceptibility). Intervals with significant clay and peat often have low susceptibility.

In Figures A1.10–A1.13, the SkyTEM inversion models have been plotted in tracks alongside the lithology log to illustrate the changes in electrical properties with depth. In general, the layering in the lithology logs is at a much finer scale than the SkyTEM inversion models. Sharp contacts in the lithology logs are detected in the sharp SkyTEM inversion, whereas the smooth SkyTEM inversion tends to highlight the trends of increasing sand or silt content. When the complete section encountered by wells LPDP 1, 4, and 5 is considered, the SkyTEM models identify the following units:

- The top 6–10 m is dominated by peat with a low resistivity (~7–10 ohm.m).
- The resistivity increases sharply at the top of a silt- and sand-dominated layer (~20–25 ohm.m).
- The sand and gravel units in LPDP 4 have a sharp base that is picked as a drop in resistivity at 50 m depth (~10–15 ohm.m).
- The silt-dominated package extending to 150 m depth (LPDP 5) has a lower resistivity (~8–15 ohm.m).
- The resistivity increases at 170 m depth when sandy units become more common (~15–35 ohm.m).
- The SkyTEM models at the location of Poukawa 97-1 show a similar pattern.
- Limestone was not reached in the wells, but the SkyTEM inversion suggests that it is less than 20 m below the bottom of hole Poukawa 97-1.

The sharp inversion models extracted at the locations of the deeper wells (LPDP 5 and Poukawa 97-1) show an increase in resistivity from 9–14 to 30 ohm.m at depths of 180 m. This increase could be interpreted as the top of the limestone; however, in both wells, the lithology logs show a slightly sandier section but not limestone. The smooth inversions show that the resistivity boundary is likely to be at 220–250 m depth, consistent with the more competent limestone being 20–30 m below the deepest units drilled at LPDP 5 and Poukawa 97-1.

An automatic assessment was also undertaken on these bores and all resistivity data within 150 m. Fractions of lithology were summed within a resistivity layer interval and assigned that resistivity where the fraction of composition exceeded a certain threshold (Table A1.7), using both the smooth and sharp models. Due to the selection of all information within a fairly wide radius (150 m), and the different algorithms used by the smooth and sharp model inversions, the P0.1 and P0.9 smooth model estimates are considered most representative of the true range related to the lithology. Here, marl (a limestone-derived clay) has low values of 7.8–8.9, silt has slightly higher values of 14.3–17.9, peat covers a wider range of values 7.9–34.0 and sand has relatively high values of 18.4–136.6 ohm.m. For gravel,

only a 30% threshold was available, and the values are only slightly higher than silt at 20.5–23.6 ohm.m. From a manual inspection of the lithological log, the gravel layers are present between thick intervals of silt and the resistivity values are heavily influenced by these silt packages.

Table A1.6 Research lithological logs (Figure A1.9).

Well	Depth (m)	Distance to Nearest Resistivity Data (m)
LPDP 1	0–35.1	22.6
LPDP 2	0–13.3	34.3
LPDP 3	0–17.8	39.2
LPDP 4	35–112.02	42.1
LPDP 5	94.4–233.97	102.2
Poukawa 97-1	0–197.7	76.1

Table A1.7 Summary of resistivity statistics (ohm.m) associated with material volume thresholds (%) within the research lithological logs (Figure A1.12).

Model	Lithology	Distance (m)	Threshold	Minimum	Maximum	P0.1	P0.9	Mean
Sharp	Gravel	150	30	21.7	23.8	21.8	23.6	22.6
Sharp	Marl	150	50	9.1	10.1	9.3	10.0	9.7
Sharp	Peat	150	80	9.1	58.9	9.6	38.8	22.6
Sharp	Silt	150	80	10.3	12.7	10.4	11.8	11.0
Sharp	Sand	150	80	9.0	141.1	13.4	120.2	75.2
Smooth	Gravel	150	30	20.1	24.0	20.5	23.6	22.0
Smooth	Marl	150	50	7.6	9.0	7.8	8.9	8.3
Smooth	Peat	150	80	7.4	50.8	7.9	34.0	20.1
Smooth	Silt	150	80	13.7	18.5	14.3	17.9	16.2
Smooth	Sand	150	80	14.4	159.3	18.4	136.6	81.6

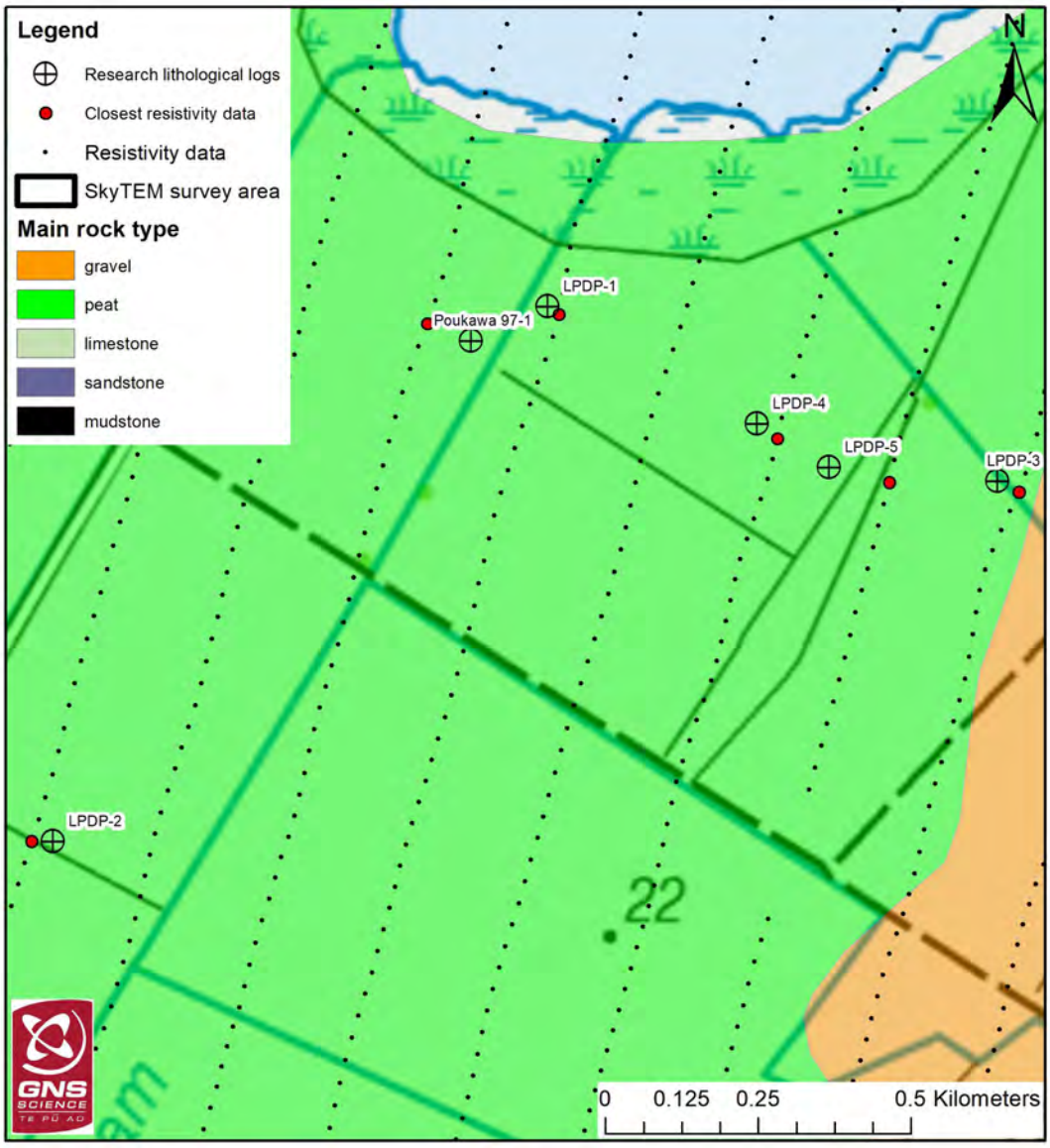

Figure A1.9 Research lithological logs and the closest resistivity data to each one (Table A1.6).

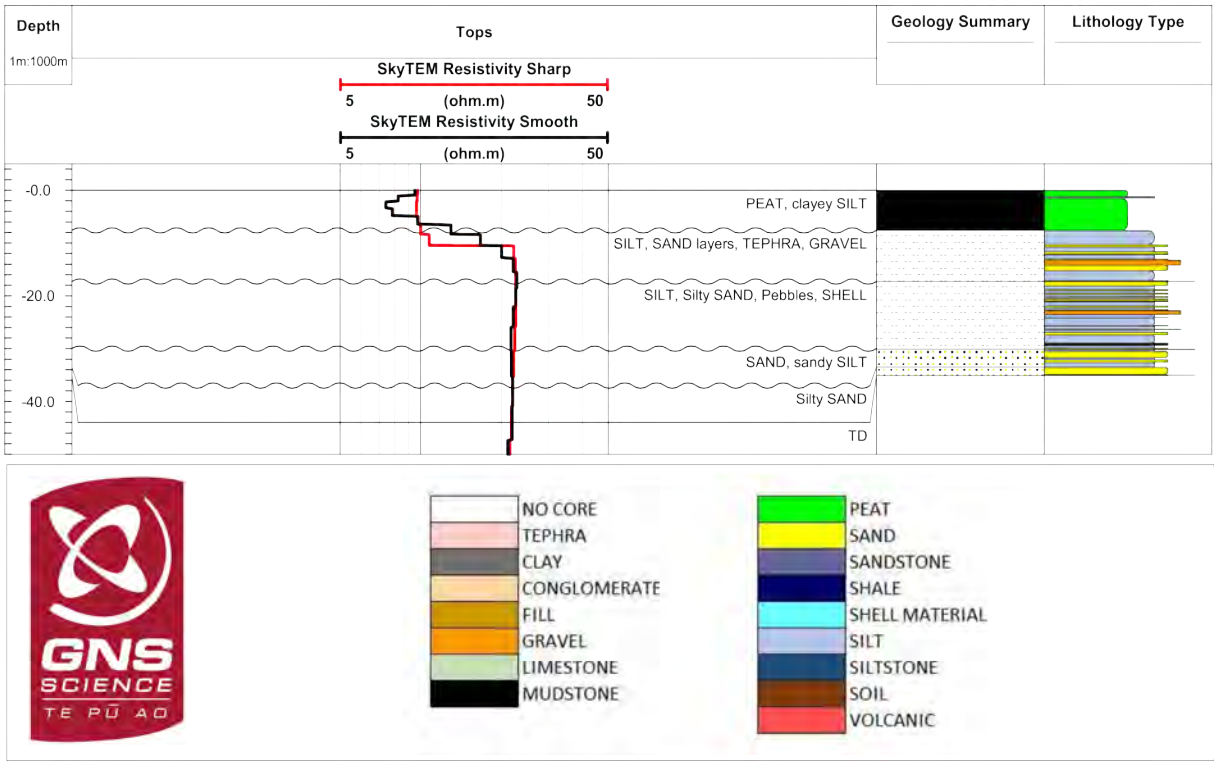

Figure A1.10 LPDP 1 lithological log compared to the sharp and smooth resistivity models.

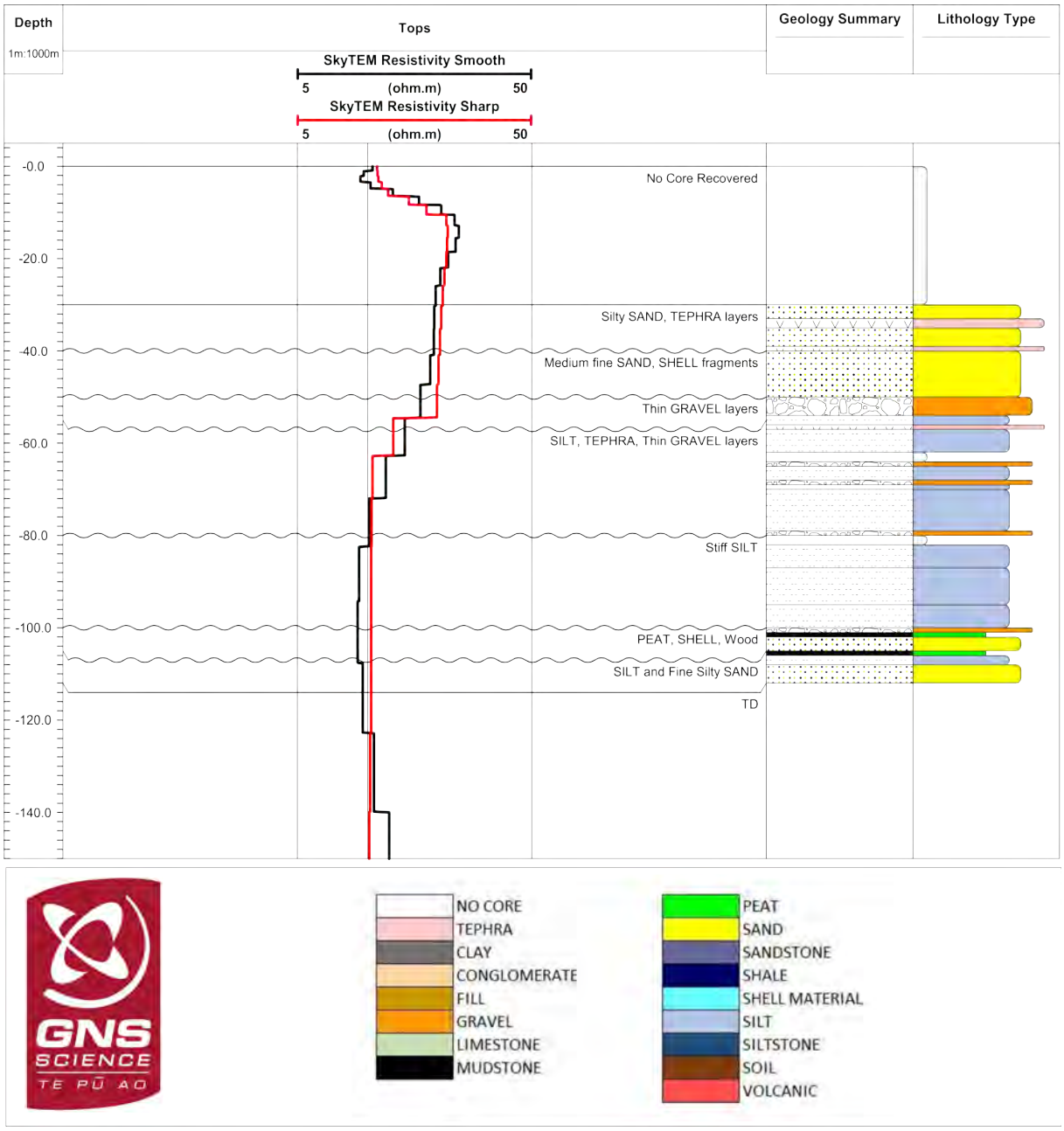

Figure A1.11 LPDP 4 lithological log compared to the sharp and smooth resistivity models.

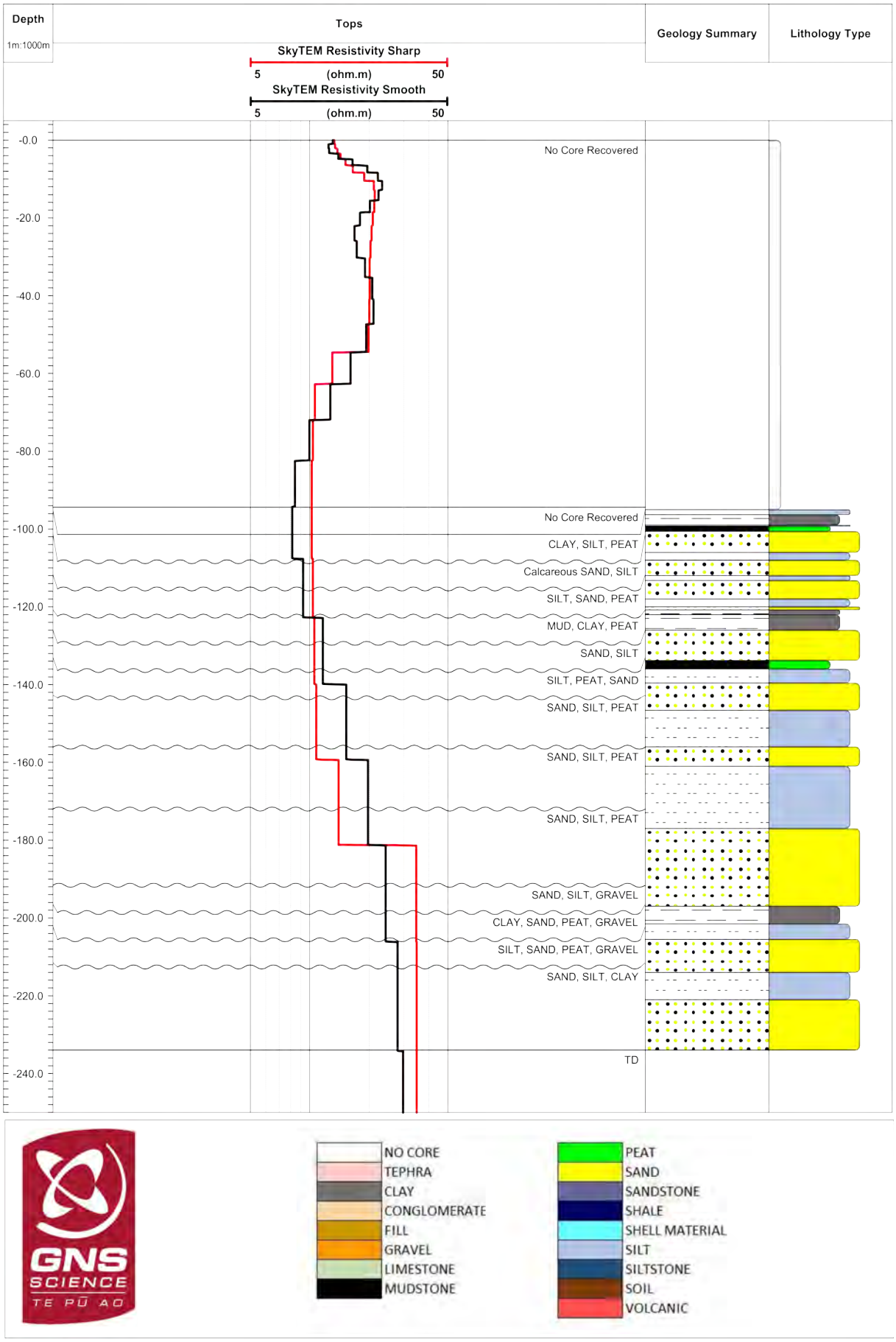

Figure A1.12 LPDP 5 lithological log compared to the sharp and smooth resistivity models.

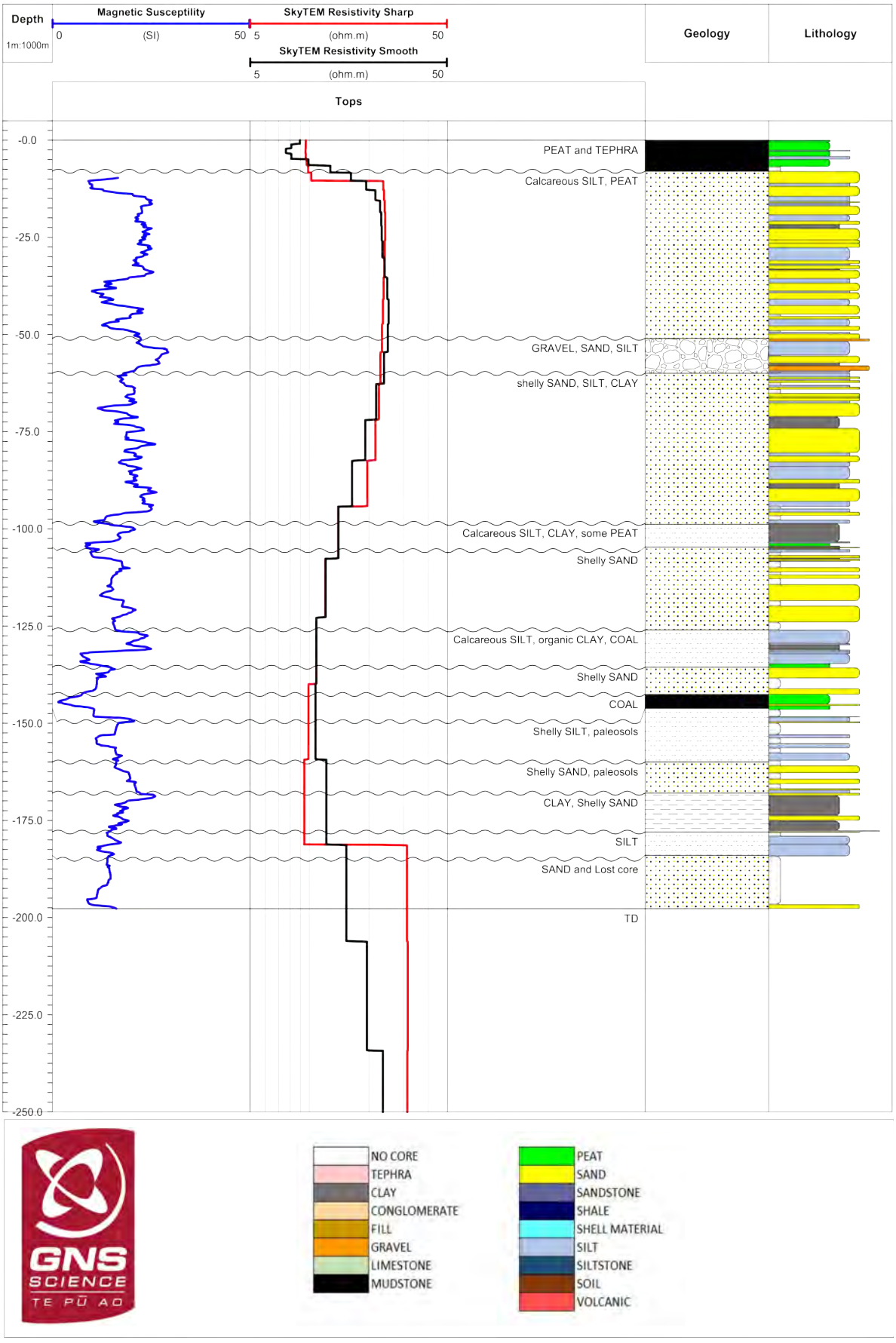

Figure A1.13 Poukawa 97-1 lithological log compared to the sharp and smooth resistivity models. Magnetic susceptibility was measured on core samples.

A1.7 Hawke's Bay Regional Council Well Database

Lithological data from the HBRC Well database (Harper 2019) were used to assess nearby resistivity information. Due to limited lithological log data, all boreholes were used except those that included the comment 'map ref. not accurate'. This resulted in 160 wells available for the assessment (Figure A1.14). All resistivity information within 100 m was selected for assessment (79 wells; Figure A1.14).

Fractions of lithology were summed within a resistivity layer interval and assigned that resistivity where the fraction of composition exceeded 80% (Table A1.8). Because of high values within the clay dataset, this was investigated more closely. Bores with ≥80 ohm.m correlated to clay were pulled out and the two datasets assessed independently (Table A1.8). Additionally, all wells with a note of 'water bearing' were selected for closer inspection (Table A1.9).

Areas expected to have a strong limestone influence provide higher resistivity values for clay, with material logged as clay falling within the porous limestone interval of Figure 1.3. It is considered that this is likely either an error in the identification of the material during logging, or that the conductive electromagnetic responses of these thin layers of clay are swamped by the thick highly resistive underlying package of limestone. Logged limestone falls within the porous limestone range and lower section of the massive limestone range within Figure 1.3. Both gravel and sand have lower values than expected from Figure 1.3, suggesting silt and clay influences. All other logged intervals are within the ranges expected from Figure 1.3.

It is known from experience that differences can exist within the HBRC well database regarding logged intervals (from close inspection of database records with driller's original logging sheets), and there is additional uncertainty associated with the boreholes having been primarily logged by drillers rather than geologists. The drilling methods utilised also impact the uncertainty of the logged descriptions. These uncertainties need to be weighed against expected resistivity values for lithological units when utilising the results of this assessment.

Table A1.8 Summary of resistivity statistics (ohm.m) associated with material volume threshold within a distance of 100 m from lithological data within the Hawke's Bay Regional Council well database. Limestone-influenced clay was identified in bores 4176, 4197, 4666, 4667, 5528, 5641 and 5643.

Lithology	Threshold (%)	Minimum	Maximum	P0.1	P0.25	P0.75	P0.9	Mean
Gravel	80	7	316	17	27	106	166	75
Sand	80	11	155	12	13	22	84	30
Peat	80	17	23	18	18	21	22	20
Silt	80	9	37	11	14	19	23	17
Clay	100	4	614	11	15	26	36	31
Clay – no major limestone influence	100	4	68	10	15	23	29	19
Clay – major limestone influence	100	13	614	17	23	141	310	105
Ash/pumice	80	27	27	27	27	27	27	27
Limestone	80	11	650	21	44	147	303	132
Sandstone	80	10	69	11	19	33	46	27
Siltstone	80	4	66	6	13	28	42	22
Mudstone	80	6	57	7	7	14	21	13

Table A1.9 Summary of resistivity statistics (ohm.m) associated with material volume threshold within a distance of 100 m from lithological data within the Hawke's Bay Regional Council well database – intervals with notes of 'water bearing'.

Lithology	Threshold (%)	Minimum	Maximum	P0.1	P0.25	P0.75	P0.9	Mean
Gravel	80	9	183	15	32	76	161	67
Sand	80	11	155	12	13	22	84	30
Limestone	80	15	360	48	67	105	165	97
Mudstone	80	16	22	16	17	20	21	19

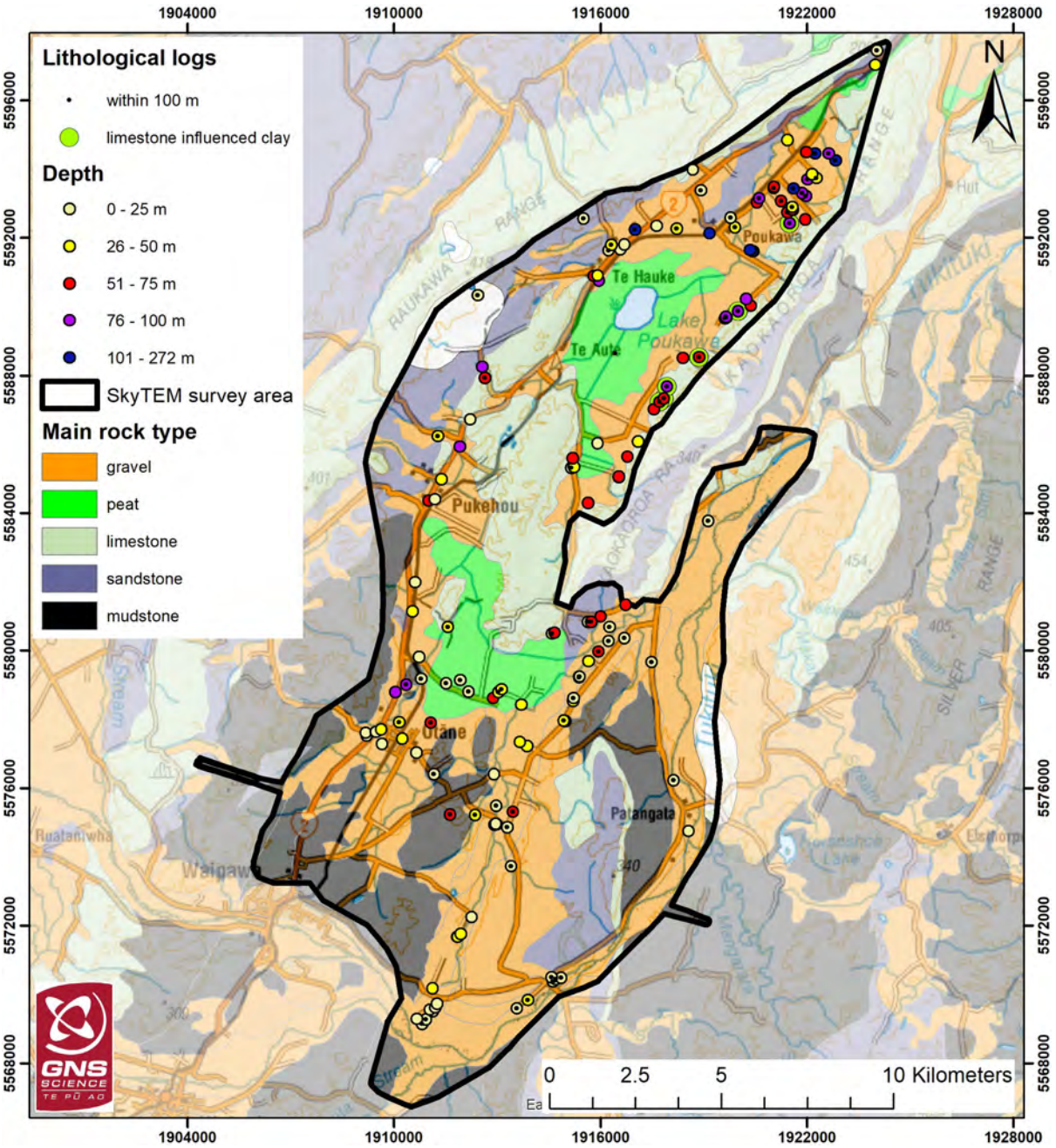

Figure A1.14 Lithological logs. Black dots identify lithological logs within 100 m of resistivity data.

www.gns.cri.nz

Principal Location

1 Fairway Drive, Avalon
Lower Hutt 5010
PO Box 30368
Lower Hutt 5040
New Zealand
T +64-4-570 1444
F +64-4-570 4600

Other Locations

Dunedin Research Centre
764 Cumberland Street
Private Bag 1930
Dunedin 9054
New Zealand
T +64-3-477 4050
F +64-3-477 5232

Wairakei Research Centre
114 Karetoto Road
Private Bag 2000
Taupo 3352
New Zealand
T +64-7-374 8211
F +64-7-374 8199

National Isotope Centre
30 Gracefield Road
PO Box 30368
Lower Hutt 5040
New Zealand
T +64-4-570 1444
F +64-4-570 4657